Research Article

Image Processing Results Of One Week Covid-19 Evolution Pneumonia X-Rays

Abhishek Bansal [1],

[1]New Era Consultancy Services, Delhi,India ; abhishekbansaL006@gmail.com

*Correspondence: abhishekbansaL006@gmail.com ;

Abstract: This paper presents the collection of 385 new images and results, obtained after performing many known image processing algorithms and digital image transformations techniques like adding noises namely Gaussian with variances, Poisson and speckle with variances; double precision, methods of Sobel, Prewitt and Robert; dehazing algorithm, pixel intensities, vector quantization, k-means clustering, fuzzy logic and morphological segmentation. Images used in this paper are five X-Rays at day 0, day3, day 4 and day 6, which are Posterior to Anterior (PA) views of the patient's lungs who was diagnosed with covid-19 Pneumonia. All results are included in the paper as well as separate images have also been uploaded on the open-access page. The data has been analyzed with histogram and mathematical polynomial fitting equations and matrices have been also submitted which can used in the digital testing of machines or computer diagnostic solutions. As these results reveal certain patterns, these further processed X-Ray results can help researchers or doctors in understanding ailment or diagnosing and to pharmacologists in making medicine or machine/therapy.

Keywords: image processing, pneumonia, X-Ray, Laplacian operator, Sobel–Feldman operator, mathematical morphology,Gaussian,white noise,variances,Poisson,speckle,single precision,double precision,Sobel,Prewitt, Robert,dehazing algorithm, pixel intensities,vector quantization, k-means clustering,fuzzy logic,edge detection, fuzzy inference system, FIS,Gaussian smoothing, intermediate difference,central difference,polynomial regression,convolution,morphological segmentation,COVID, windpipe,covid-19 ,respiratory tract

1. Introduction

It is known that images can be processed through computer using algorithms. There are many open-source and proprietary tools and softwares like in Python[1], OpenCV[3], FuzzyLite[4], PyTorch[10],TensorFlow[11] etc. The techniques like Laplacian Operator[5], Sobel–Feldman operator[6], Mathematical morphology[7], Fuzzy Logic[8],double precision, methods of Sobel,Prewitt and Robert gradients,Gaussian,Canny, dehazing algorithm, pixel intensities,vector quantization, k-means clustering, fuzzy logic and morphological segmentation. are known and widely implemented in digital camera images,

Face detection, Edge Detection, traffic vehicles, etc.

The author has used all these various digital image transformations techniques on the X-rays or Datasets from[1]. The use of these image processing algorithms is in research by many researchers/post-doctorate fellows/clinical doctors, even the source[1] has python script and other scripts on tensorflow, openCV or proprietary software scripts can be located on internet. The techniques used in this paper are mentioned along side with the processed-image. Algorithms have not been explained as they are known and it would be a plagiarism.‡

The paper is organized as : In the Section II, five original-rays are included.

The subsequent five sections are related to the results of processed images of Day0(L), Day0(PA),Day3(PA), Day4(PA) and Day6(PA).

The Day0(L) results are from page 4-28.

The Day0(PA) results are from page 29-52.

The Day3(PA) results are from page 53-75.

The Day4(PA) results are from page 75-98.

The Day6(PA) results are from page 99 - 121.

The conclusion is given on page 121.

The subsections are organized as :

1) Firstly X-Ray of the section is converted to single precision grayscale and double precision in Subsection 1 titled as ‘X-Ray Converted’

2) In Subsection 2- ‘Double Precision Noise Addition’, noises namely Gaussian, Poisson and speckle noises are added to the converted double-precision X-Ray.

3) In Subsection 3-'Gradient Magnitude and Direction' of single precision X-Ray are plotted using four methods.

‡ *Many will say just known code and image processing, elementary, which is true as the author has modified known scripts and image results obtained. On the other side, many paid freshers or paid employees! will want to know code. Modified code is not shareable but the author can render services at some monetary price. Overload computations have caused many times computer crashes with complete corruption of files.*

4) In Subsection 4-'Directional Gradients' of single precision X-Ray are plotted using four methods.

5) In Subsection 5- 'Gaussian Noises & Sobel Gradient', Gaussain noise with variances are added to single precision grayscale X-Ray.

6) In Subsection 6- 'Poisson Noise & Sobel Gradient', noise is added to single precision grayscale X-Ray.

7) In Subsection 7- 'Speckle Noise & Sobel Gradient', Speckle noise with variances are added to single precision grayscale X-Ray.

8) In Subsection 8- 'Pixel Intensities & Contrast', original X-Ray is contrasted and mathematical formulation of the pixels are given.

9) In Subsection 9- 'Fuzzy Logic' is used and edge detection using FIS and edge algorithm given.

10) In Subsection 10- 'K-means Clustering', a vector quantization technique is used to obtain clusters and the mathematical formulation is again given.

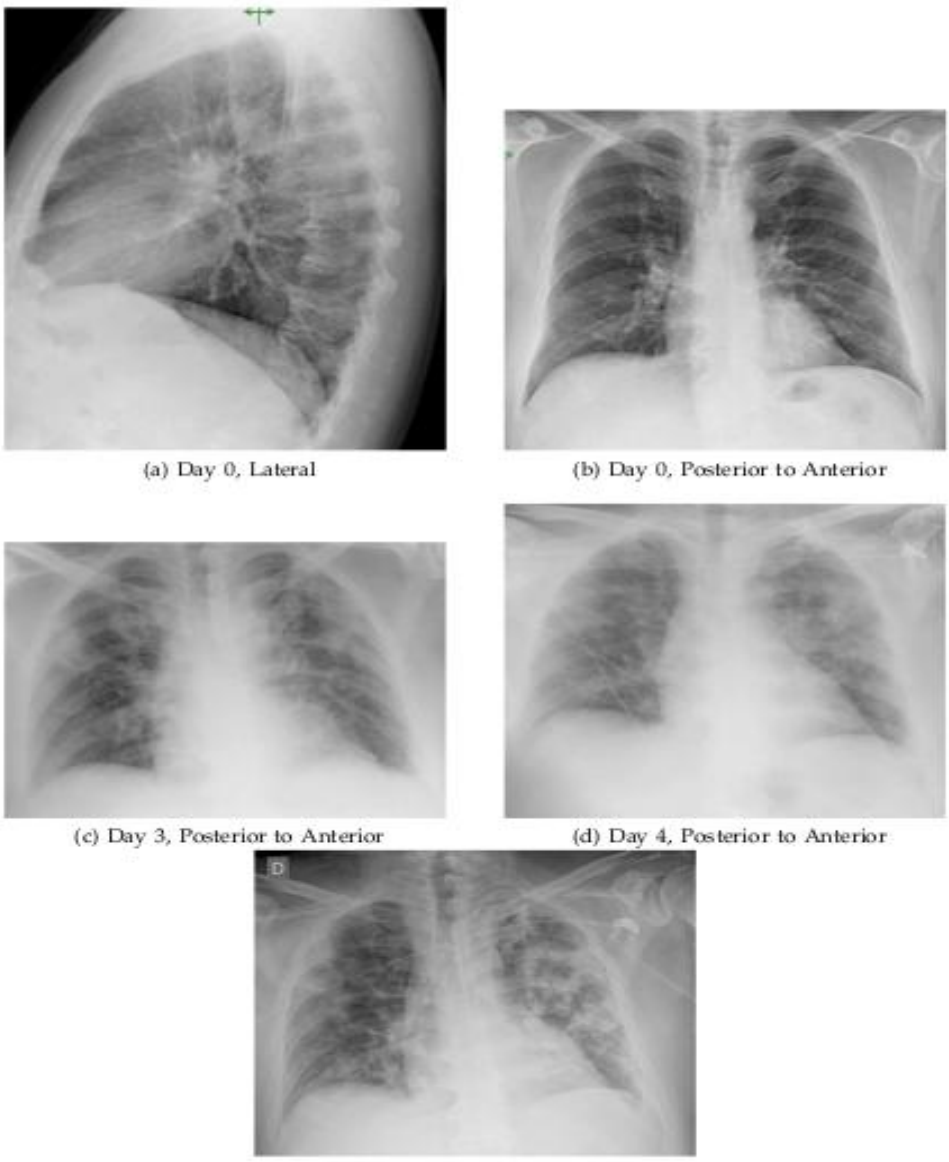
11) Subsection 11- 'Morphological Segmentation' results are given.

12) Subsection 12- 'Dehazing Algorithm' is used and its results are given.

2. Original X-Rays

The five X-Rays are taken from [1] are shown in Fig. 1, which are evolution of covid-

19-pneumonia over a week from Day 0 to Day 6. On these X-rays, the above mentioned popular elementary and advanced algorithms will be implemented.



(a) Day 0, Lateral

(b) Day 0, Posterior to Anterior

(c) Day 3, Posterior to Anterior

(d) Day 4, Posterior to Anterior

(e) Day 6, Posterior to Anterior

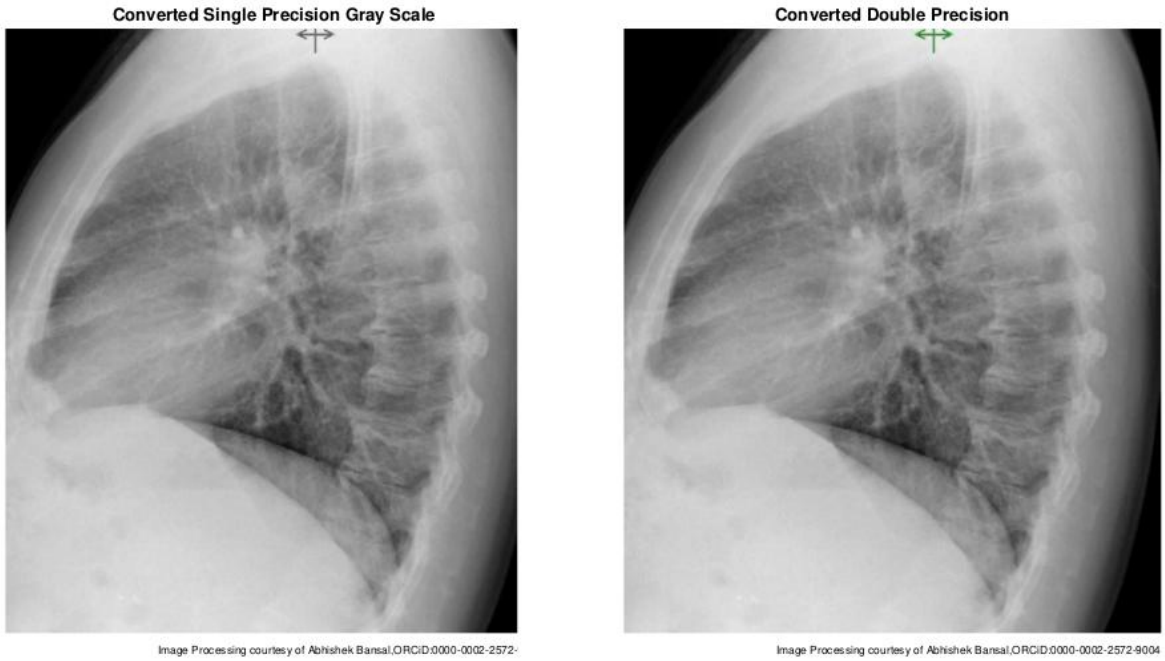
Fig. 1: Original X-Rays from [1]

3. Results : Day 0,Lateral

3.1. X-Ray Converted

In this subsection, X-Ray(L) of Day 0 is converted to single precision gray-scale and double precision, on which all further image processing s will be done. These are shown

in Fig. 2.

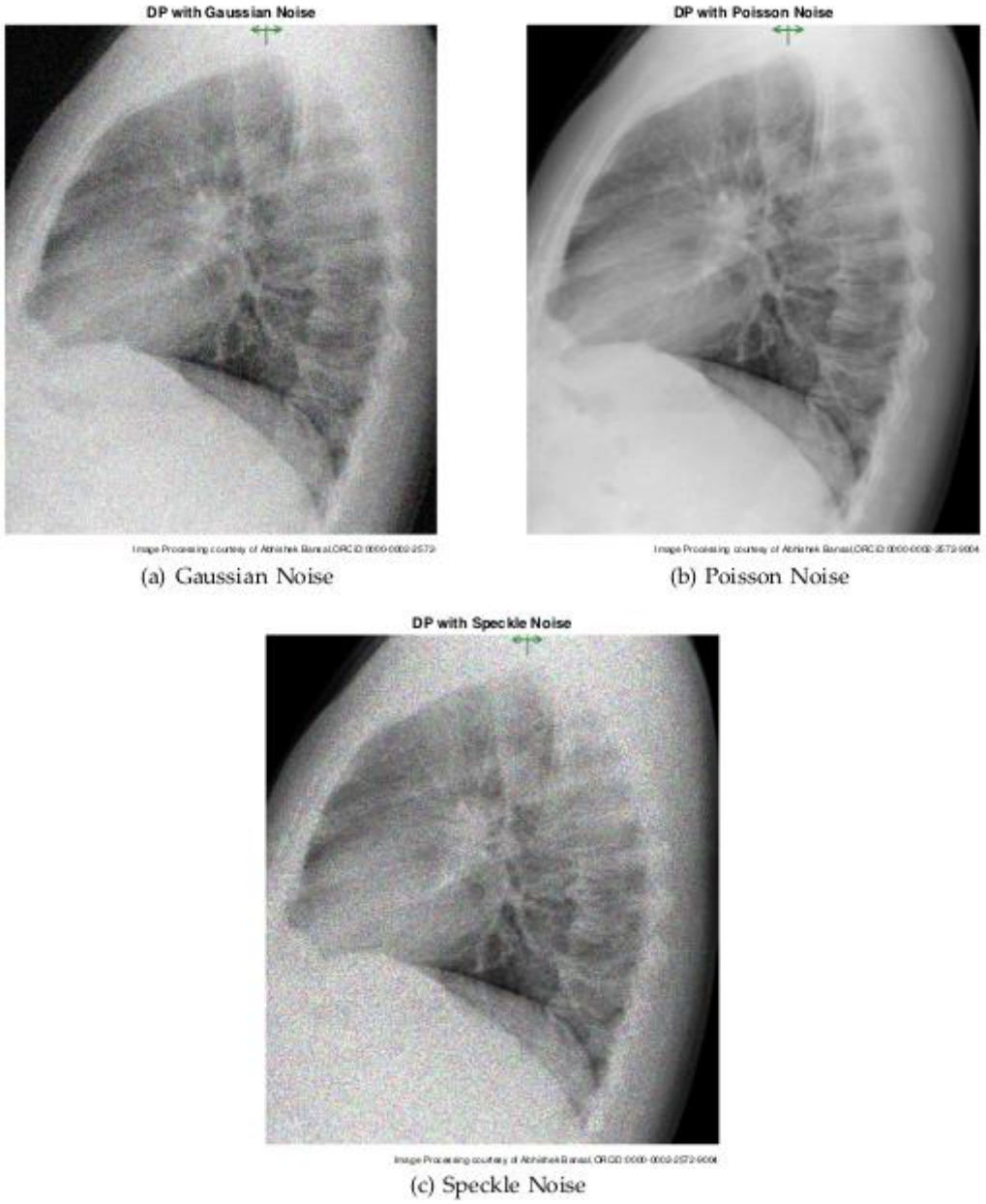


(a) Single Precision (b) Double Precision

Fig. 2: Converted to Single Precision & Double Precision

3.2. Double Precision Noise Addition

In this subsection, the double precision X-Ray of Day 0 (Fig 2(b)) of the previous subsection is subjected to noises namely Gaussian with variance 0.01, Poisson Noise and speckle noise with variance 0.05. These are shown in Fig. 3.



(a) Gaussian Noise (b) Poisson Noise

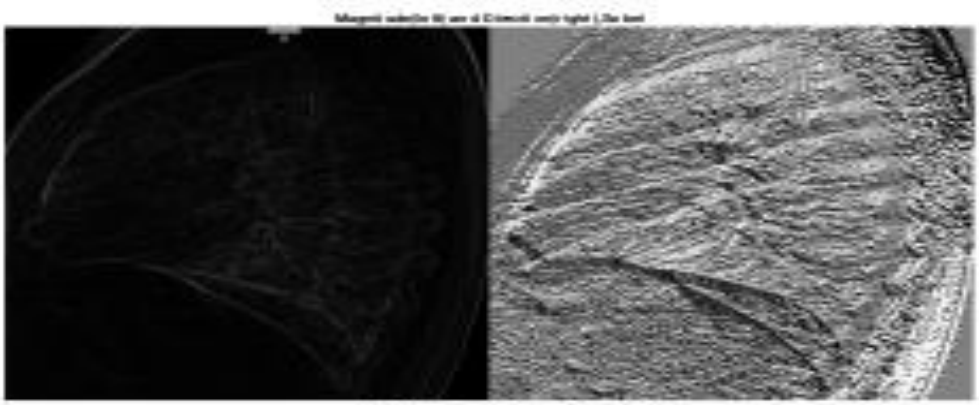
(c) Speckle Noise

Fig. 3: Noises Added to Double Precision

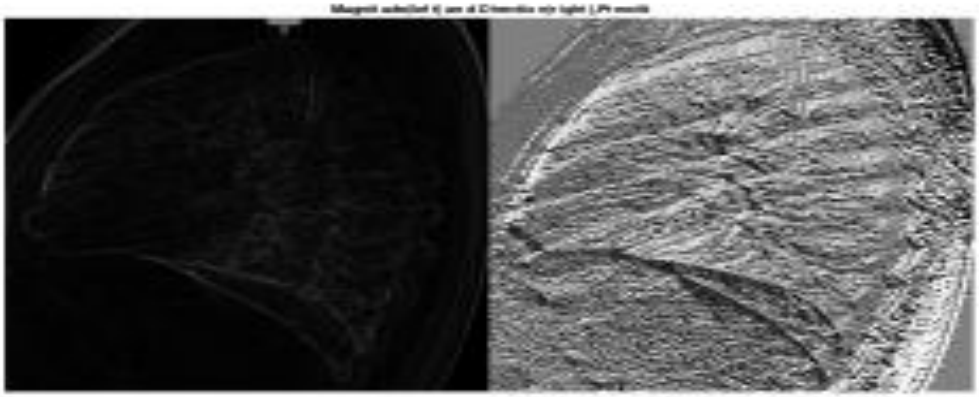
3.3. Gradient Magnitude and Direction

In this subsection, the gradient of the single precision X-Ray of Day 0 (Fig 2(a)) is obtained and its magnitude and direction is plotted using methods of Sobel, Prewitt, central difference and intermediate difference. These are shown in Fig. 4.

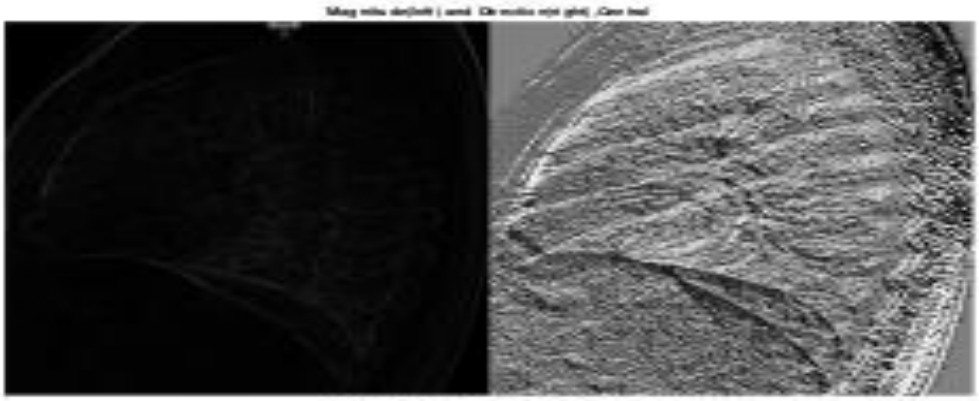
178
179
180
181



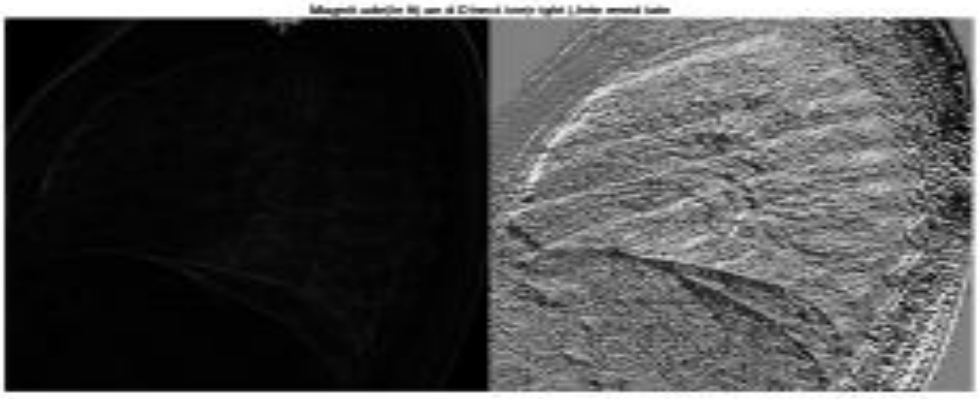
(a) Sobel Method



(b) Prewitt Method



(c) Central Difference

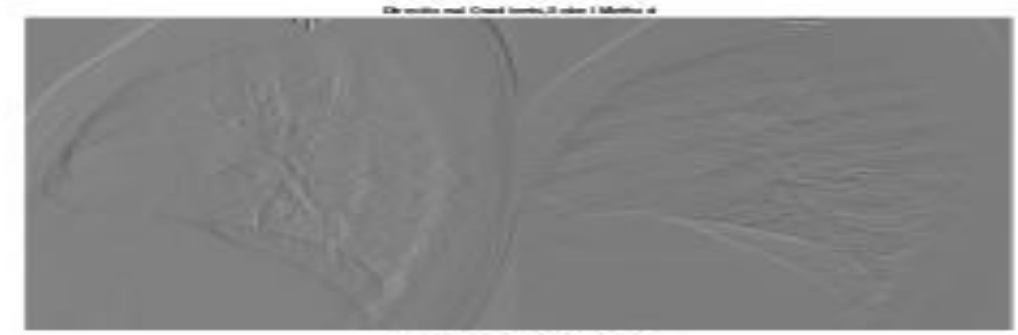


(d) Intermediate Difference

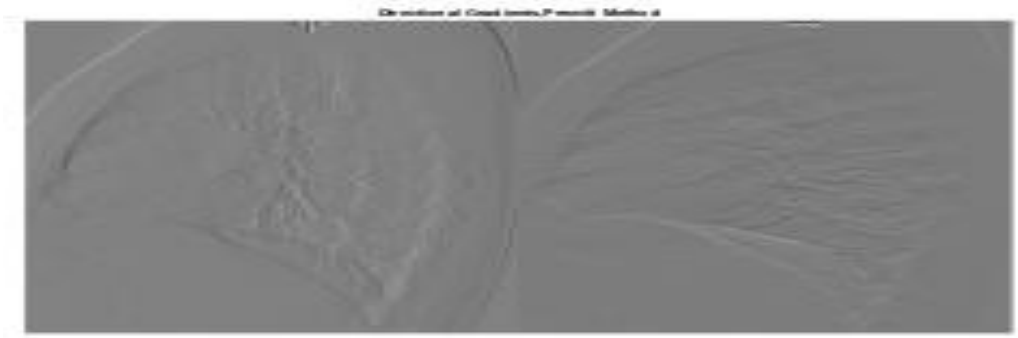
Fig. 4: X-Ray Gradient Magnitude and Direction

3.4. Directional Gradients

In this subsection, the directional gradient of the single precision X-Ray of Day 0 (Fig 2(a)) is plotted using methods of Sobel, Prewitt, central difference and intermediate difference. These are shown in Fig. 5.



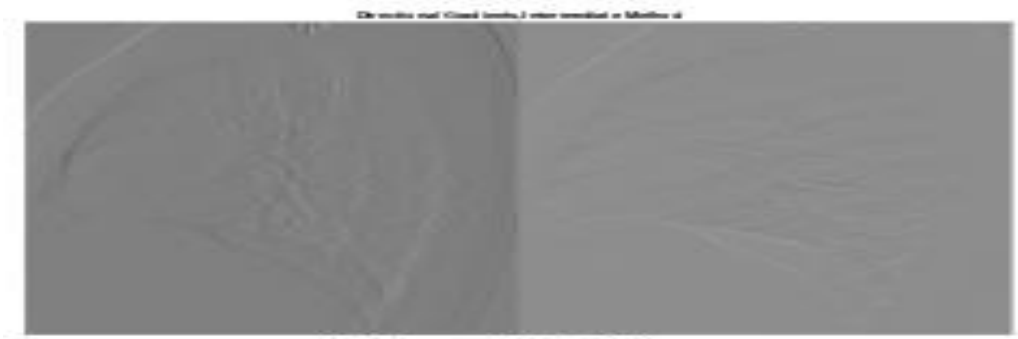
(a) Sobel Method



(b) Prewitt Method



(c) Central Difference

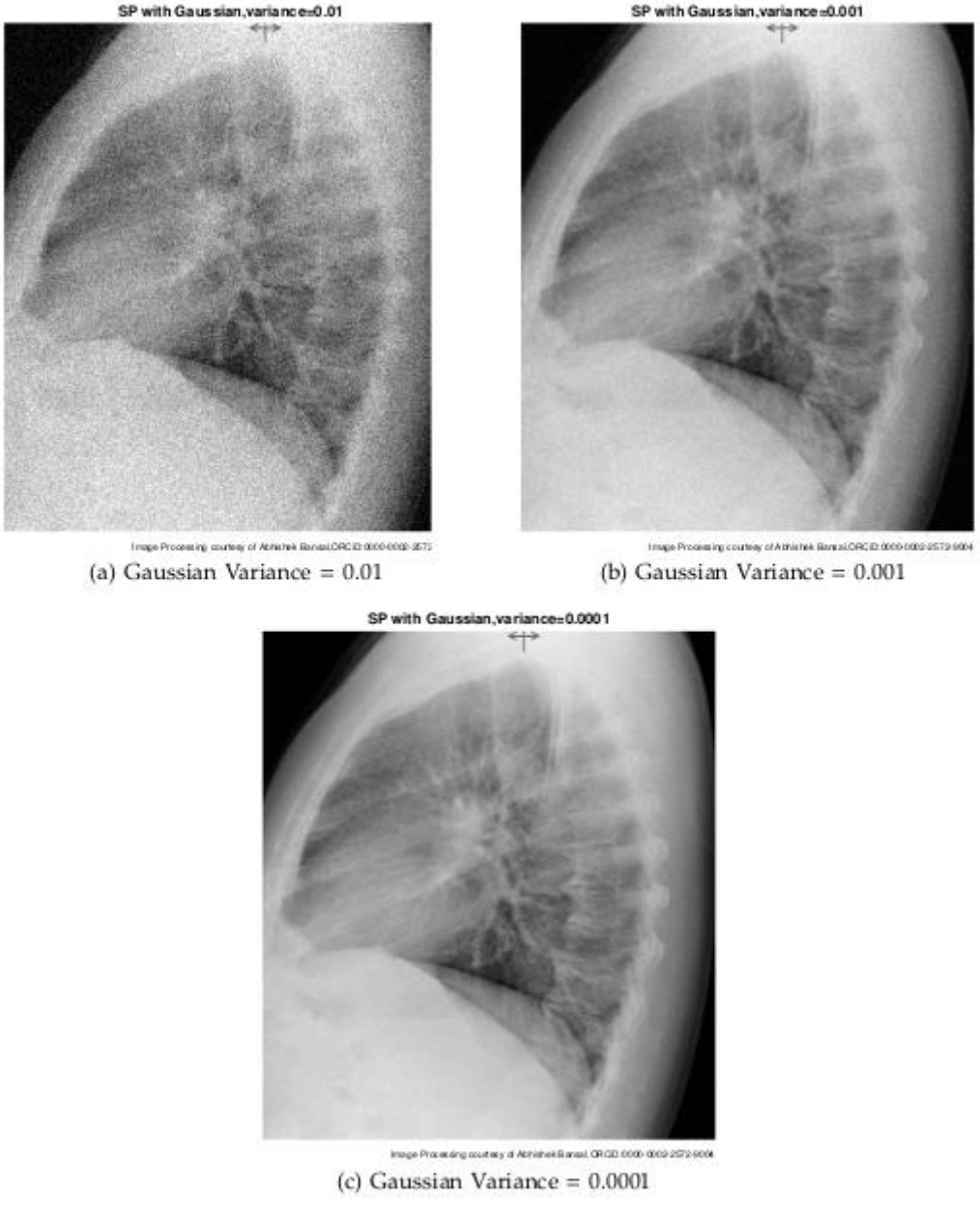


(d) Intermediate Difference

Fig. 5: Directional Gradients

3.5. Gaussian Noises & Sobel Gradient

In this subsection, the single precision X-Ray of Day 0 (Fig 2(a)) is subjected to Gaussian noise with three variances of 0.01, 0.001 and 0.0001. These are shown in Fig. 6. The gradient magnitude of these noisy X-Rays are plotted using Sobel method, which are shown in Fig. 7. The figures of gradient magnitude of Fig. 7 are further smoothed using 2-D Gaussian smoothing. The Gaussian smoothing and central difference gradient are shown in Fig. 8. The Gaussian smoothing and intermediate difference gradient are shown in Fig. 9.



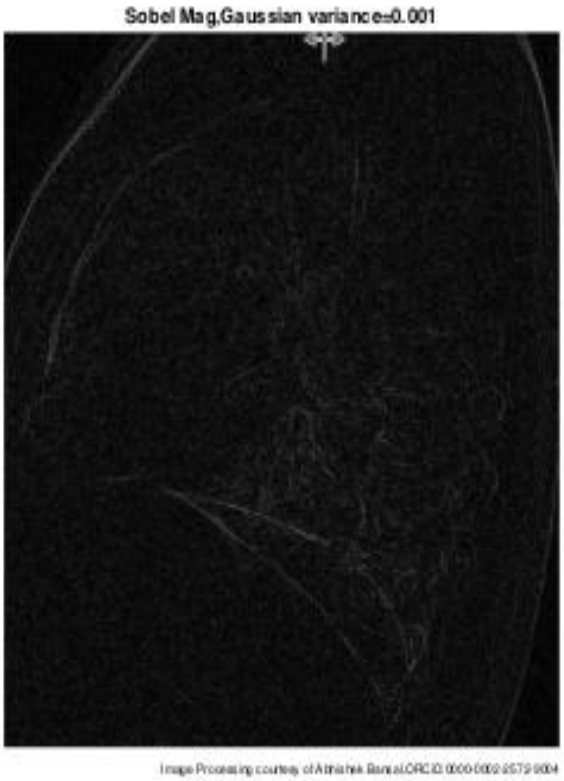
(a) Gaussian Variance = 0.01 (b) Gaussian Variance = 0.001

(c) Gaussian Variance = 0.0001

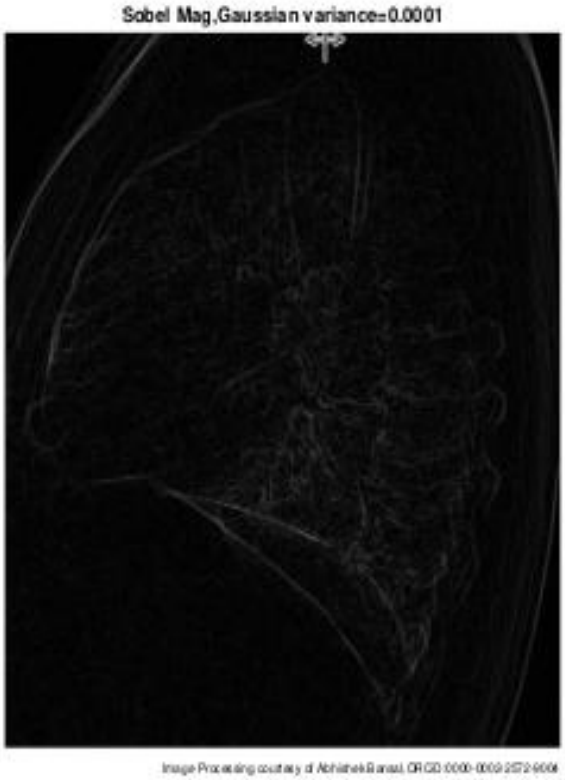
Fig. 6: Gaussian White Noise added to Image



(a) Gaussian Variance = 0.01



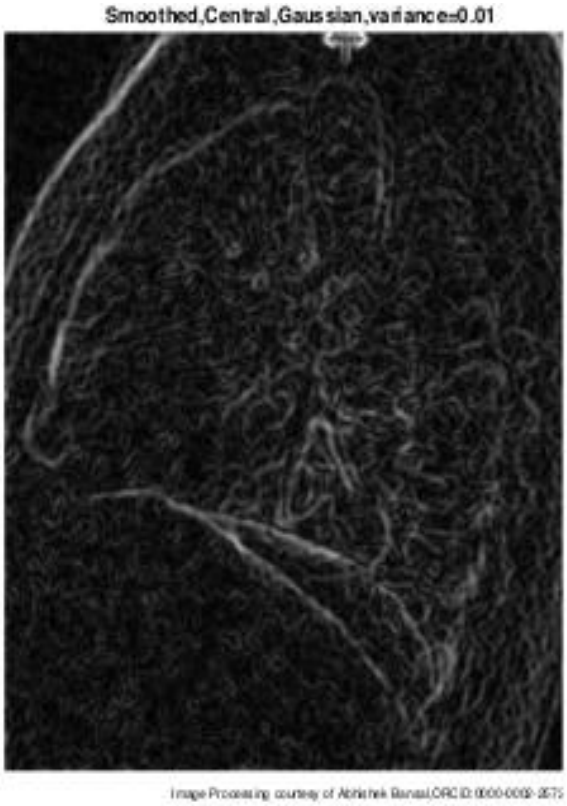
(b) Gaussian Variance = 0.001



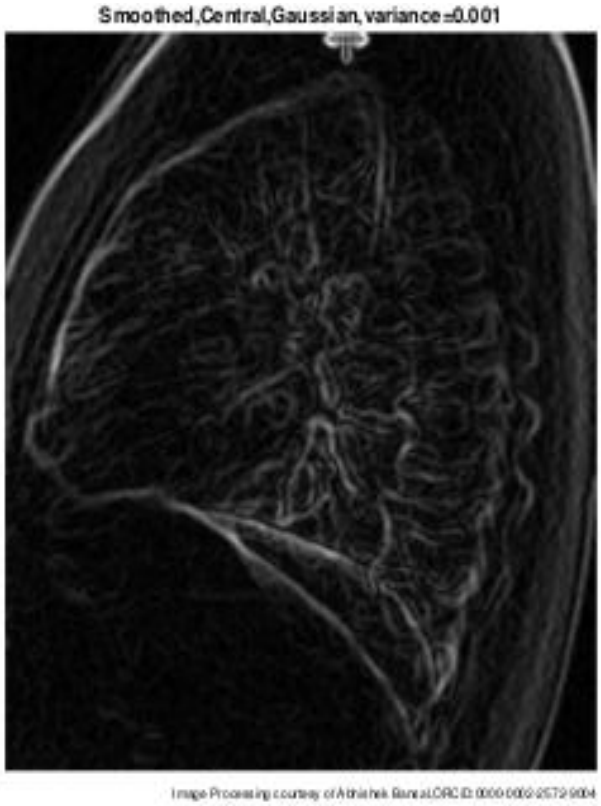
(c) Gaussian Variance = 0.0001

Fig. 7: Gradient of Noisy X-Ray using Sobel Method

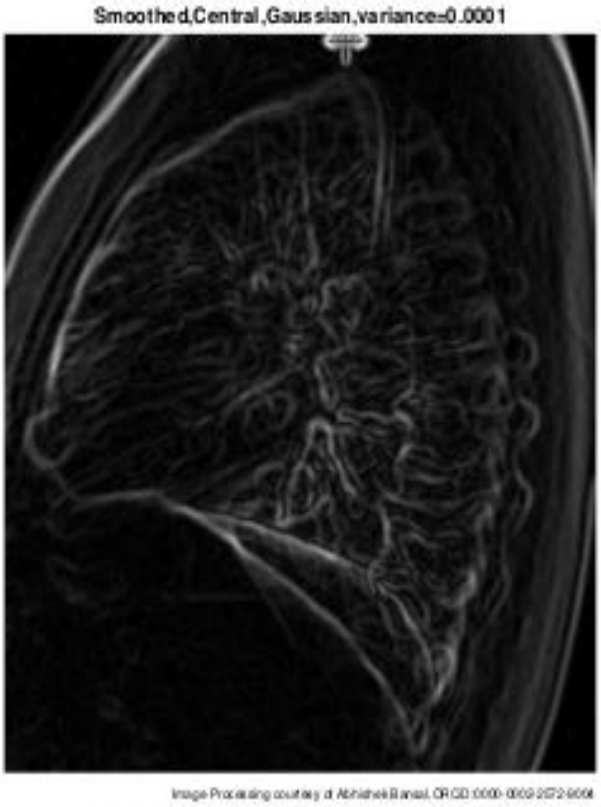
International Journal of Advanced Computing and Intelligent System (IJACIS)
Volume 1, Issue 1 (2023)
DOI: 10.66917/ijacis.a000003
https://msis-press.com/journals/ijacis



(a) Gaussian Variance = 0.01



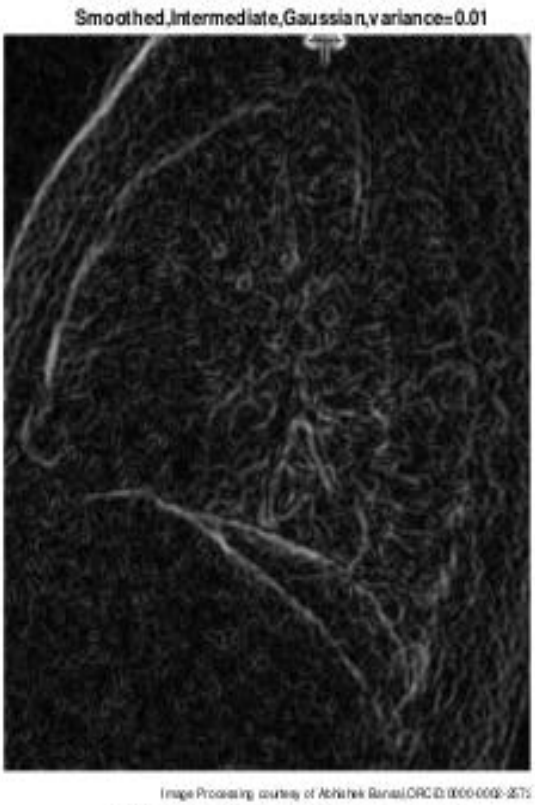
(b) Gaussian Variance = 0.001



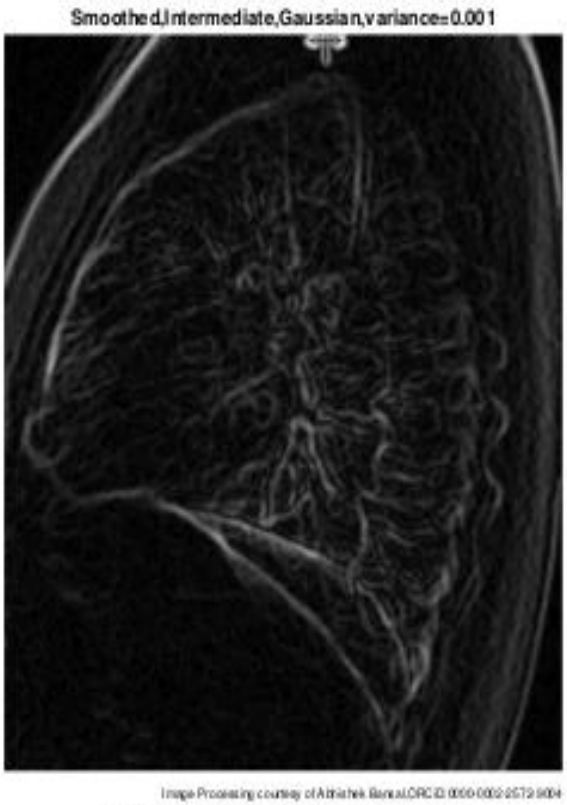
(c) Gaussian Variance = 0.0001

Fig. 8: Gaussian smoothing & central difference gradient

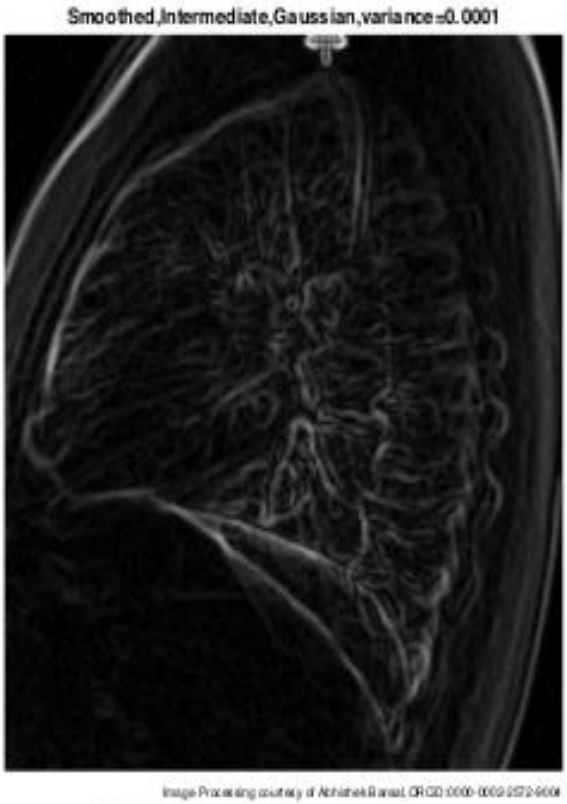
International Journal of Advanced Computing and Intelligent System (IJACIS)
Volume 1, Issue 1 (2023)
DOI: 10.66917/ijacis.a000003
https://msis-press.com/journals/ijacis



(a) Gaussian Variance = 0.01



(b) Gaussian Variance = 0.001



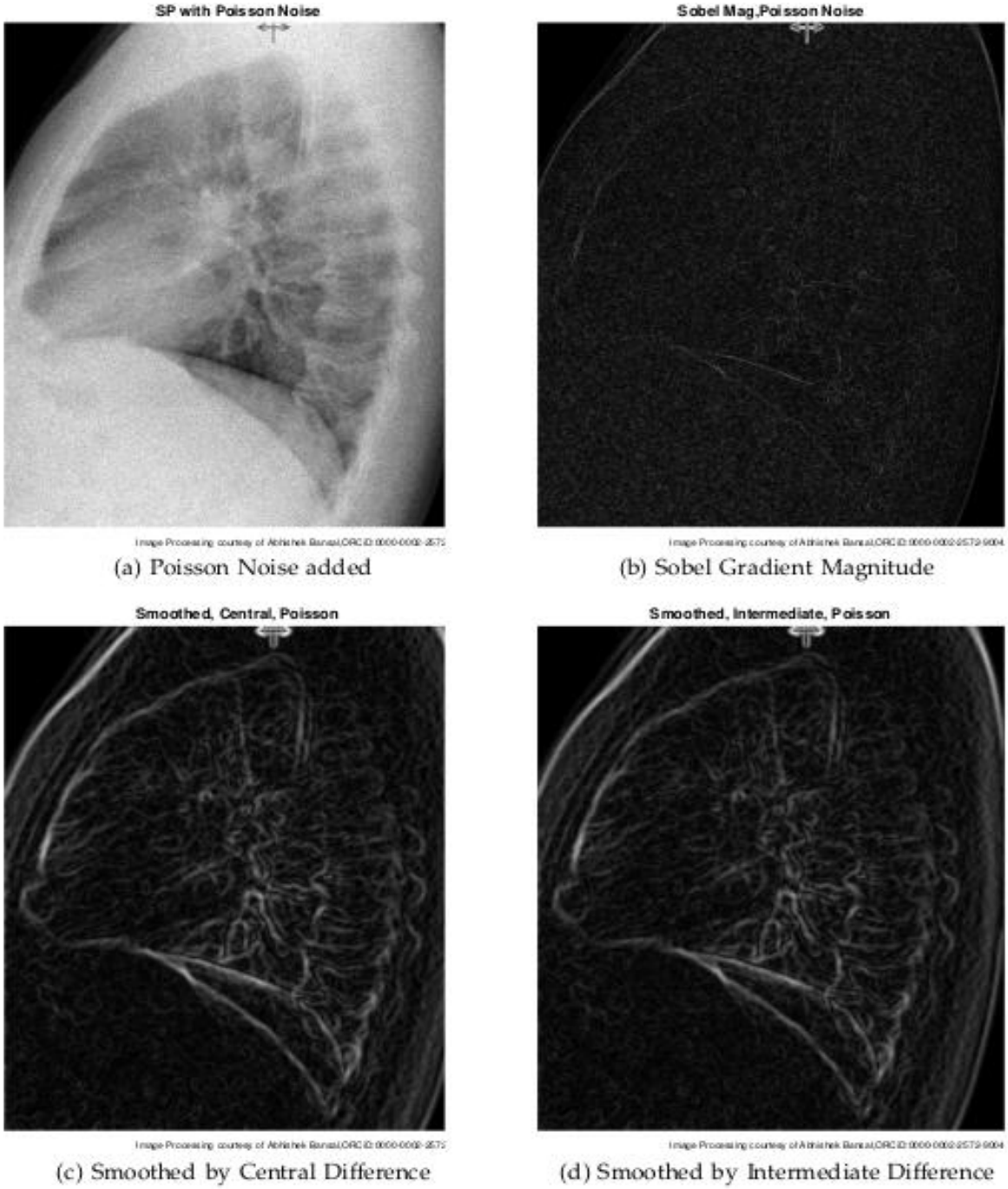
(c) Gaussian Variance = 0.0001

Fig. 9: Gaussian smoothing & intermediate difference gradient

International Journal of Advanced Computing and Intelligent System (IJACIS)
Volume 1, Issue 1 (2023)
DOI: 10.66917/ijacis.a000003
https://msis-press.com/journals/ijacis

3.6. Poisson Noise & Sobel Gradient

In this subsection, the single precision X-Ray of Day 0 (Fig 2(a)) is subjected to Poisson Noise,Fig. 10(a). The gradient magnitude of Poisson noise X-Ray is plotted using Sobel method, which are shown in Fig. 10(b). This is further smoothed using 2-D Gaussian smoothing and central difference gradient in Fig. 10(c); and 2-D Gaussian smoothing and intermediate difference gradient in Fig. 10(d).



(a) Poisson Noise added

(b) Sobel Gradient Magnitude

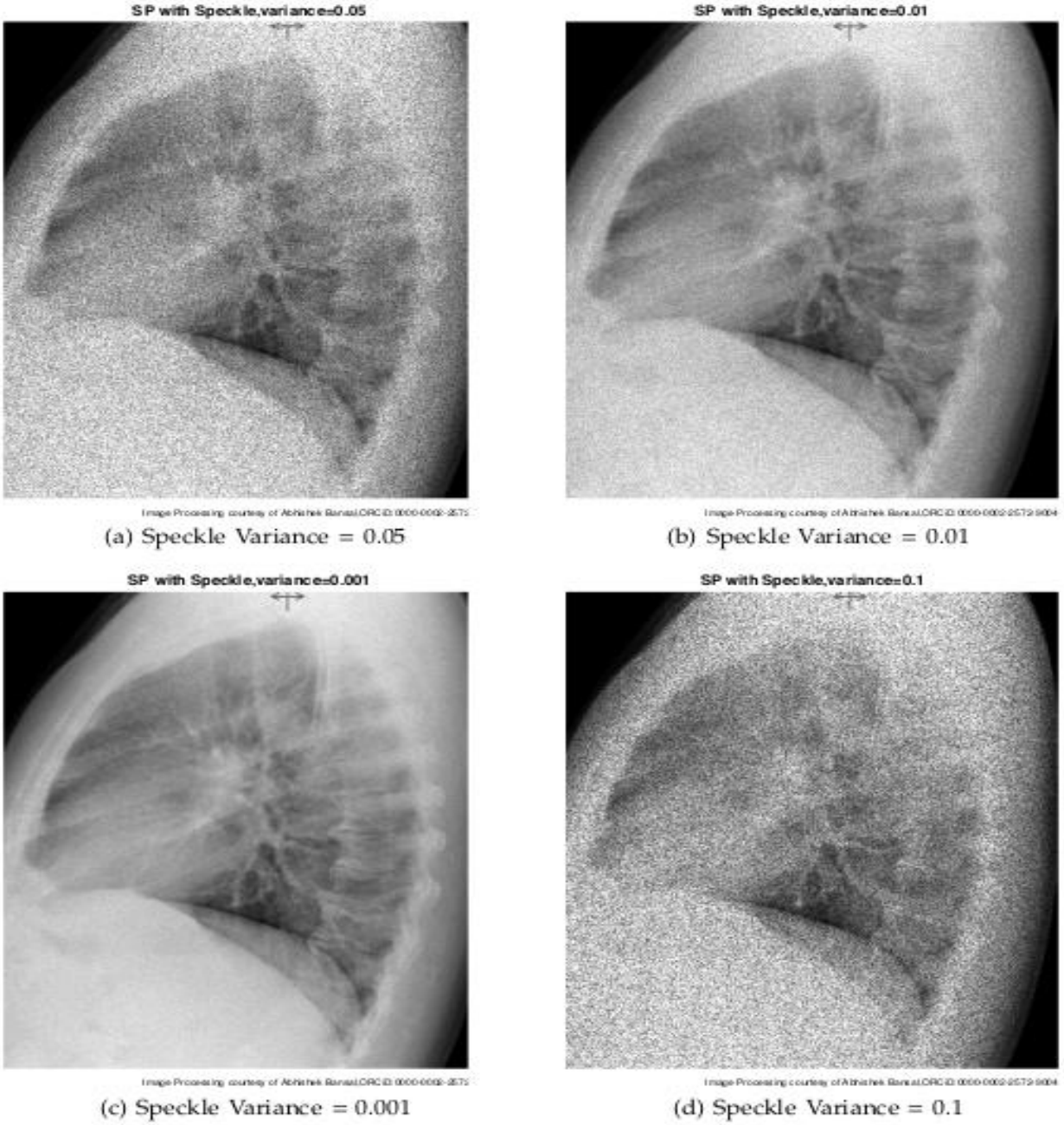
(c) Smoothed by Central Difference

(d) Smoothed by Intermediate Difference

Fig. 10: Poisson Noise & Gradient Magnitude

3.7. Speckle Noise & Sobel Gradient

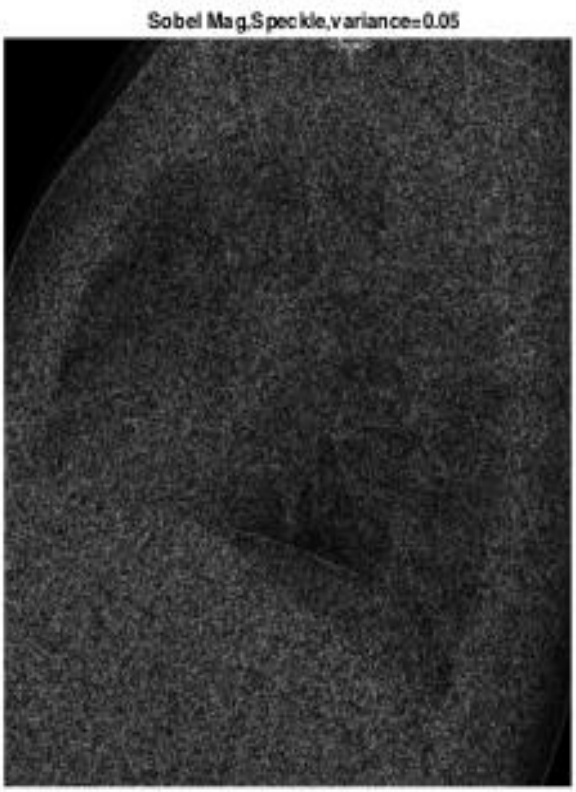
In this subsection, the single precision X-Ray of Day 0 (Fig 2(a)) is subjected to Speckle noise with four variances of 0.05, 0.01, 0.001 and 0.1. These are shown in Fig. 11[a-d]. The gradient magnitude of these noisy X-Rays are plotted using Sobel method, which are shown in Fig. 12. These are further smoothed using 2-D Gaussian smoothing. The Gaussian smoothing and central difference gradient are shown in Fig. 13. The Gaussian smoothing and intermediate difference gradient are shown in Fig. 14.



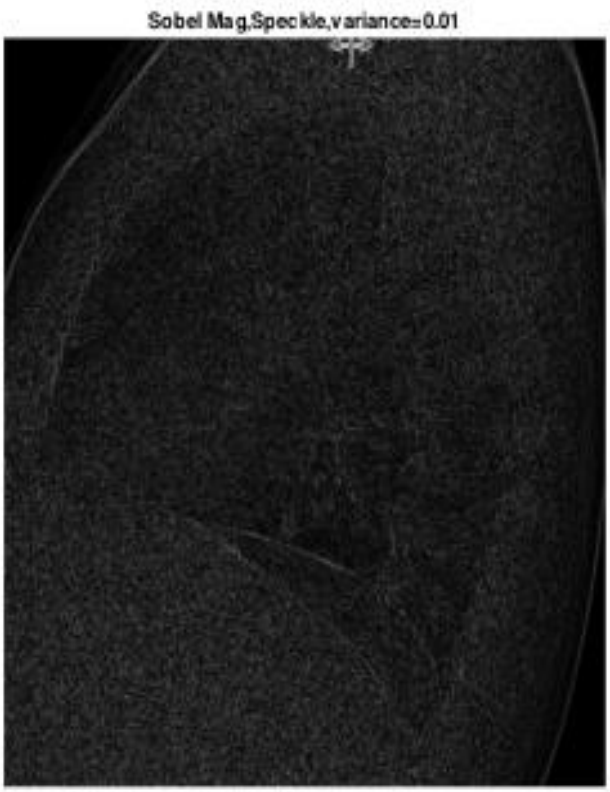
(a) Speckle Variance = 0.05 (b) Speckle Variance = 0.01

(c) Speckle Variance = 0.001 (d) Speckle Variance = 0.1

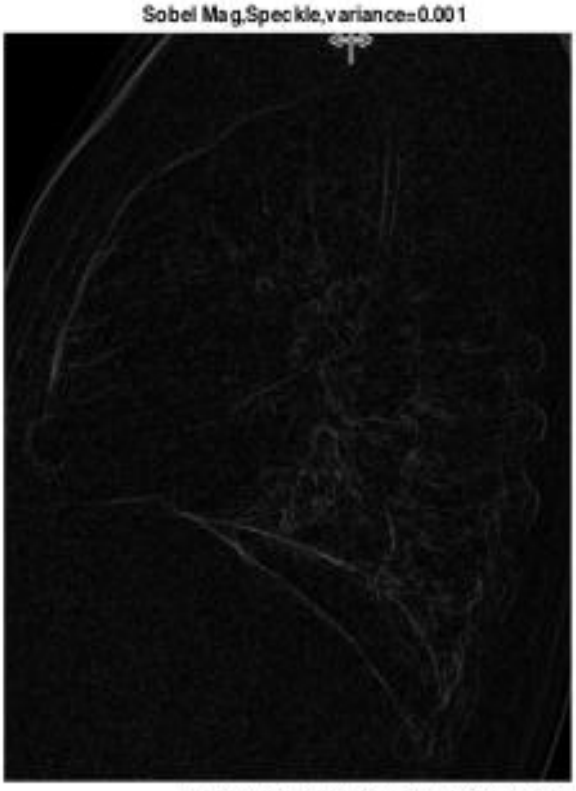
Fig. 11: Speckle Noise added to Image



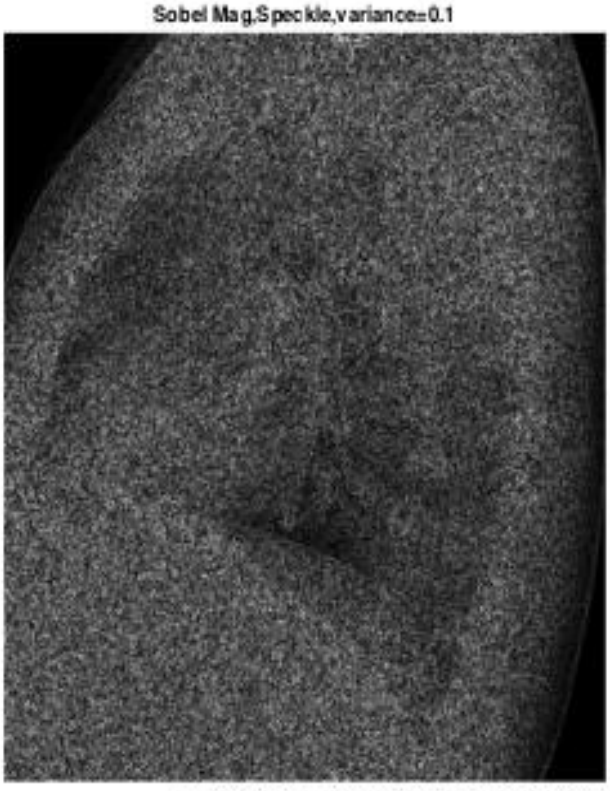
(a) Speckle Variance = 0.05



(b) Speckle Variance = 0.01



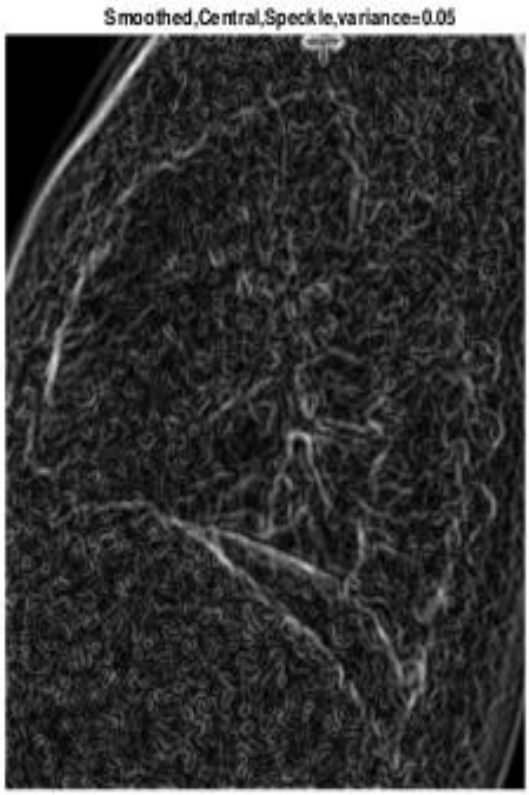
(c) Speckle Variance = 0.001



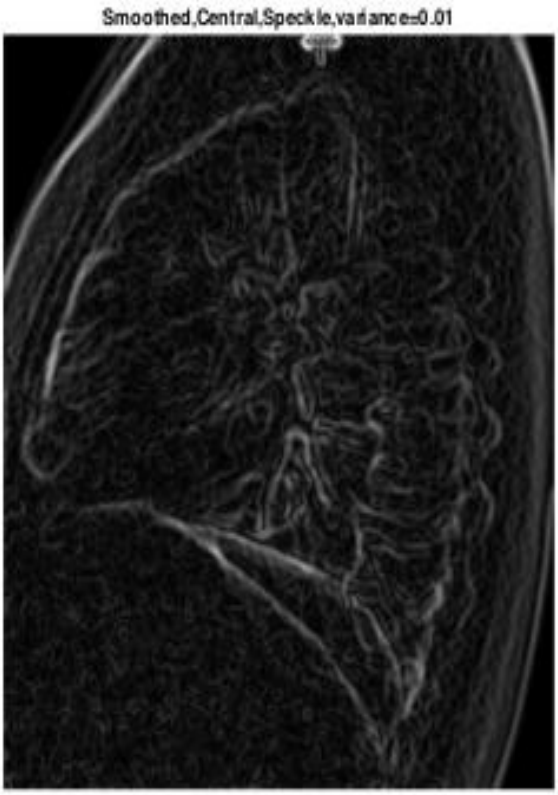
(d) Speckle Variance = 0.1

Fig. 12: Gradient of Noisy X-Ray using Sobel Method

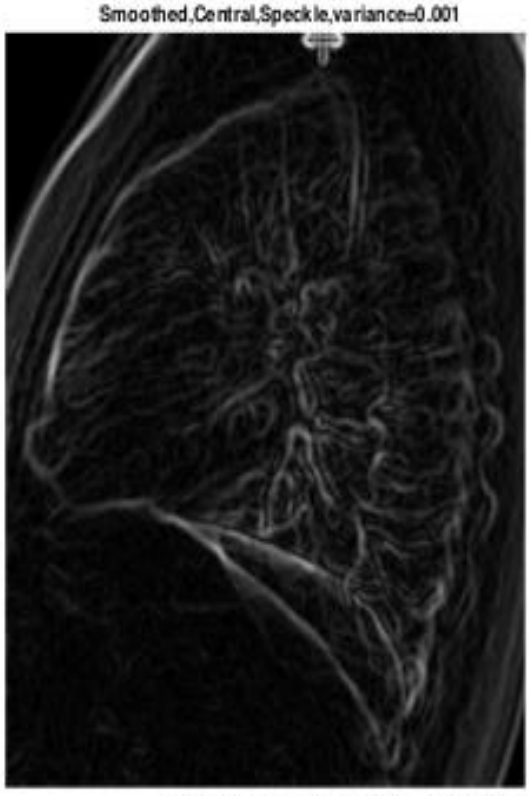
International Journal of Advanced Computing and Intelligent System (IJACIS)
Volume 1, Issue 1 (2023)
DOI: 10.66917/ijacis.a000003
https://msis-press.com/journals/ijacis



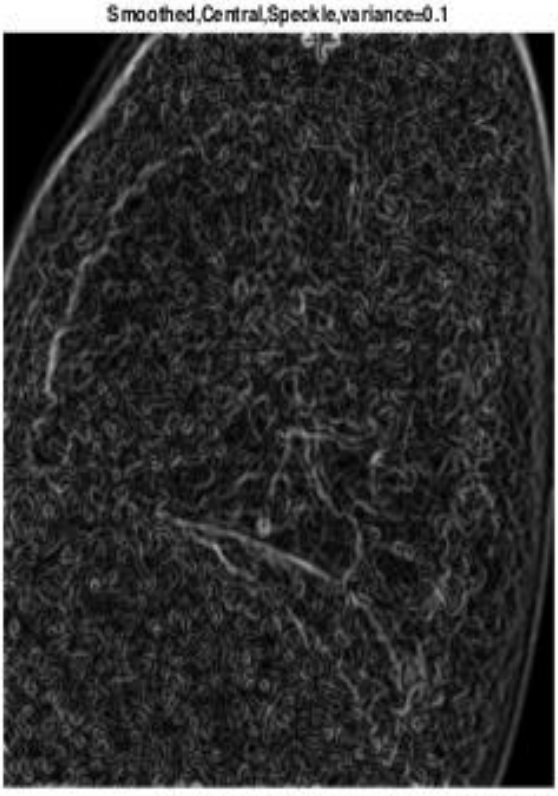
(a) Speckle Variance = 0.05



(b) Speckle Variance = 0.01



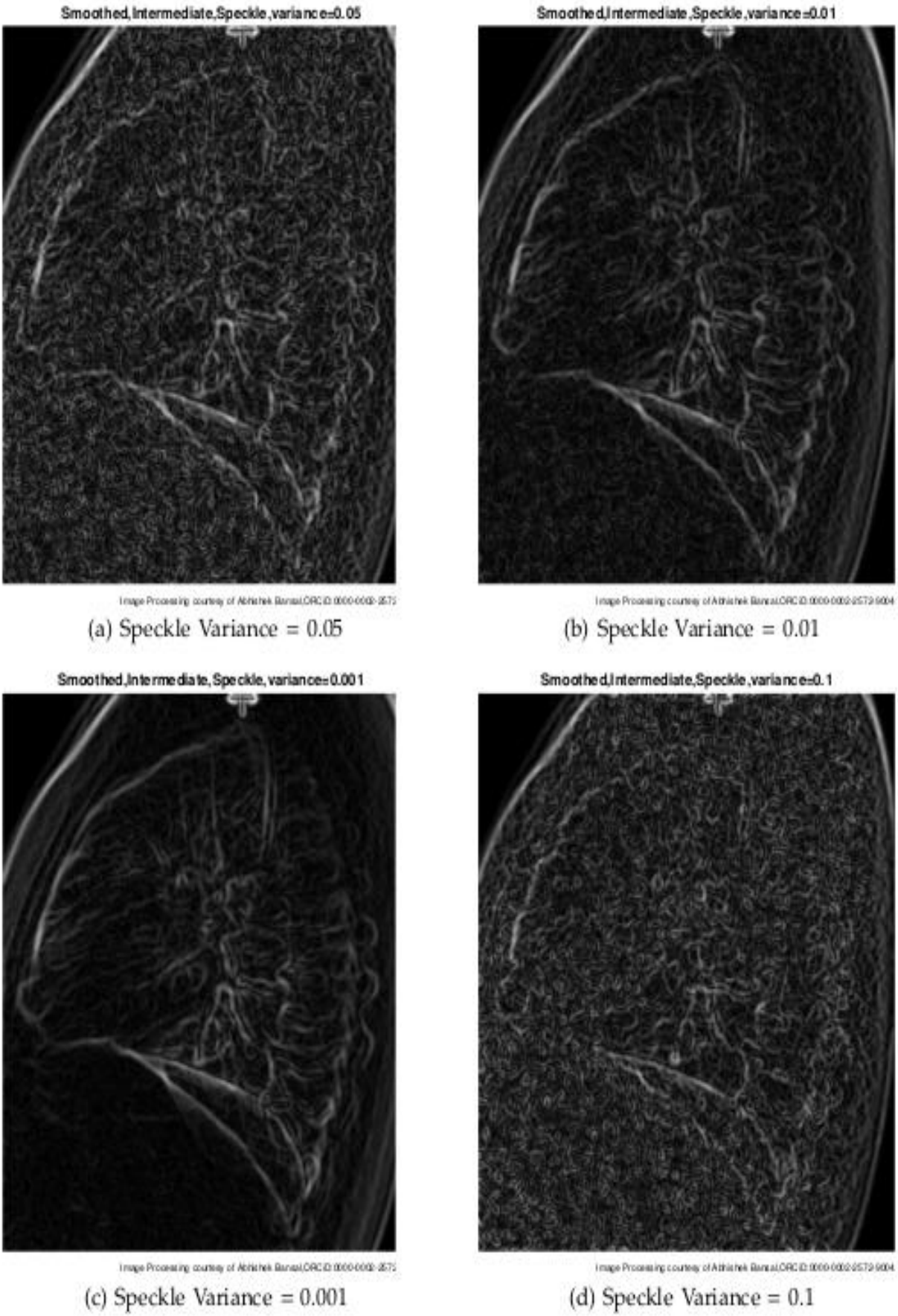
(c) Speckle Variance = 0.001



(d) Speckle Variance = 0.1

Fig. 13: Gaussian smoothing & central difference gradient

International Journal of Advanced Computing and Intelligent System (IJACIS)
Volume 1, Issue 1 (2023)
DOI: 10.66917/ijacis.a000003
https://msis-press.com/journals/ijacis



(a) Speckle Variance = 0.05 (b) Speckle Variance = 0.01

(c) Speckle Variance = 0.001 (d) Speckle Variance = 0.1

Fig. 14: Gaussian smoothing & intermediate difference gradient

International Journal of Advanced Computing and Intelligent System (IJACIS)
Volume 1, Issue 1 (2023)
DOI: 10.66917/ijacis.a000003
https://msis-press.com/journals/ijacis

3.8. Pixel Intensities & Contrast

In this subsection, the original X-Ray (without converting to single precision or double precision) is contrasted for study and analysis.

Let the center fit

$$z = \frac{(x - 127.5)}{74.05}$$

then from polynomial regression

$$y = -1049 \times z^9 + 2661 \times z^8 + 6199 \times z^7 - 1.429 \times 10^4 \times z^6 - 1.22 \times 10^4 \times z^5 + 2.406 \times 10^4 \times z^4 + 7439 \times z^3 - 1.476 \times 10^4 \times z^2 + 1640 \times z + 5288$$

Let $\bar{y}$ be the mean of y, $\hat{y}$ the calculated values of y, then the coefficient of determination, R^2

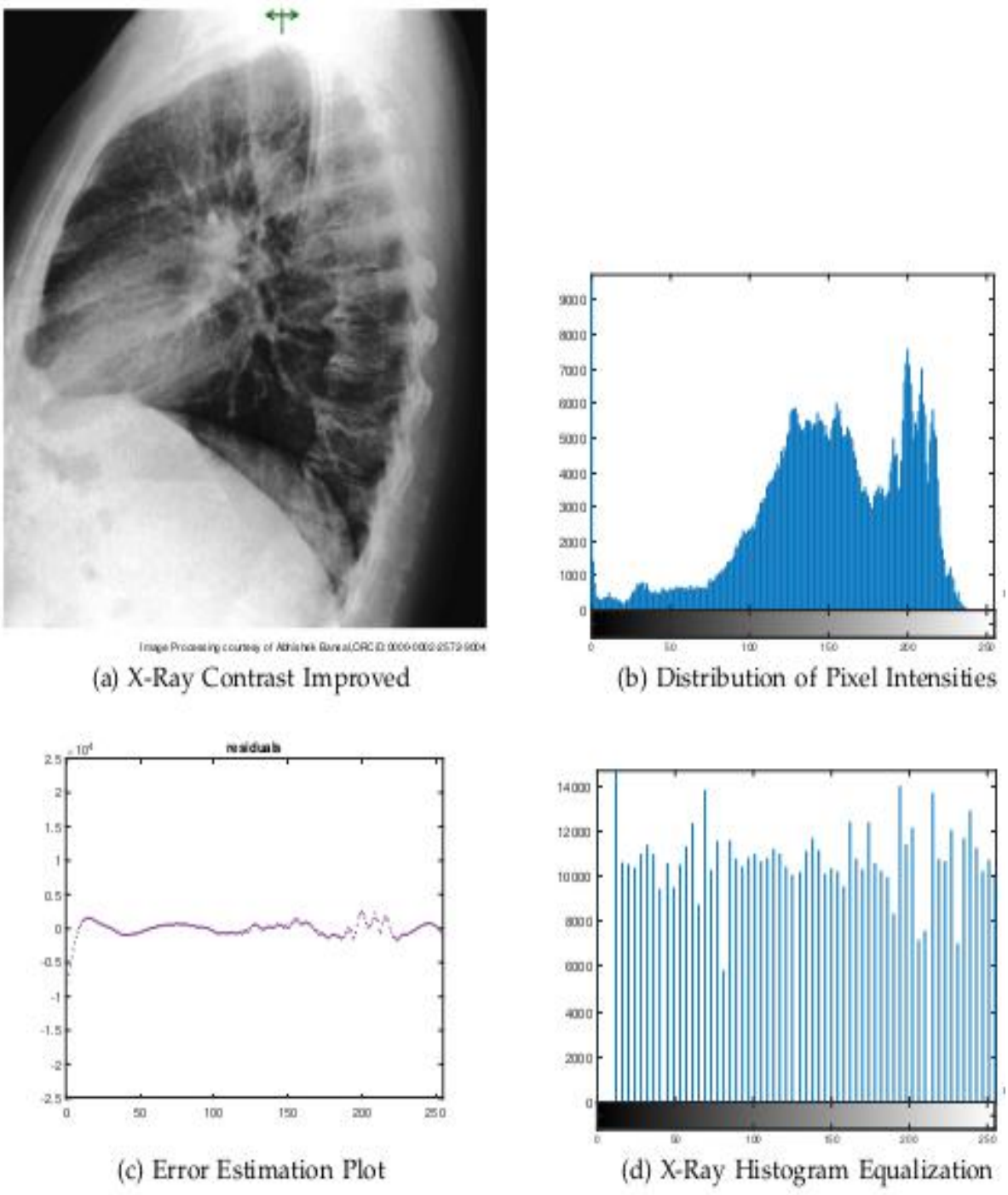
$$R^2 = 1 - \frac{\sum_{\iota=1}^{n}(y_i - \hat{y})^2}{\sum_{\iota=1}^{n}(y_i - \bar{y})^2} = 0.6302$$

The measure of the goodness of fit given by norm of residuals is 2.758 × 104 . Here, the polynomial of degree 9 chosen here is the global which can be focused on the areas of interest (to be decided by infection part or researchers/doctors interest) and separate equations can be obtained for each particular area of interest. This gives insight in mathematical formulation and has been used in the Novel B-Mathematical Modeling of Respiratory System.

TABLE I: Data Statistics for Fig. 15(b)

	X	Y
min	0	0
max	255	3.214×10^4
mean	127.5	2668
median	127.5	2082
mode	0	300
std deviation	74.05	2840
range	255	3.214×10^4

The Fig.15(a) shows that X-Ray contrast is improved for analysis when compared with Fig. 1(a). Fig. 15(b) shows the distribution of X-Ray pixel intensities. Fig. 15(c) shows the error estimation plot, which is the plot of the residuals. Fig. 15(d) shows the X-Ray histogram equalization which is the spreading of the intensity values over the full range.



(a) X-Ray Contrast Improved

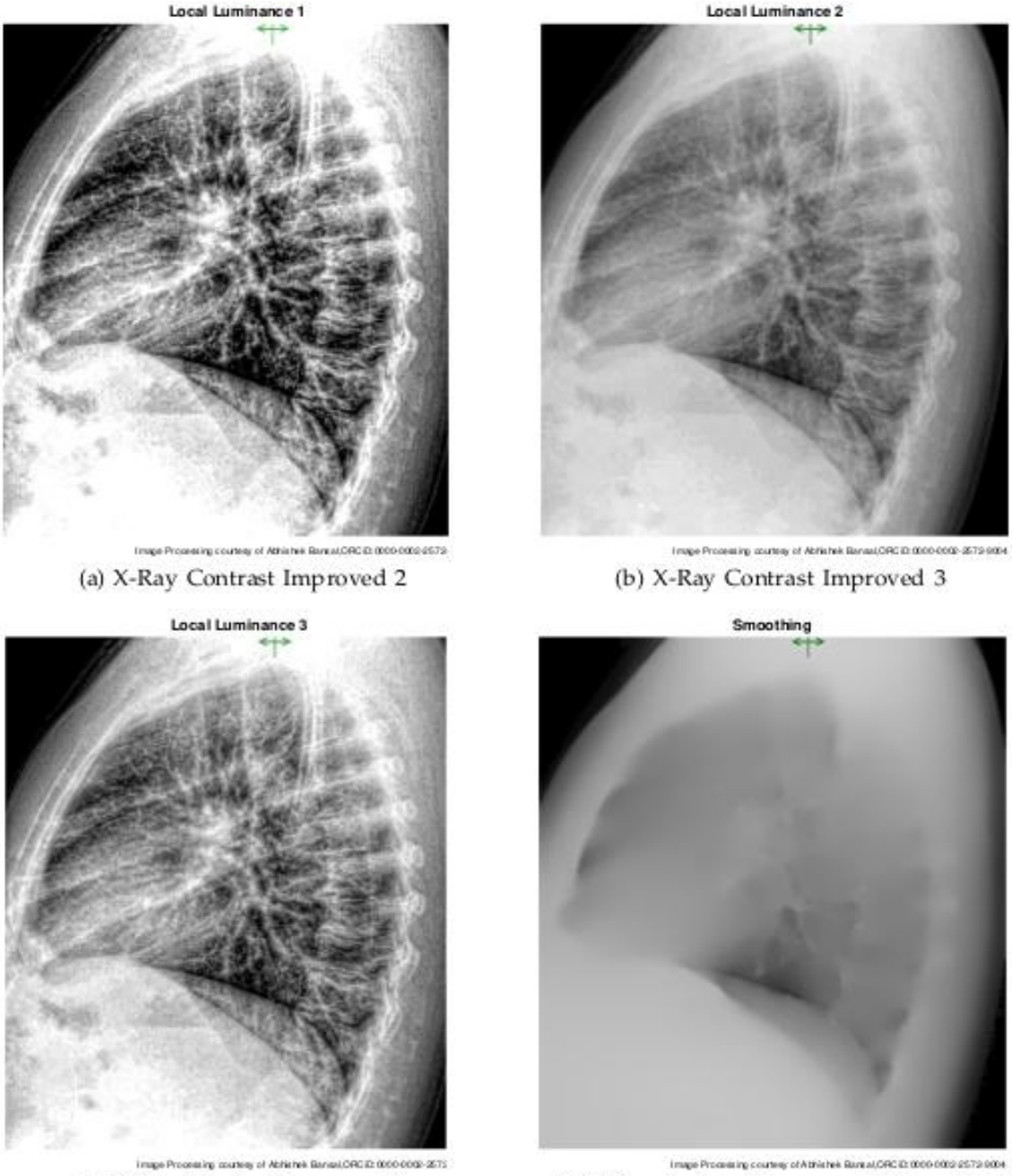
(b) Distribution of Pixel Intensities

(c) Error Estimation Plot

(d) X-Ray Histogram Equalization

Fig. 15: Distribution of Pixel Intensities in X-Ray

In Fig. 16, X-Ray Contrast is improved with five local luminances. The original Fig. 2(a) X-Ray contrast is improved with four more local luminances by varying the intensity values at low and high intensities. These are shown in Fig 16(a), Fig. 16(b) and Fig. 16(c). In Fig. 16(d), the original Fig. 2(a) X-Ray is contrasted with fifth value of improvement but smoothing technique is applied after it.



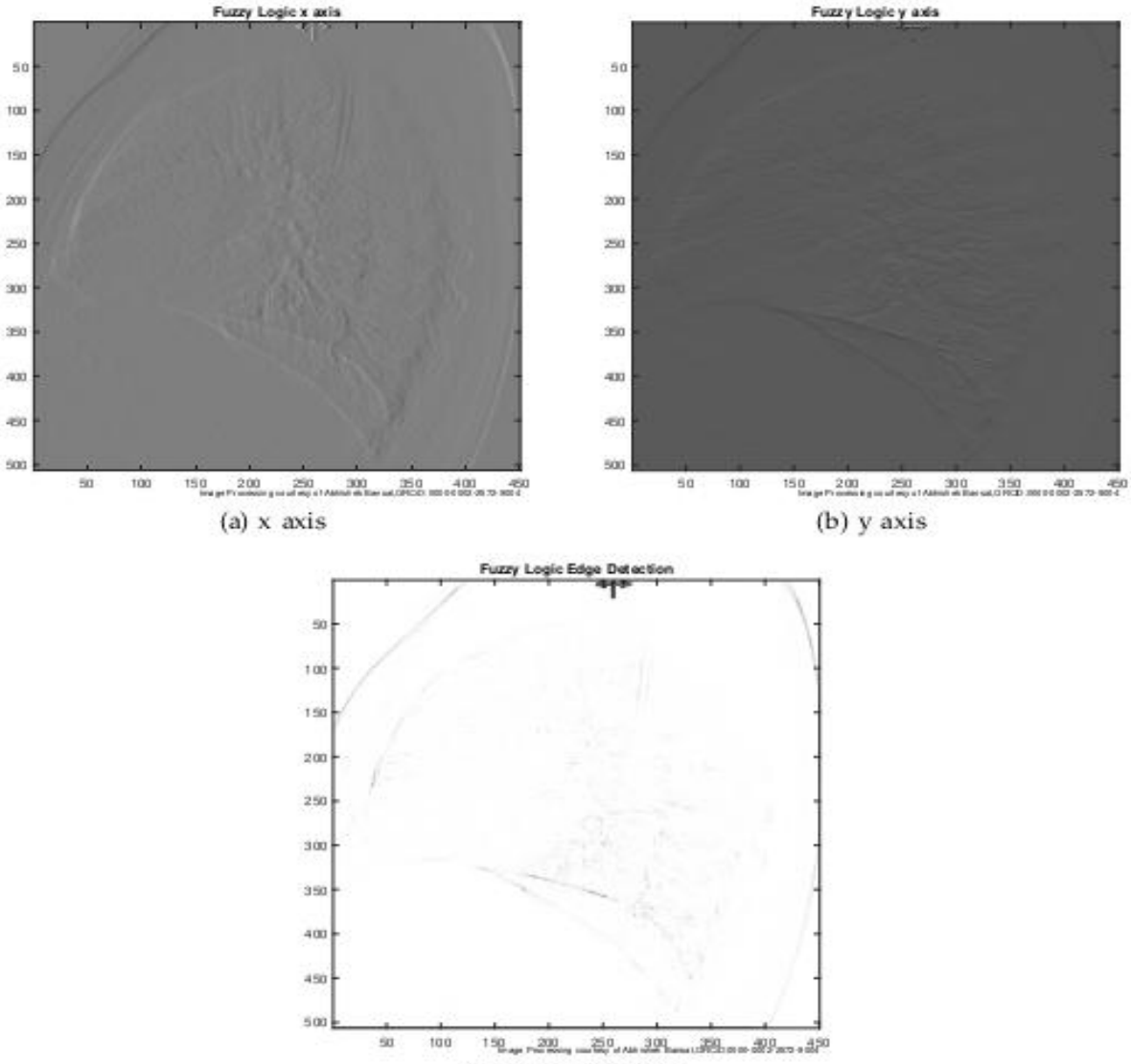
(a) X-Ray Contrast Improved 2 (b) X-Ray Contrast Improved 3

(c) X-Ray Contrast Improved 4 (d) X-Ray Contrast Improved & Smoothed

Fig. 16: X-Ray Contrast Improved with Five Local Luminances

3.9. Fuzzy Logic

In this subsection, the images obtained using fuzzy logic edge-detection algorithm and Fuzzy Inference System (FIS) are given. Two 2-D Convolution are performed. The x-axis of directional gradient is convolved with x-axis gradients of double-precision X-Ray obtained in Fig. 2(b) and the X-Ray gradient of fuzzy logic x-axis is given in Fig. 17(a). The y-axis of directional gradient is convolved with y-axis gradients of double-precision X-Ray obtained in Fig. 2(b) and the X-Ray gradient of fuzzy logic y-axis is given in Fig. 17(b). The edge detection is shown in Fig. 17(c).



(a) x axis

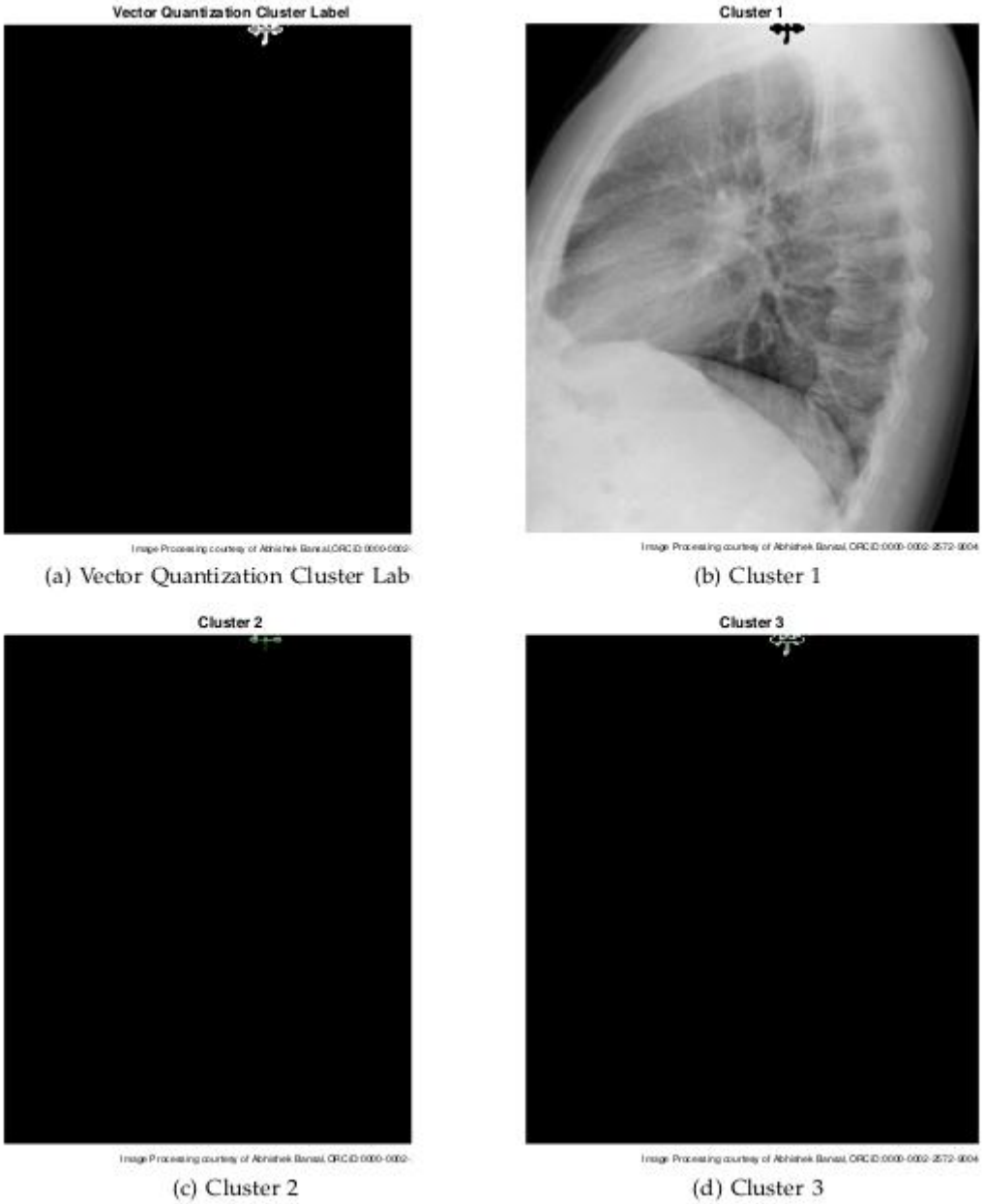
(b) y axis

(c) Edge Detection

Fig. 17: Fuzzy Logic

3.10. K-means Clustering

In this subsection, the popular vector quantization technique of K-Means clustering is applied to X-Ray. In this technique, firstly CIE XYZ tristimulus technique is used to know the color information and thus, the information of luminosity layer 'L*', chromaticity-layer 'a*' and chromaticity-layer 'b*' is obtained. Then every pixel is clustered with its pixel label and partitioned into three clusters. The clustering obtained is shown in Fig. 18(a), Vector Quantization Cluster Label. And three clusters Cluster 1, Cluster 2 and Cluster 3 obtained are shown in Fig. 18(b), Fig. 18(c) and Fig. 18(d) respectively.

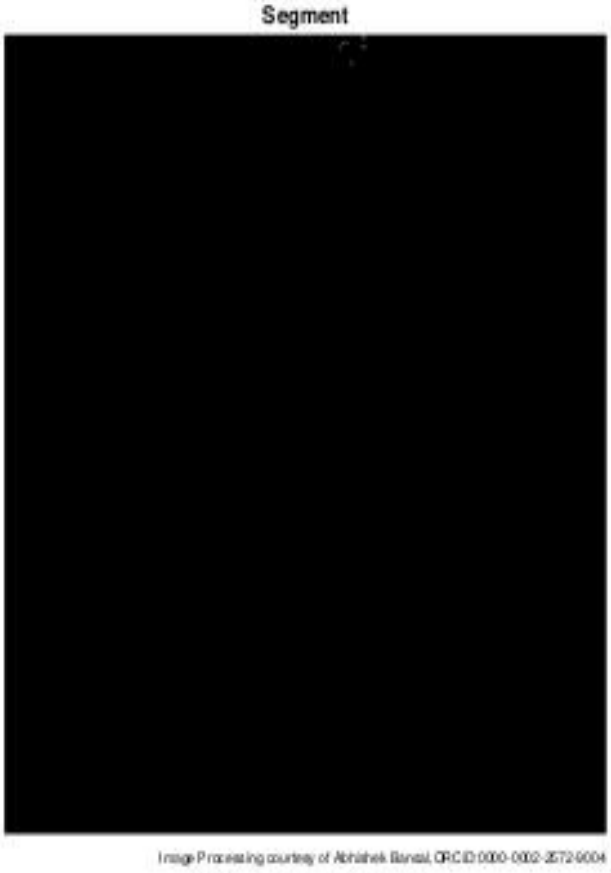


(a) Vector Quantization Cluster Lab (b) Cluster 1

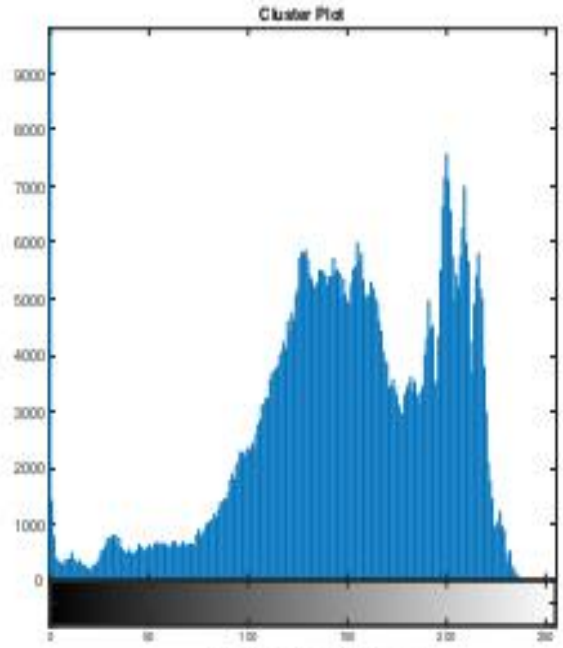
(c) Cluster 2 (d) Cluster 3

Fig. 18: Vector Quantization,K-means Clustering

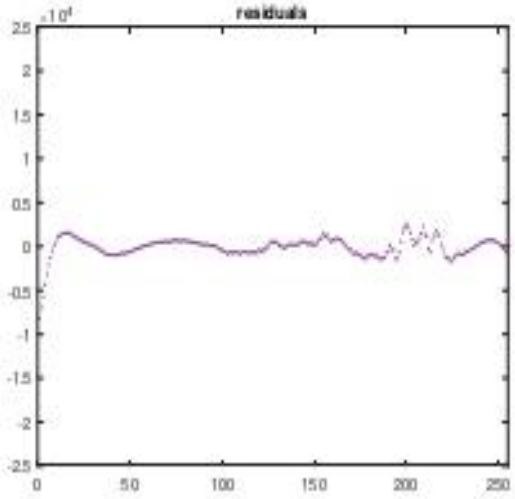
In Fig. 19(a), segmentation is applied and Fig. 19(b) and Fig. 19(c) shows respectively the cluster plot and the plot of error estimation, that is, the plot of residuals.



(a) Segmentation



(b) Cluster Plot



(c) Cluster Plot Residuals

Fig. 19: Clustering Plot and Segment

Moving in similar way as in the Subsection-8 and choosing same

$$z = \frac{(x - 127.5)}{74.05}$$

we have

$$y = -1091 \times z^9 + 2695 \times z^8 + 6434 \times z^7 - 1.445 \times 10^4 \times z^6 - 1.263 \times 10^4 \times z^5 + 2.43 \times 10^4 \times z^4 + 7715 \times z^3 - 1.487 \times 10^4 \times z^2 + 1595 \times z + 5292$$

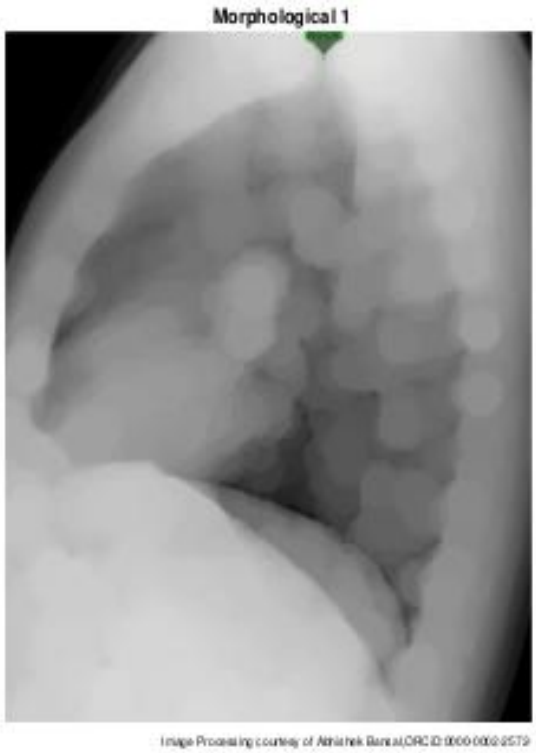
$R^2 = 0.6213$, and Norm of Residuals = 2.828×10^4

TABLE II: Data Statistics for Fig. 18(b)

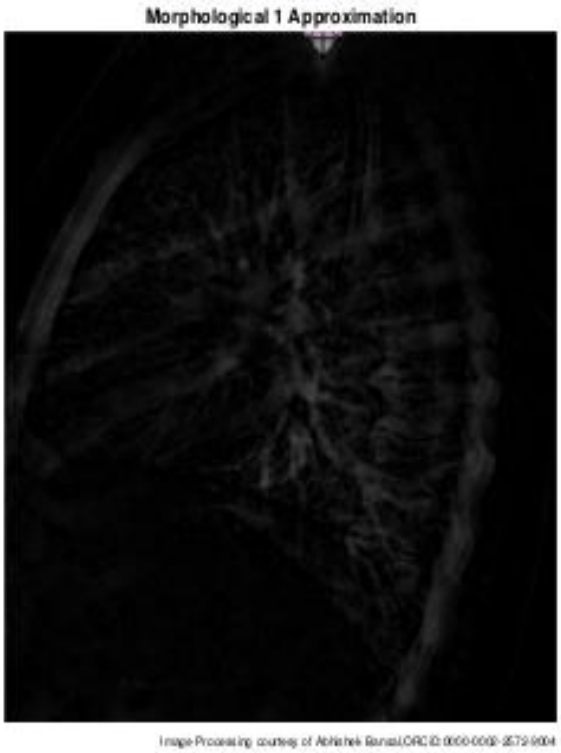
	X	Y
min	0	0
max	255	3.308×10^4
mean	127.5	2668
median	127.5	2075
mode	0	0
std deviation	74.05	2878
range	255	3.308×10^4

3.11. Morphological Segmentation

In this subsection, known morphological segmentation technique is applied on X-Rays. Three morphological openings are used. The morphological opening with structuring element of disk shaped with three different radius are shown in Fig. 20(a), Fig. 20(c) and Fig. 21(a). The background approximation images of X-Ray obtained after subtracting from the original image are shown in Fig. 20(b), Fig. 20(d) and Fig. 21(b).



(a) Morphological Opening 1



(b) Background Approximation Removed from Fig. 19(a)



(c) [Morphological Opening 2

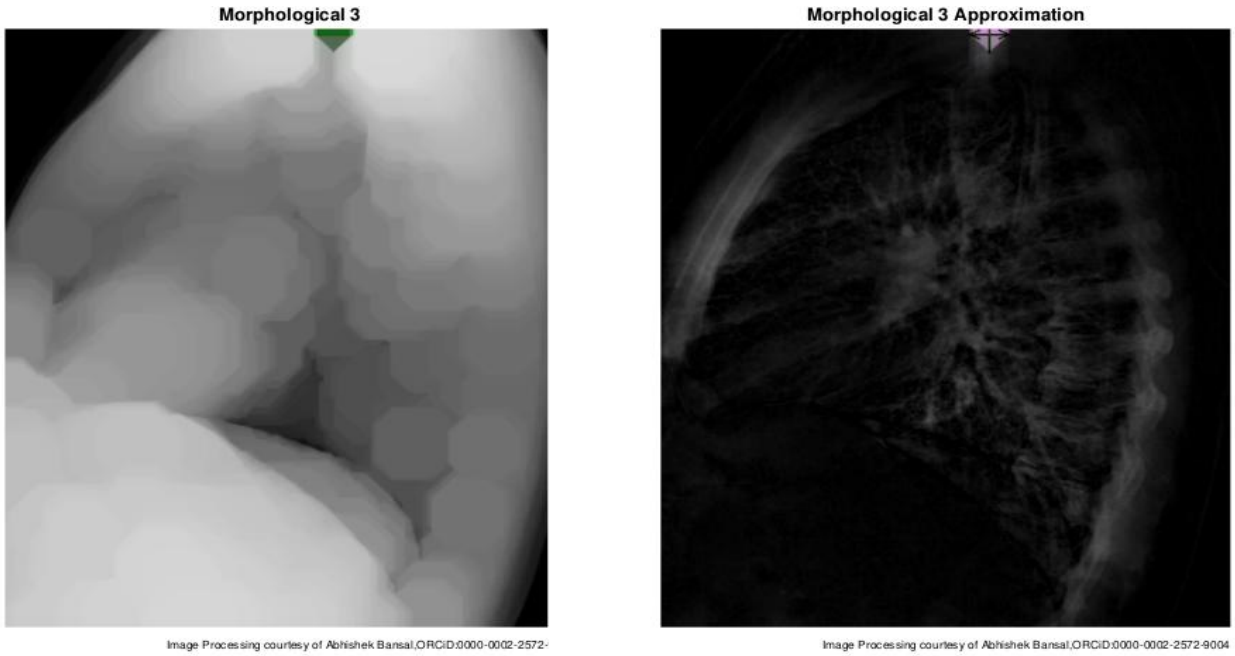


(d) Background Approximation Removed from Fig. 19(c)

Fig. 20: Morphological Segmentation

330

331



(a) Morphological Opening 3

(b) Background Approximation Removed from Fig. 20(a)

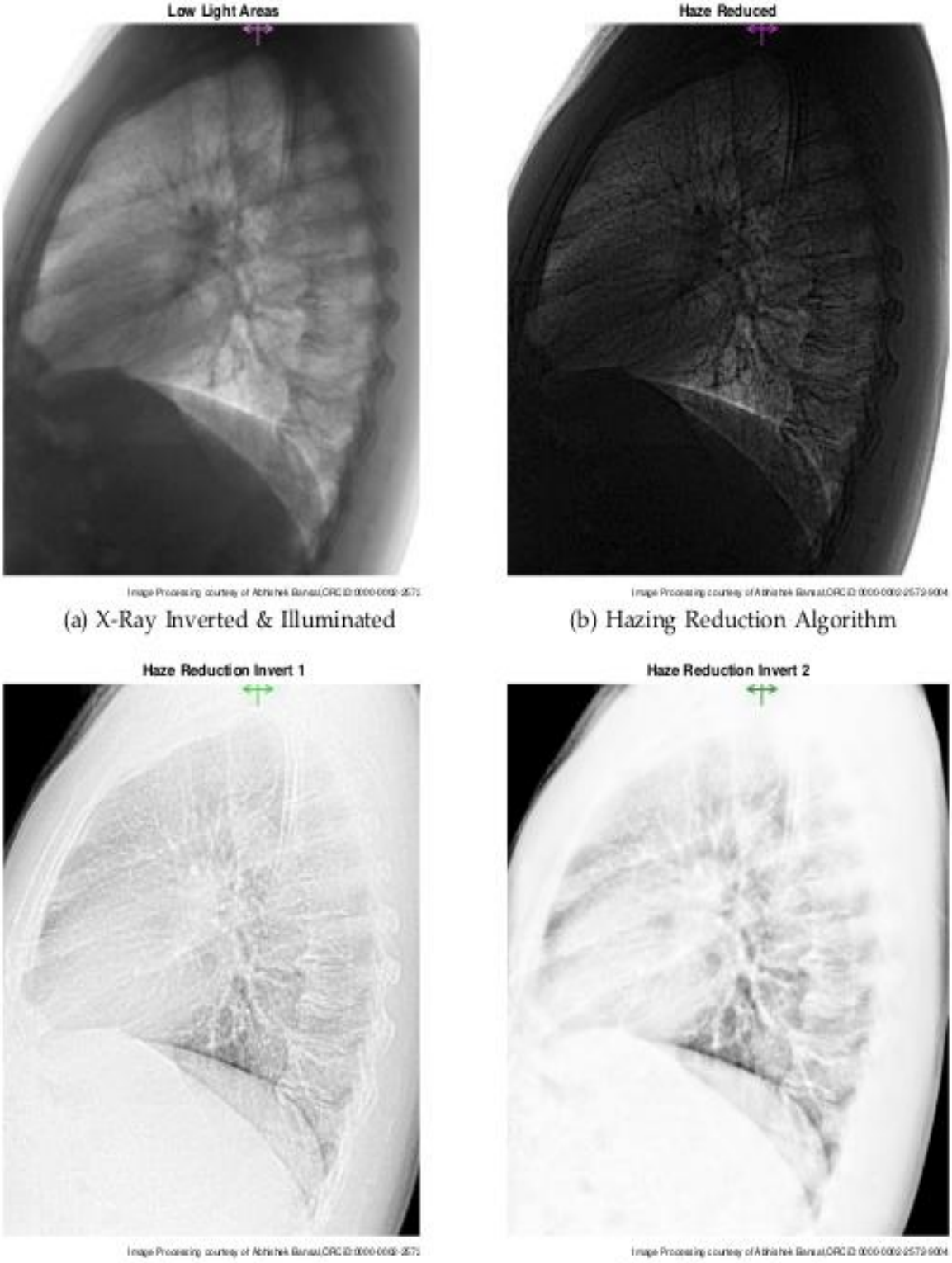
Fig. 21: Morphological Segmentation

3.12. Dehazing Algorithm

In Fig. 22(a), the original Fig. 2(a) X-Ray is inverted and the low-light areas and focused and the new X-Ray is obtained.

The hazing obtained in Fig.22(a) is reduced by hazing reduction algorithm.

On the new X-Ray of Fig.22(b), dehazing algorithm is applied and its result is in Fig.22(c,d). Fig. 23[a-d] has four more such combinations on which dehazing algorithm is implemented.



(a) X-Ray Inverted & Illuminated

(b) Hazing Reduction Algorithm

(c) Dehazing Algorithm

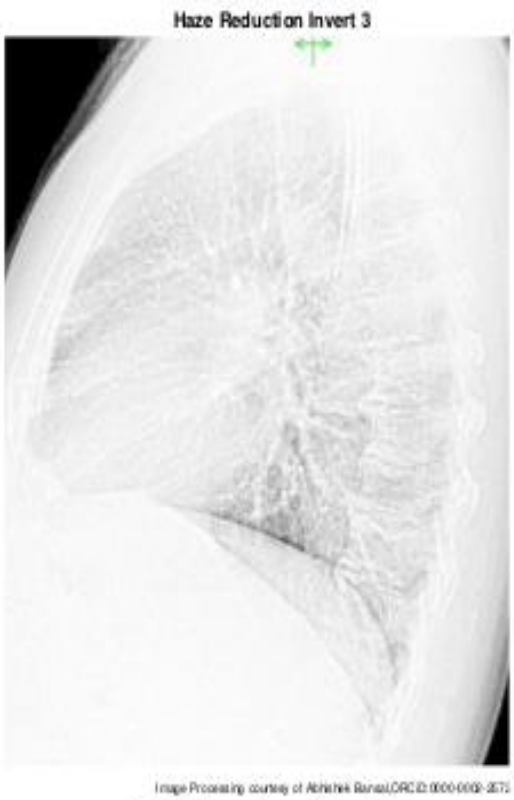
(d) Dehazing Algorithm

Fig. 22: Dehazing Algorithm

345

346

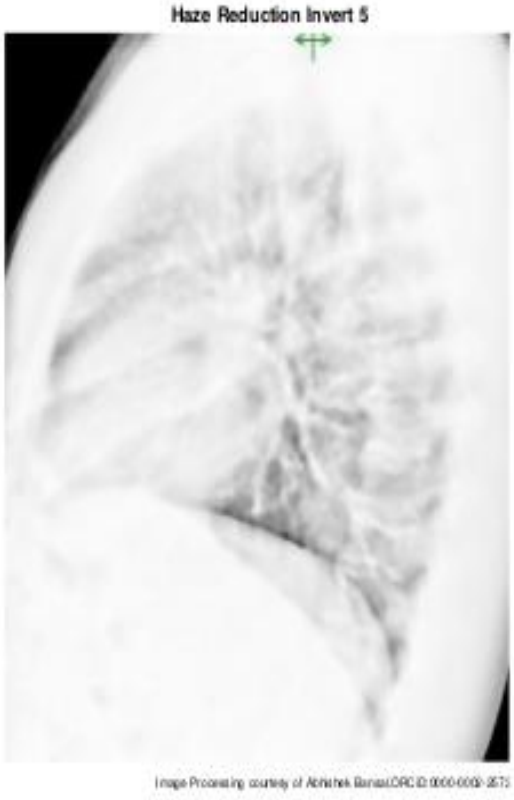
347



(a) Dehazing Algorithm



(b) Dehazing Algorithm



(c) Dehazing Algorithm



(d) Dehazing Algorithm

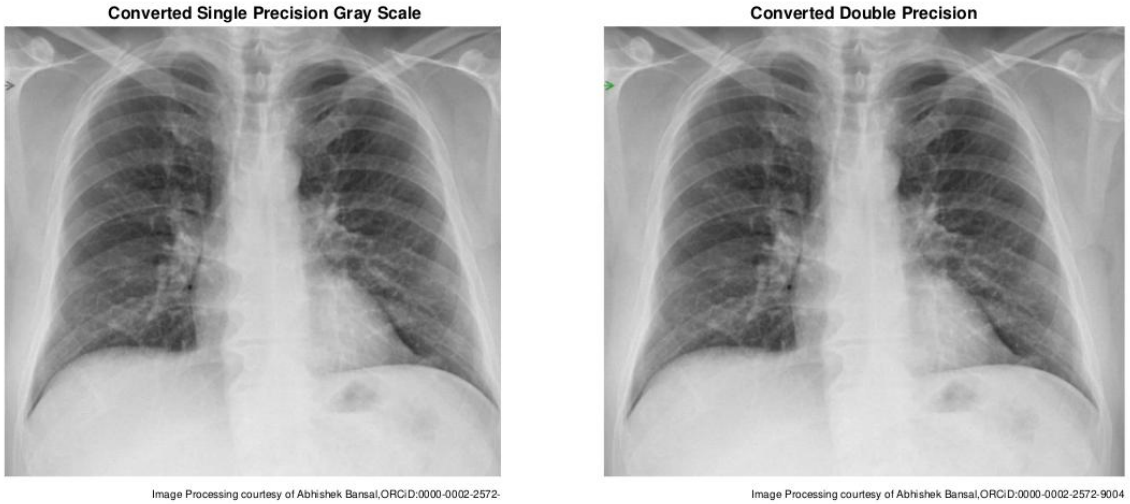
Fig. 23: Dehazing Algorithm

International Journal of Advanced Computing and Intelligent System (IJACIS)
Volume 1, Issue 1 (2023)
DOI: 10.66917/ijacis.a000003
https://msis-press.com/journals/ijacis

4. Results : Day 0, PA

4.1. X-Ray Converted

In this subsection, X-Ray(PA) of Day 0 is converted to single precision gray-scale and double precision, on which all further image processing's will be done. These are shown in Fig. 24.

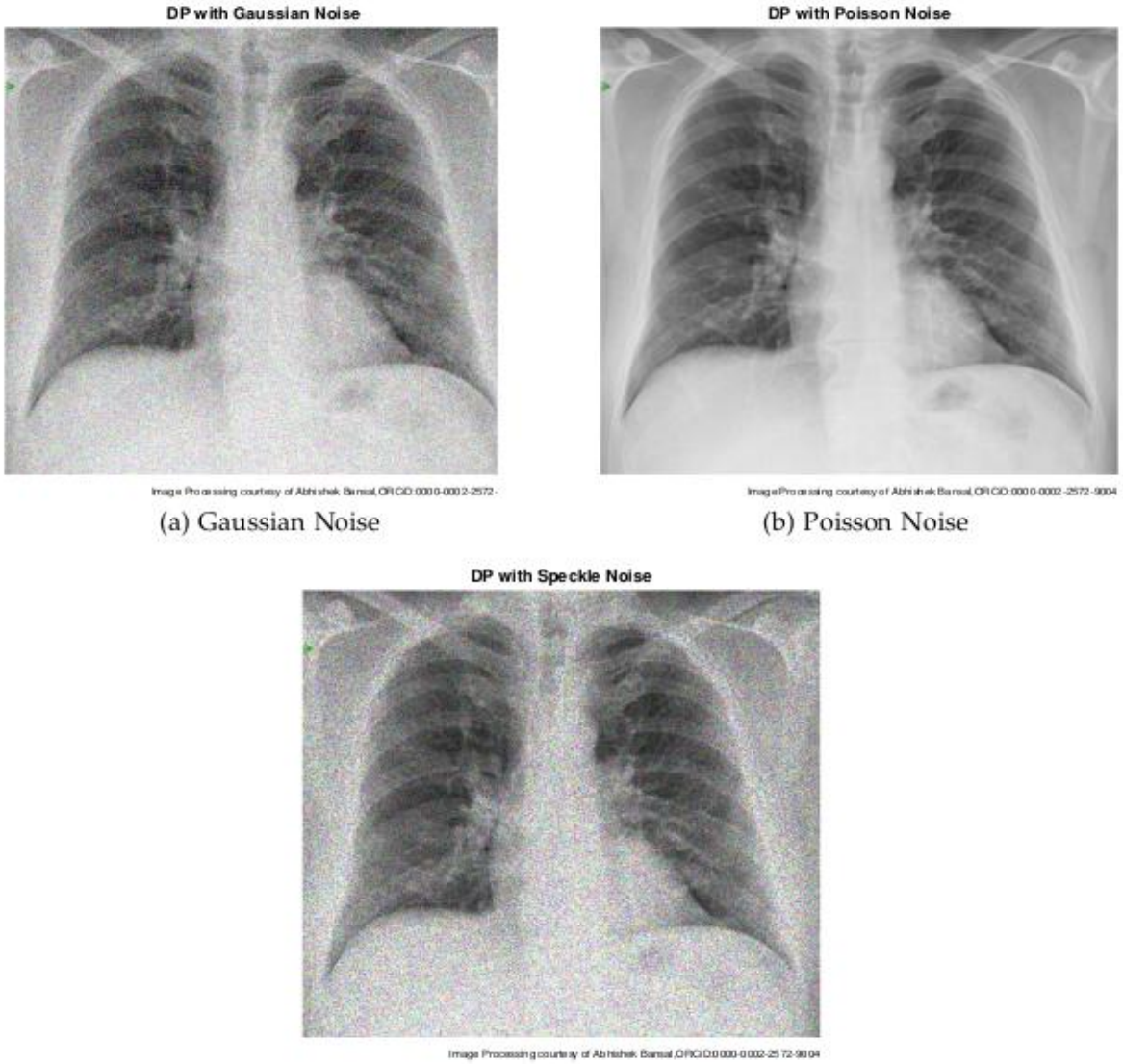


(a) Single Precision (b) Double Precision

Fig. 24: Converted to Single Precision & Double Precision

4.2. Double Precision Noise Addition

In this subsection, the double precision X-Ray of Day 0 (Fig 24(b)) of the previous subsection is subjected to noises namely Gaussian with variance 0.01, Poisson Noise and speckle noise with variance 0.05. These are shown in Fig. 25.



(a) Gaussian Noise

(b) Poisson Noise

(c) Speckle Noise

Fig. 25: Noises Added to Double Precision

363

364

365

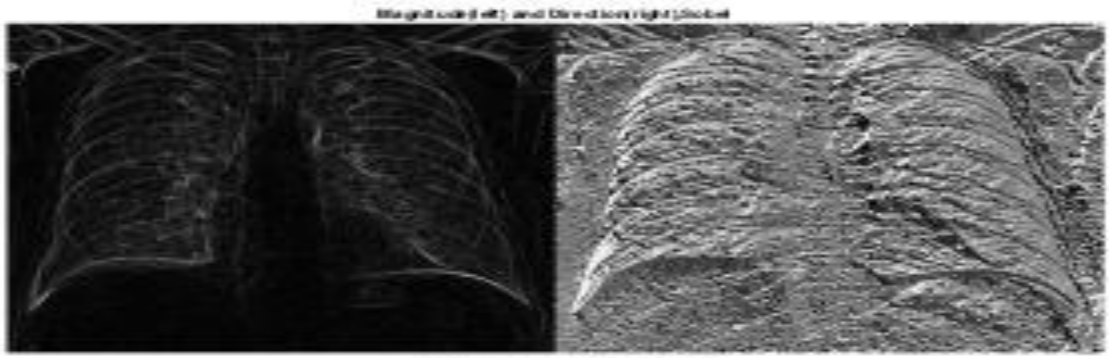
366 4.3. Gradient Magnitude and Direction

367 In this subsection, the gradient of the single precision X-Ray of Day 0 (Fig 24(a)) is

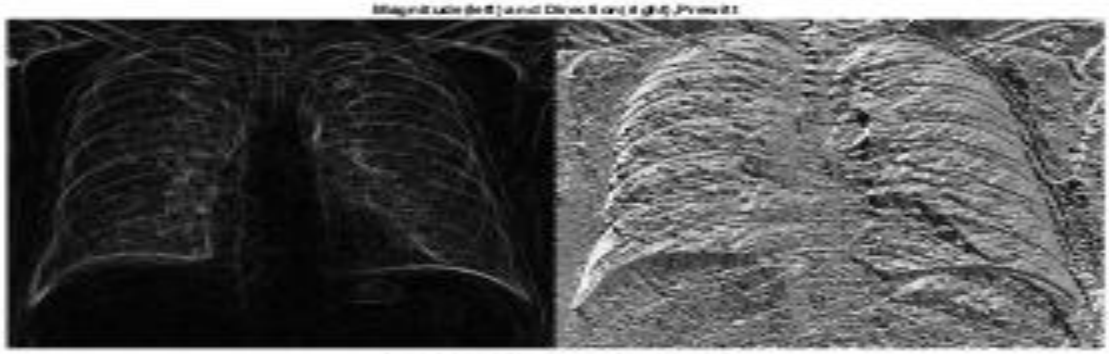
368 obtained and its magnitude and direction is plotted using methods of Sobel, Prewitt,

369 central difference and intermediate difference. These are shown in Fig. 26.

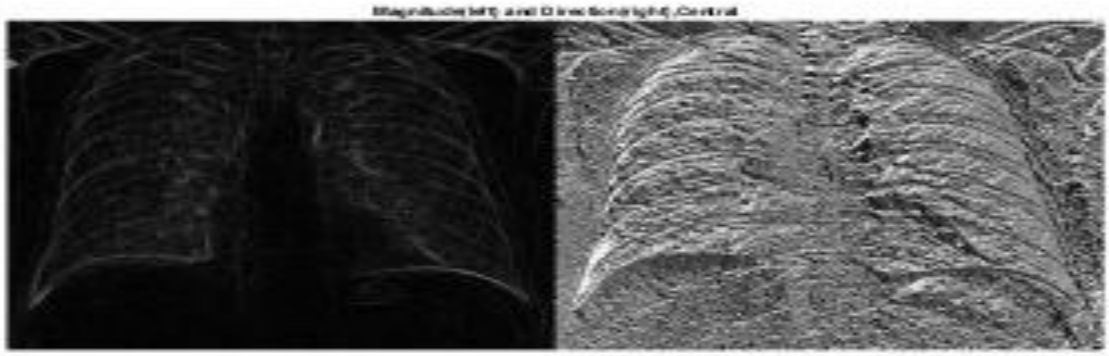
370



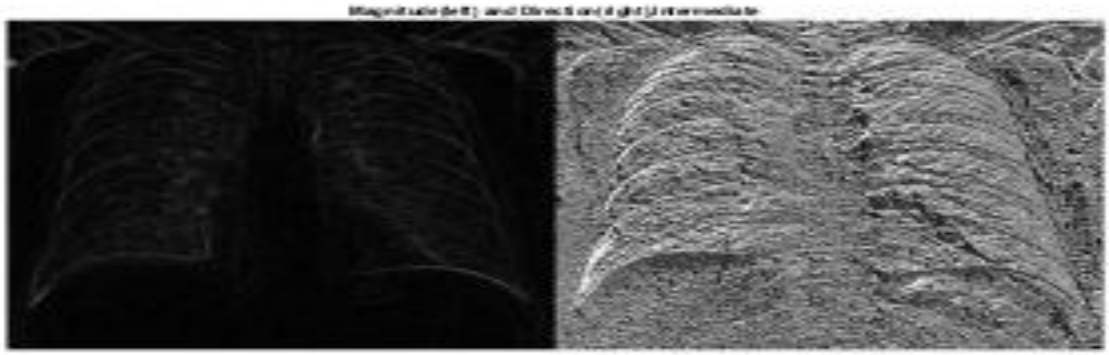
(a) Sobel Method



(b) Prewitt Method



(c) Central Difference



(d) Intermediate Difference

Fig. 26: X-Ray Gradient Magnitude and Direction

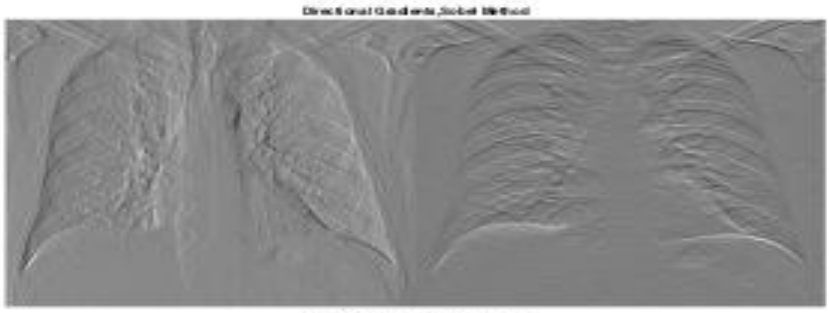
371

372

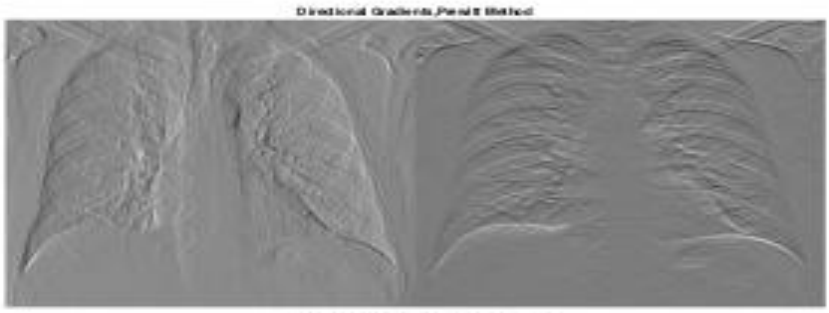
373 4.4. Directional Gradients

374 In this subsection, the directional gradient of the single precision X-Ray of Day 0 (Fig
375 24(a)) is plotted using methods of Sobel, Prewitt, central difference and intermediate
376 difference. These are shown in Fig. 27.

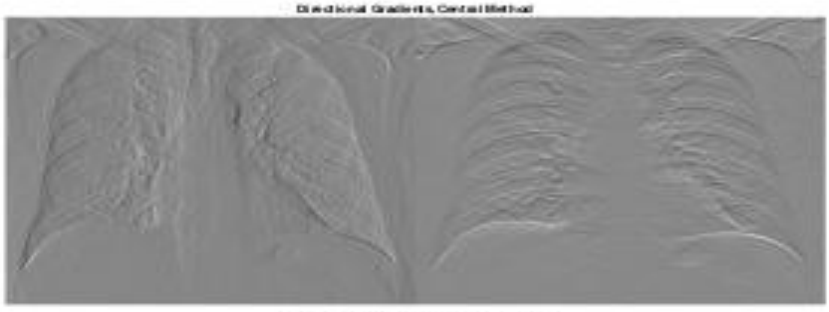
377



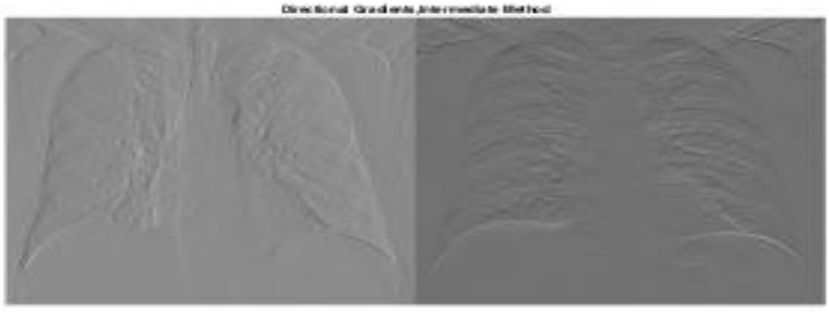
(a) Sobel Method



(b) Prewitt Method



(c) Central Difference



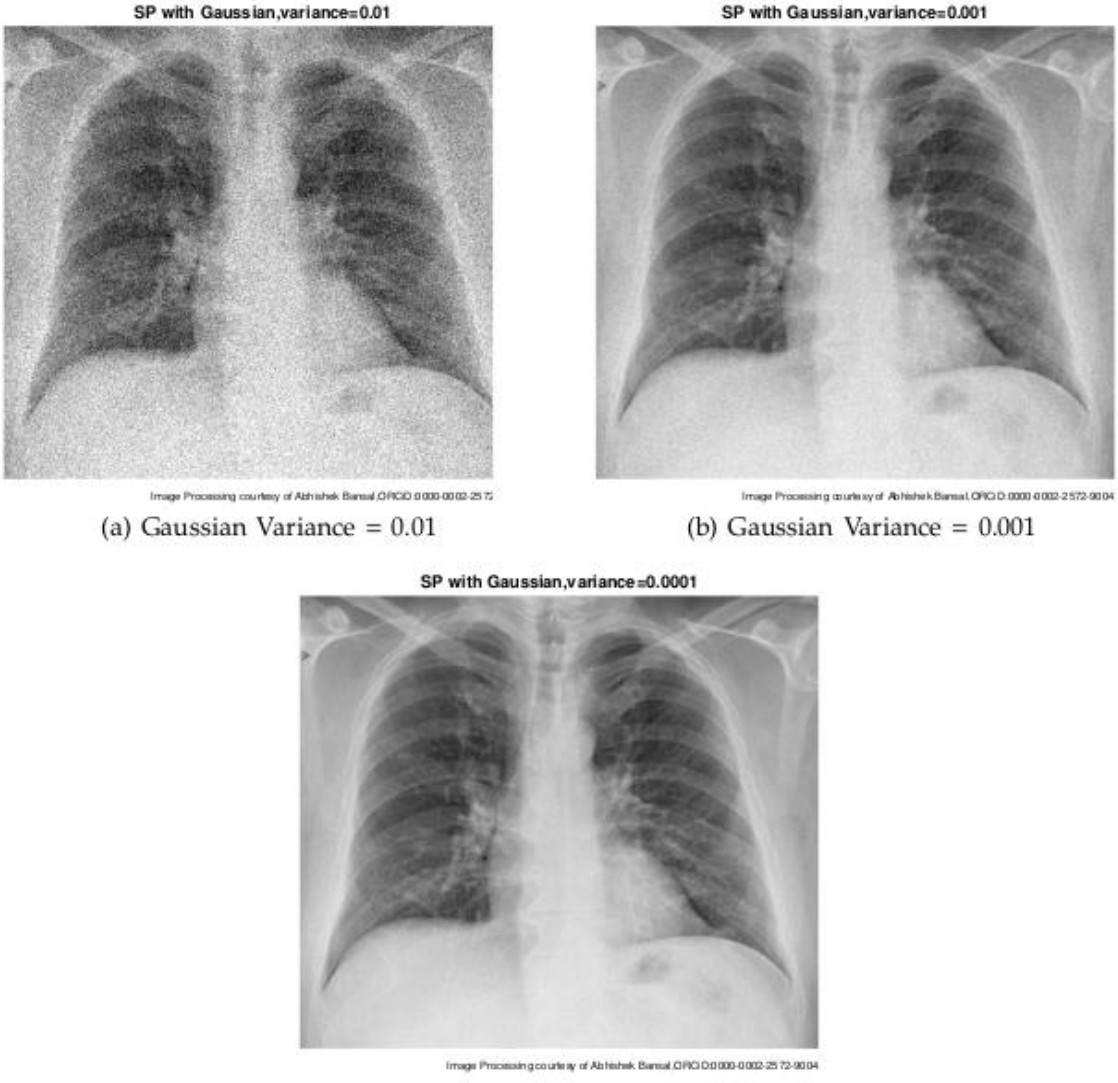
(d) Intermediate Difference

Fig. 27: Directional Gradients

382 4.5. Gaussian Noises & Sobel Gradient

383 In this subsection, the single precision X-Ray of Day 0 (Fig 24(a)) is subjected to
384 Gaussian noise with three variances of 0.01, 0.001 and 0.0001. These are shown in Fig.
385 28. The gradient magnitude of these noisy X-Rays are plotted using Sobel method, which
386 are shown in Fig. 29. The figures of gradient magnitude of Fig. 29 are further smoothed
387 using 2-D Gaussian smoothing. The Gaussian smoothing and central difference gradient
388 are shown in Fig. 30. The Gaussian smoothing and intermediate difference gradient are
389 shown in Fig. 31.

390



(a) Gaussian Variance = 0.01

(b) Gaussian Variance = 0.001

(c) Gaussian Variance = 0.0001

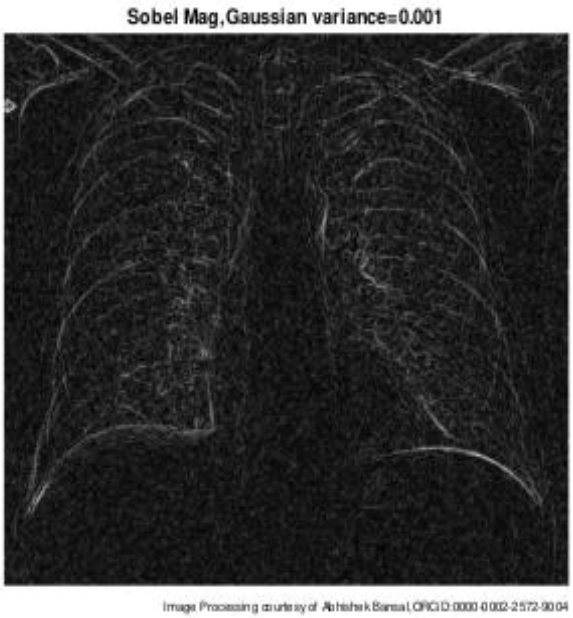
Fig. 28: Gaussian White Noise added to Image

391

392



(a) Gaussian Variance = 0.01



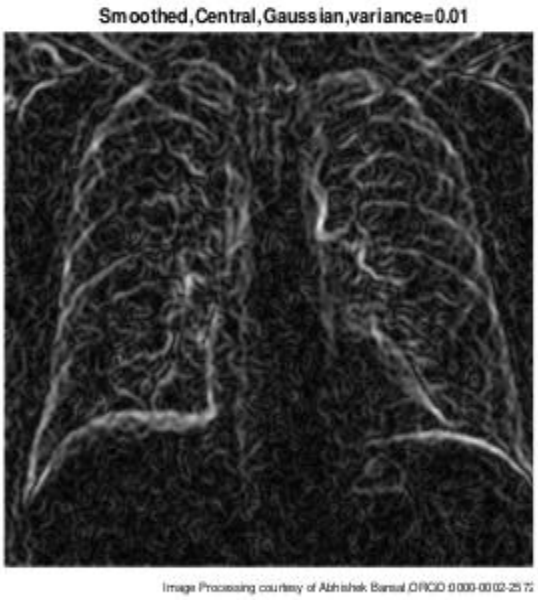
(b) Gaussian Variance = 0.001



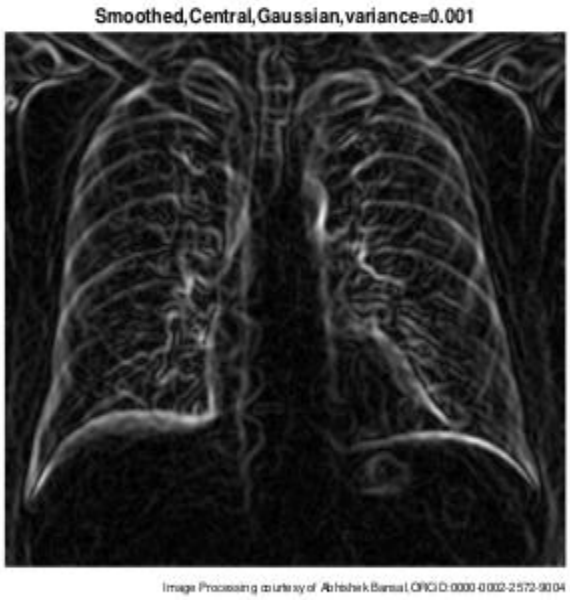
(c) Gaussian Variance = 0.0001

Fig. 29: Gradient of Noisy X-Ray using Sobel Method

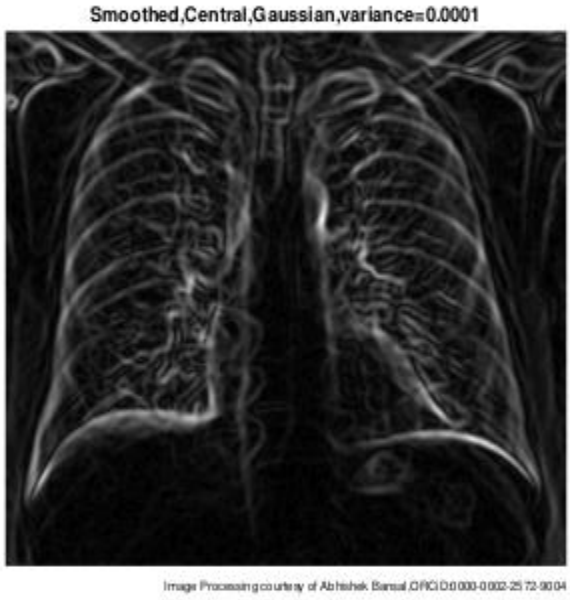
393



(a) Gaussian Variance = 0.01



(b) Gaussian Variance = 0.001



(c) Gaussian Variance = 0.0001

Fig. 30: Gaussian smoothing & central difference gradient

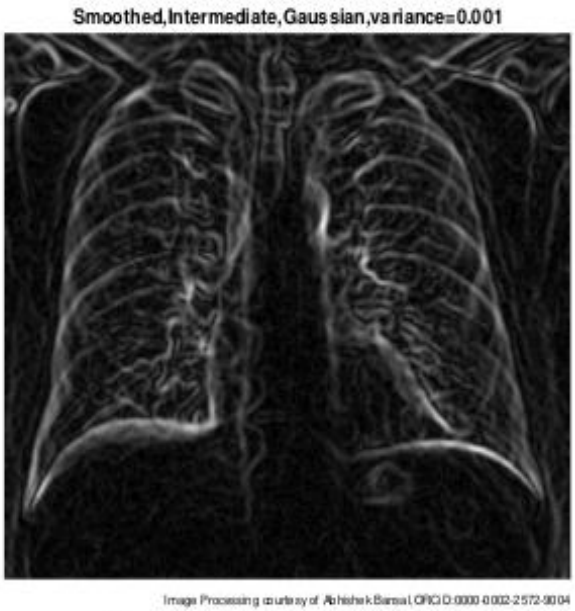
394

395

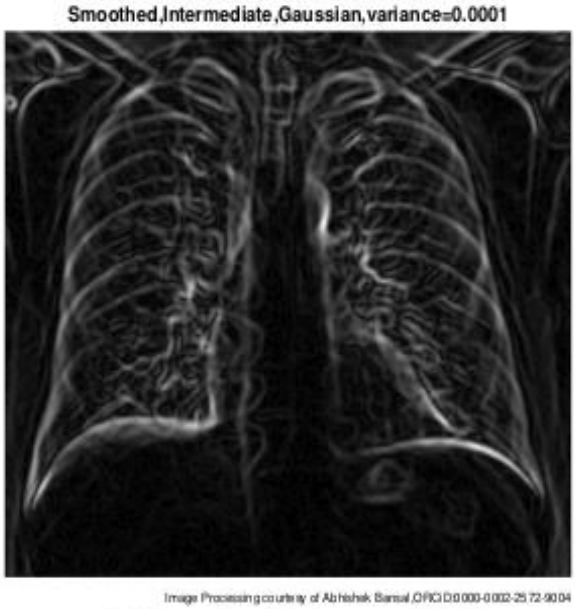
396



(a) Gaussian Variance = 0.01



(b) Gaussian Variance = 0.001



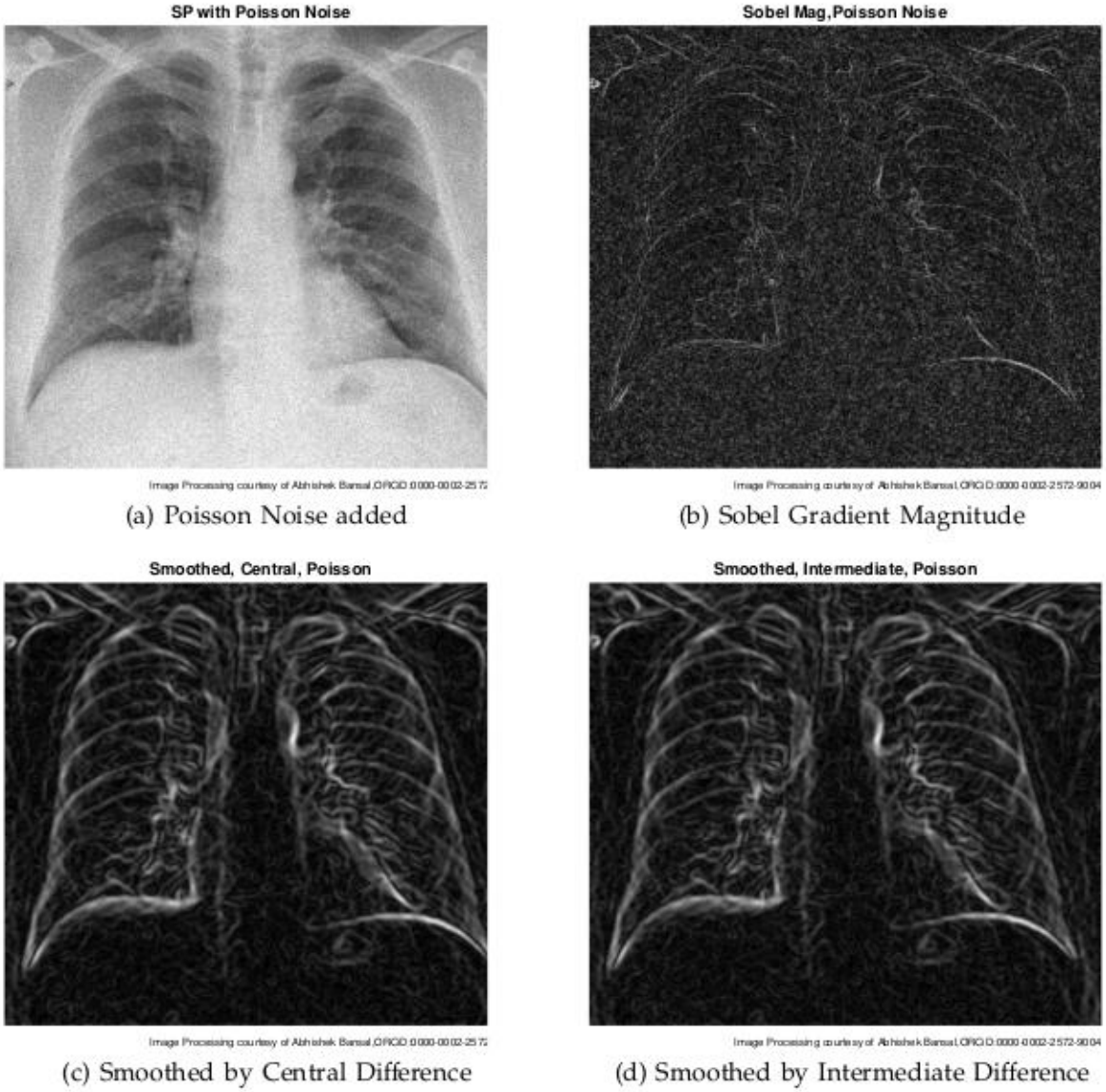
(c) Gaussian Variance = 0.0001

Fig. 31: Gaussian smoothing & intermediate difference gradient

397

4.6. Poisson Noise & Sobel Gradient

In this subsection, the single precision X-Ray of Day 0 (Fig 24(a)) is subjected to Poisson Noise,Fig. 32(a). The gradient magnitude of Poisson noise X-Ray is plotted using Sobel method, which are shown in Fig. 32(b). This is further smoothed using 2-D Gaussian smoothing and central difference gradient in Fig. 32(c); and 2-D Gaussian smoothing and intermediate difference gradient in Fig. 32(d).



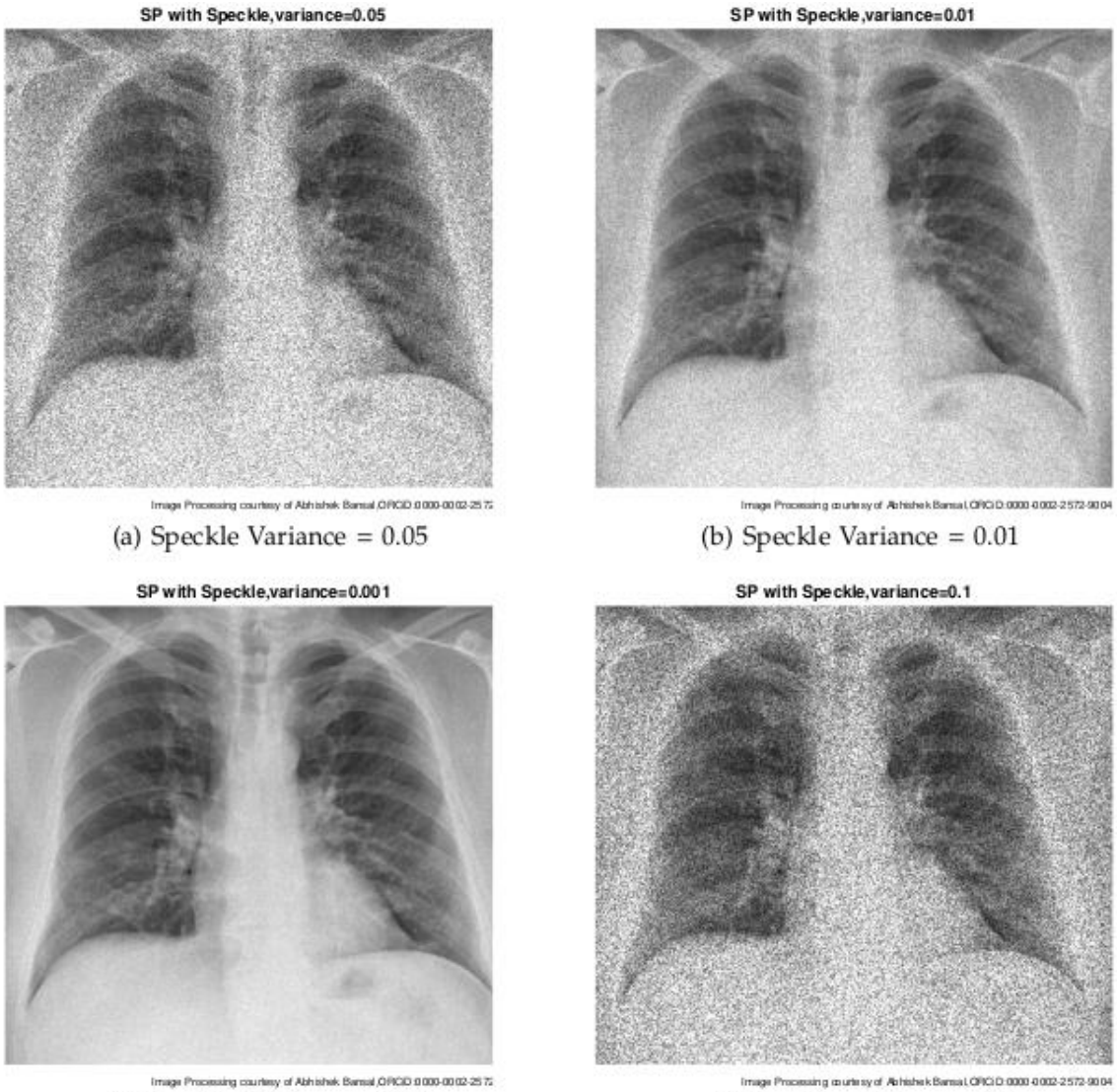
(a) Poisson Noise added (b) Sobel Gradient Magnitude

(c) Smoothed by Central Difference (d) Smoothed by Intermediate Difference

Fig. 32: Poisson Noise & Gradient Magnitude

4.7. Speckle Noise & Sobel Gradient

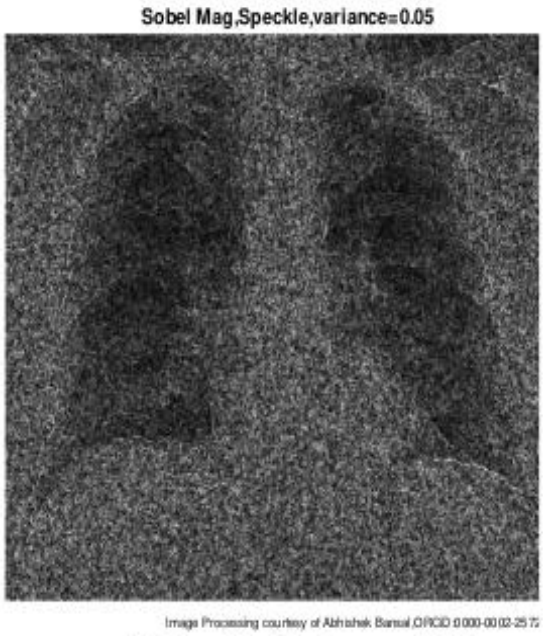
In this subsection, the single precision X-Ray of Day 0 (Fig 24(a)) is subjected to Speckle noise with four variances of 0.05, 0.01, 0.001 and 0.1. These are shown in Fig. 33[a-d]. The gradient magnitude of these noisy X-Rays are plotted using Sobel method, which are shown in Fig. 34. These are further smoothed using 2-D Gaussian smoothing. The Gaussian smoothing and central difference gradient are shown in Fig. 35. The Gaussian smoothing and intermediate difference gradient are shown in Fig. 36.



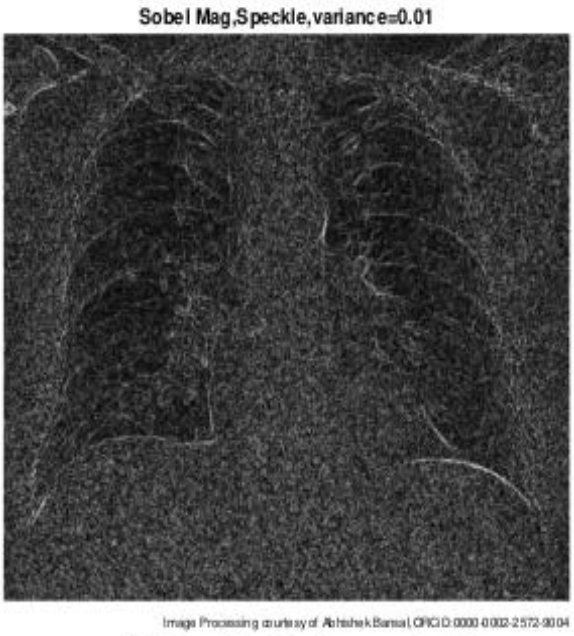
(a) Speckle Variance = 0.05 (b) Speckle Variance = 0.01

(c) Speckle Variance = 0.001 (d) Speckle Variance = 0.1

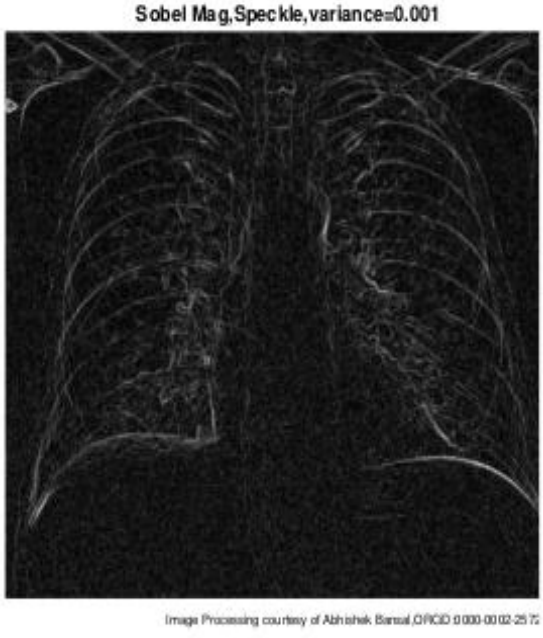
Fig. 33: Speckle Noise added to Image



(a) Speckle Variance = 0.05



(b) Speckle Variance = 0.01



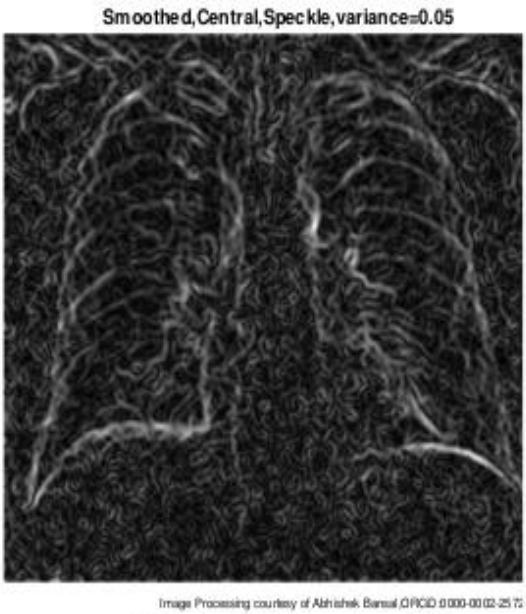
(c) Speckle Variance = 0.001



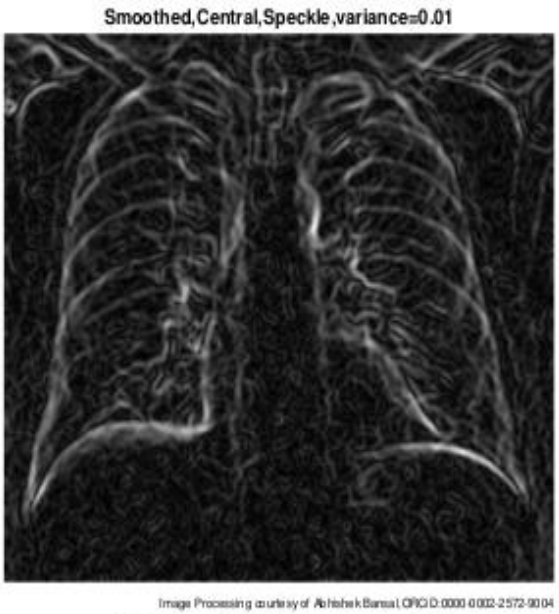
(d) Speckle Variance = 0.1

Fig. 34: Gradient of Noisy X-Ray using Sobel Method

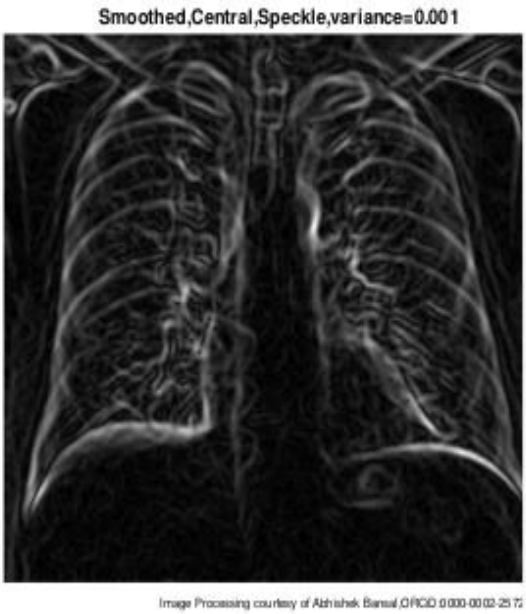
International Journal of Advanced Computing and Intelligent System (IJACIS)
Volume 1, Issue 1 (2023)
DOI: 10.66917/ijacis.a000003
https://msis-press.com/journals/ijacis



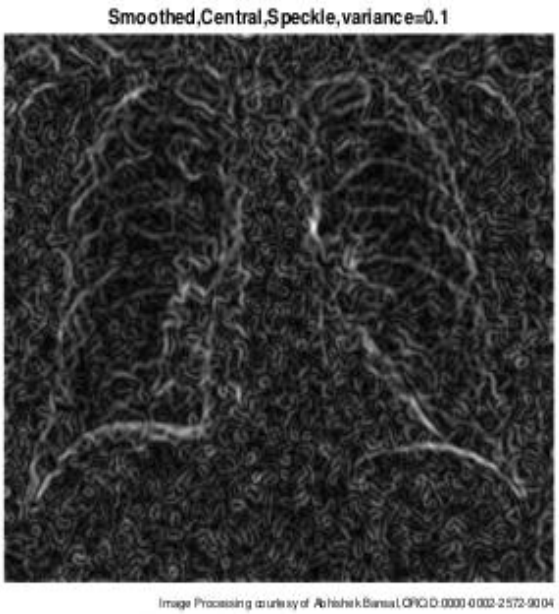
(a) Speckle Variance = 0.05



(b) Speckle Variance = 0.01



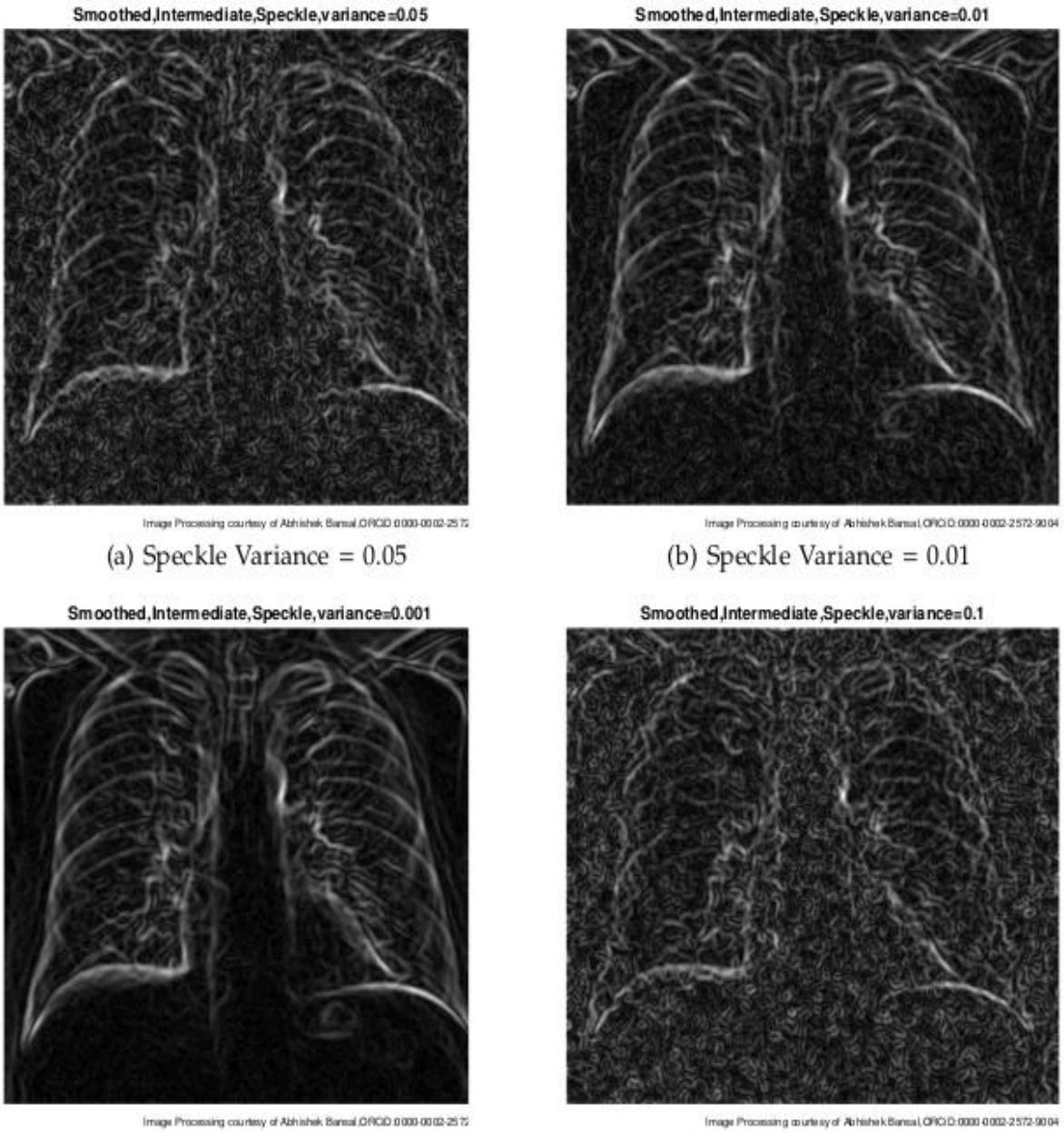
(c) Speckle Variance = 0.001



(d) Speckle Variance = 0.1

Fig. 35: Gaussian smoothing & central difference gradient

417



(a) Speckle Variance = 0.05

(b) Speckle Variance = 0.01

(c) Speckle Variance = 0.001

(d) Speckle Variance = 0.1

Fig. 36: Gaussian smoothing & intermediate difference gradient

418

4.8. Pixel Intensities & Contrast

In this subsection, the original X-Ray (without converting to single precision or double precision) is contrasted for study and analysis.

Let the center fit

$$z = \frac{(x - 127.5)}{74.05}$$

then from polynomial regression

$$y = 68.38 \times z^9 + 79.92 \times z^8 + 508.3 \times z^7 + 211.7 \times z^6 - 3969 \times z^5 - 2424 \times z^4 + 5591 \times z^3 + 2489 \times z^2 + 45.89 \times z + 2385$$

Let $\bar{y}$ be the mean of y, $\hat{y}$ the calculated values of y, then the coefficient of determination, R^2

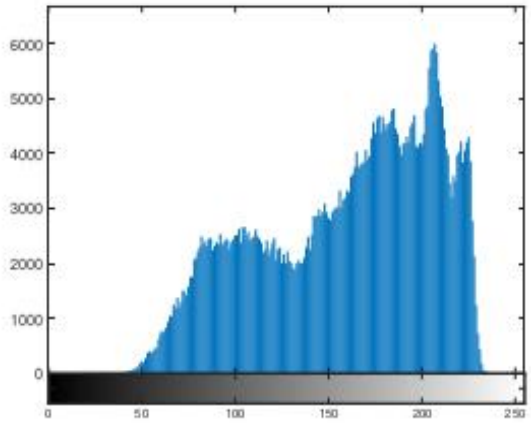
$$R^2 = 1 - \frac{\sum_{i=1}^{n} (y_i - \hat{y})^2}{\sum_{i=1}^{n} (y_i - \bar{y})^2} = 0.9428$$

The measure of the goodness of fit given by norm of residuals is 6536. Here, the polynomial of degree 9 chosen here is the global which can be focused on the areas of interest (to be decided by infection part or researchers/doctors interest) and separate equations can be obtained for each particular area of interest. This gives insight in mathematical formulation and has been used in the Novel B-Mathematical Modeling of Respiratory System.

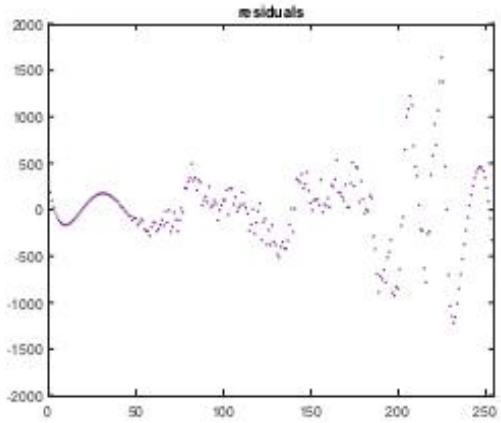
The Fig.37(a) shows that X-Ray contrast is improved for analysis when compared with Fig. 1(a). Fig. 37(b) shows the distribution of X-Ray pixel intensities. Fig. 37(c) shows the error estimation plot, which is the plot of the residuals. Fig. 37(d) shows the X-Ray histogram equalization which is the spreading of the intensity values over the full range.



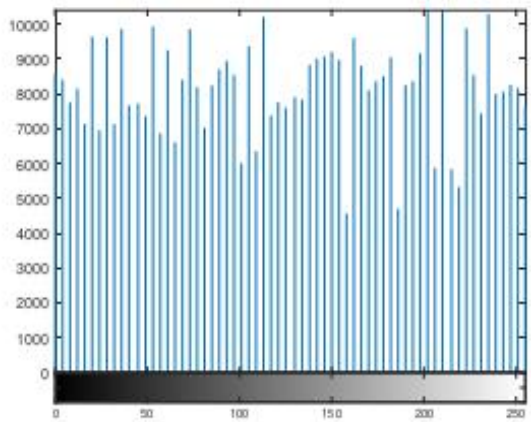
(a) X-Ray Contrast Improved



(b) Distribution of Pixel Intensities



(c) Error Estimation Plot



(d) X-Ray Histogram Equalization

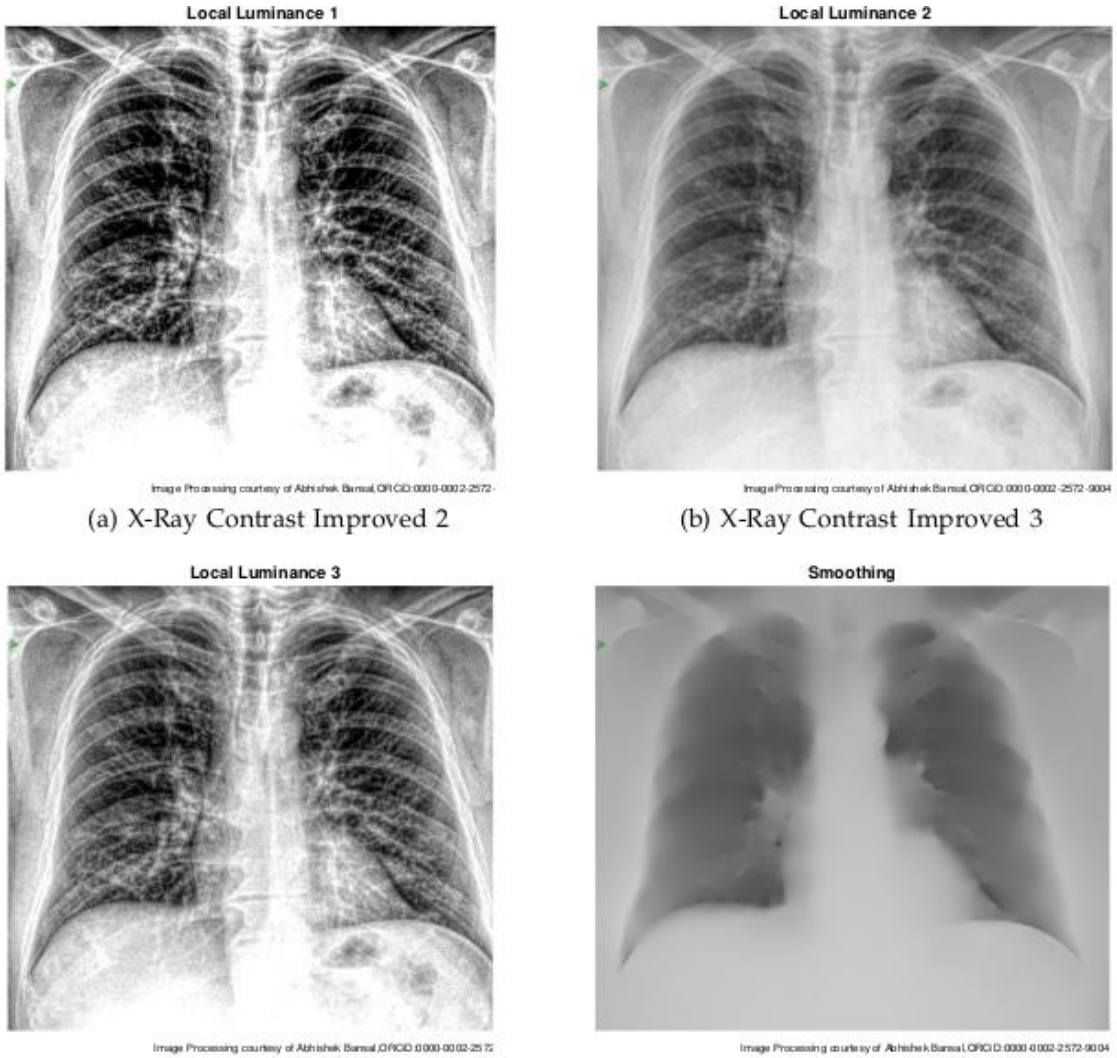
Fig. 37: Distribution of Pixel Intensities in X-Ray

445

TABLE III: Data Statistics for Fig. 37(b)

	X	Y
min	0	0
max	255	5996
mean	127.5	2051
median	127.5	2257
mode	0	0
std deviation	74.05	1711
range	255	5996

In Fig. 38, X-Ray Contrast is improved with five local luminances. The original Fig. 24(a) X-Ray contrast is improved with four more local luminances by varying the intensity values at low and high intensities. These are shown in Fig 38(a), Fig. 38(b) and Fig. 38(c). In Fig. 38(d), the original Fig. 24(a) X-Ray is contrasted with fifth value of improvement but smoothing technique is applied after it.



(a) X-Ray Contrast Improved 2 (b) X-Ray Contrast Improved 3

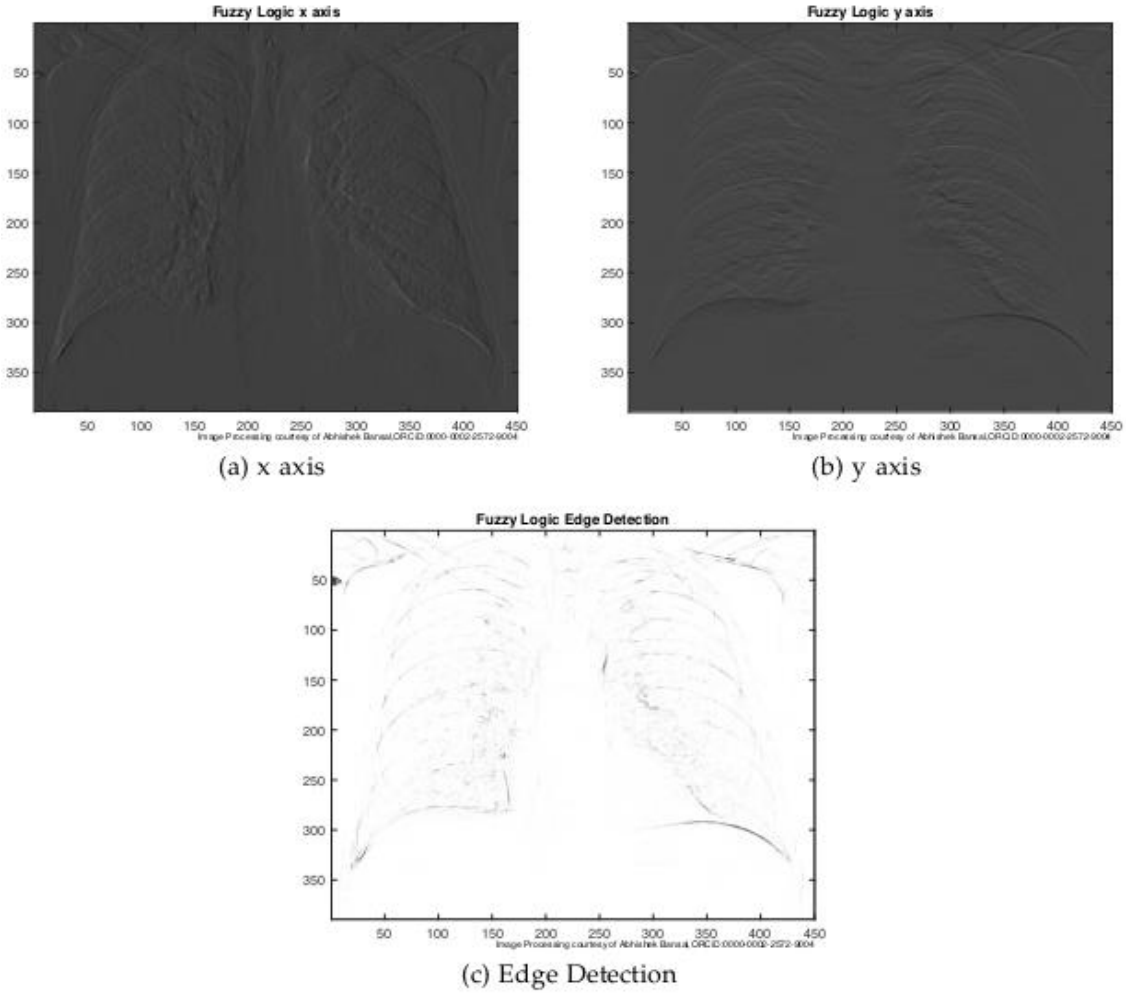
(c) X-Ray Contrast Improved 4 (d) X-Ray Contrast Improved & Smoothed

Fig. 38: X-Ray Contrast Improved with Five Local Luminances

4.9. Fuzzy Logic

In this subsection, the images obtained using fuzzy logic edge-detection algorithm and Fuzzy Inference System (FIS) are given. Two 2-D Convolution are performed. The x-axis of directional gradient is convolved with x-axis gradients of double-precision X-

Ray obtained in Fig. 24(b) and the X-Ray gradient of fuzzy logic x-axis is given in Fig. 39(a). The y-axis of directional gradient is convolved with y-axis gradients of double-precision X-Ray obtained in Fig. 24(b) and the X-Ray gradient of fuzzy logic y-axis is given in Fig. 39(b). The edge detection is shown in Fig. 39(c).



(a) x axis (b) y axis

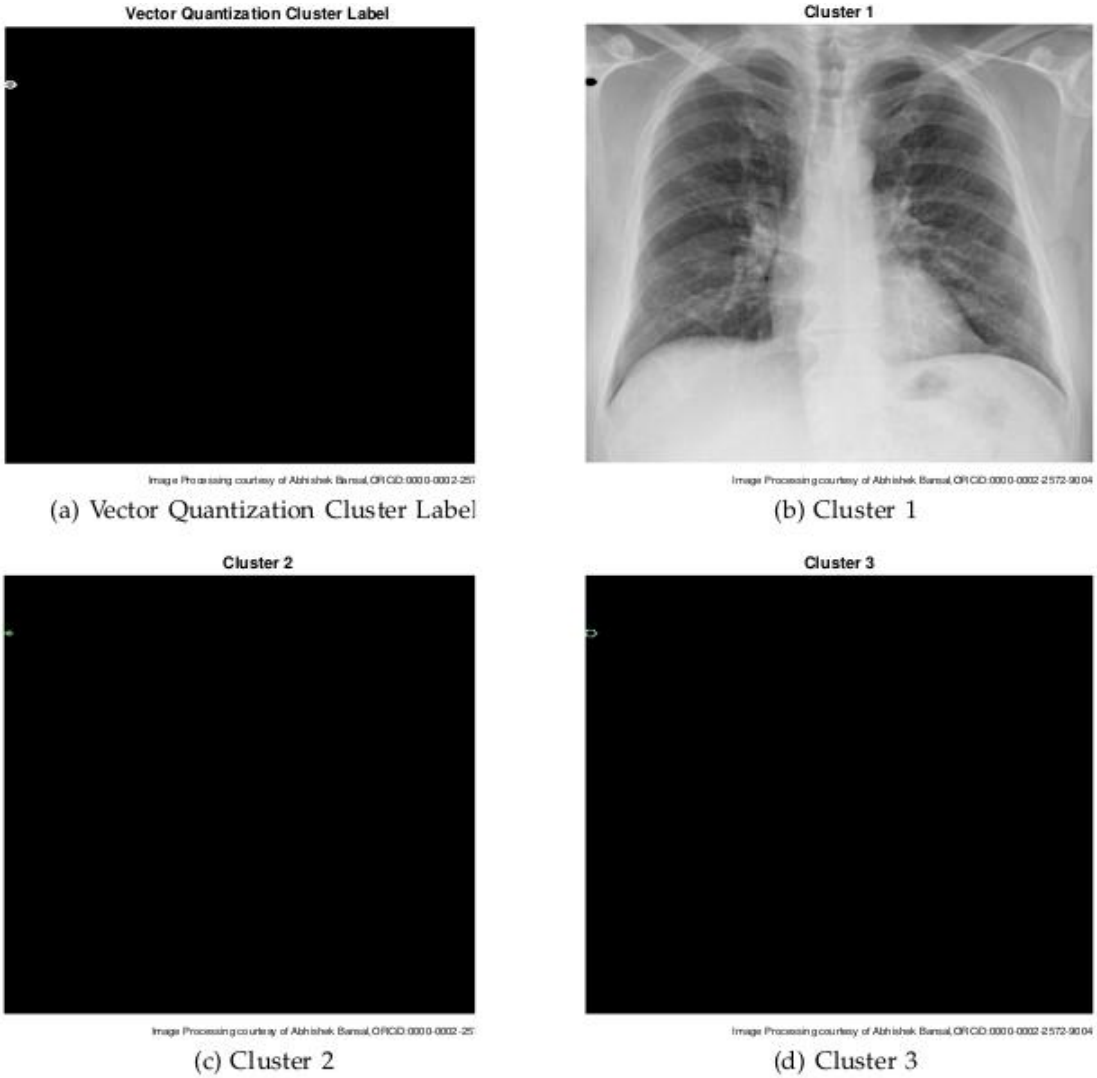
(c) Edge Detection

Fig. 39: Fuzzy Logic

4.10. K-means Clustering

In this subsection, the popular vector quantization technique of K-Means clustering is applied to X-Ray. In this technique, firstly CIE XYZ tristimulus technique is used to know the color information and thus, the information of luminosity layer 'L*', chromaticity-layer 'a*' and chromaticity-layer 'b*' is obtained. Then every pixel is

clustered with its pixel label and partitioned into three clusters. The clustering obtained is shown in Fig. 40(a), Vector Quantization Cluster Label. And three clusters Cluster 1, Cluster 2 and Cluster 3 obtained are shown in Fig. 40(b), Fig. 40(c) and Fig. 40(d) respectively.

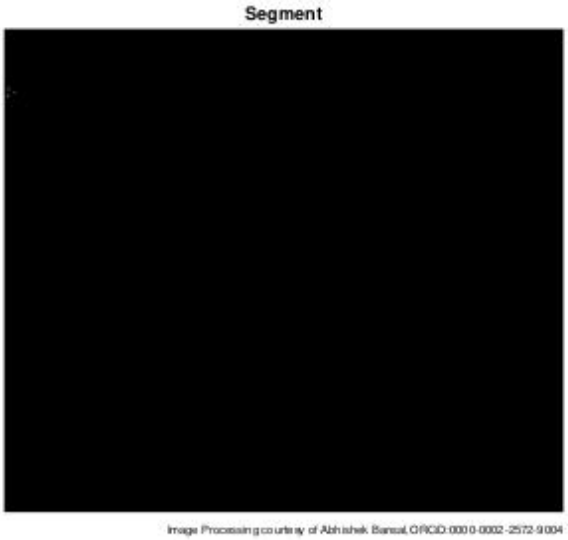


(a) Vector Quantization Cluster Label (b) Cluster 1

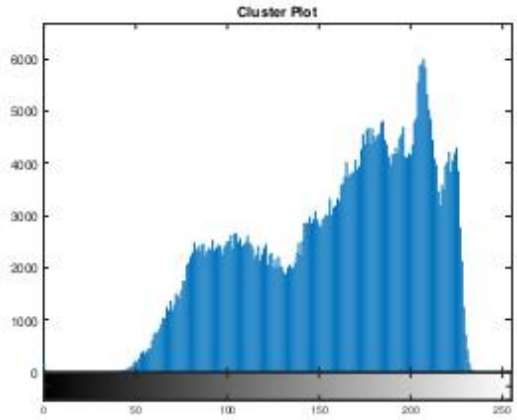
(c) Cluster 2 (d) Cluster 3

Fig. 40: Vector Quantization,K-means Clustering

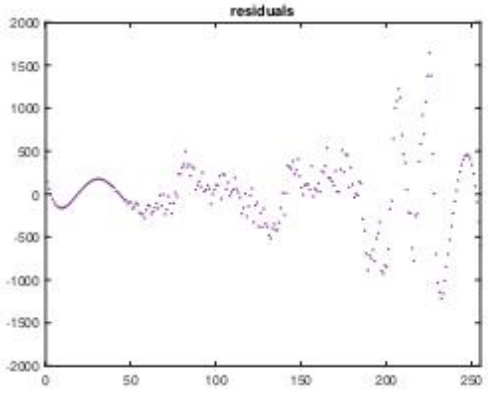
In Fig. 41(a), segmentation is applied and Fig. 41(b) and Fig. 41(c) shows respectively the cluster plot and the plot of error estimation, that is, the plot of residuals.



(a) Segmentation



(b) Cluster Plot



(c) Cluster Plot Residuals

Fig. 41: Clustering Plot and Segment

482

483

484 Moving in similar way as in the Subsection-8 and choosing same

$$z = \frac{(x - 127.5)}{74.05}$$

487 we have,

$$y = 60.64 \times z^9 + 87.05 \times z^8 + 551.5 \times z^7 + 176.3 \times z^6 - 4048 \times z^5 - 2370 \times z^4 + 5643 \times z^3 + 2464 \times z^2 + 36.35 \times z + 2386$$

488

489 $R^2 = 0.9425$ and Norm of Residuals = 6546

490

TABLE IV: Data Statistics for Fig. 40(b)

	X	Y
min	0	0
max	255	5996
mean	127.5	2051
median	127.5	2256
mode	0	0
std deviation	74.05	1710
range	255	5996

4.11. Morphological Segmentation

In this subsection, known morphological segmentation technique is applied on X-Rays. Three morphological openings are used. The morphological opening with structuring element of disk shaped with three different radius are shown in Fig. 42(a), Fig. 42(c) and Fig. 43(a). The background approximation images of X-Ray obtained after subtracting from the original image are shown in Fig. 42(b), Fig. 42(d) and Fig. 43(b).



(a) Morphological Opening 1



(b) Background Approximation Removed from Fig. 19(a)



(c) [Morphological Opening 2



(d) Background Approximation Removed from Fig. 19(c)

Fig. 42: Morphological Segmentation



(a) Morphological Opening 3



(b) Background Approximation Removed from Fig. 20(a)

Fig. 43: Morphological Segmentation

International Journal of Advanced Computing and Intelligent System (IJACIS)
Volume 1, Issue 1 (2023)
DOI: 10.66917/ijacis.a000003
https://msis-press.com/journals/ijacis

512

513 4.12. Dehazing Algorithm

514 In Fig. 44(a), the original Fig. 24(a) X-Ray is inverted and the low-light areas and

515 focused and the new X-Ray is obtained.

516

517 The hazing obtained in Fig. 44(a) is reduced

518 by hazing reduction algorithm.

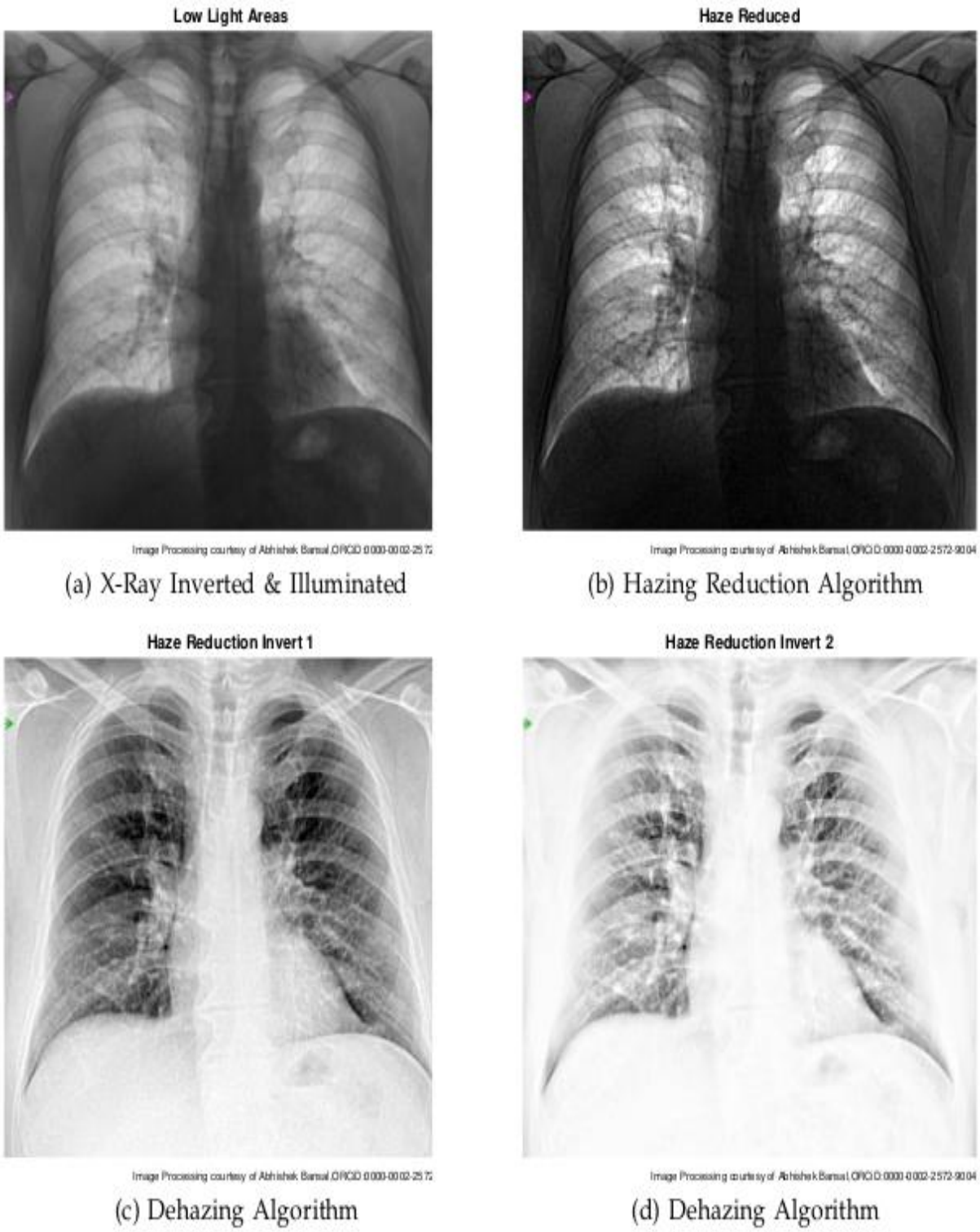
519

520 On the new X-Ray of Fig. 44(b), dehazing algorithm is applied and its result is in Fig.

521 44(c,d). Fig. 45[a-d] has four more such combinations on which dehazing algorithm is

522 implemented.

523



(a) X-Ray Inverted & Illuminated

(b) Hazing Reduction Algorithm

(c) Dehazing Algorithm

(d) Dehazing Algorithm

Fig. 44: Dehazing Algorithm

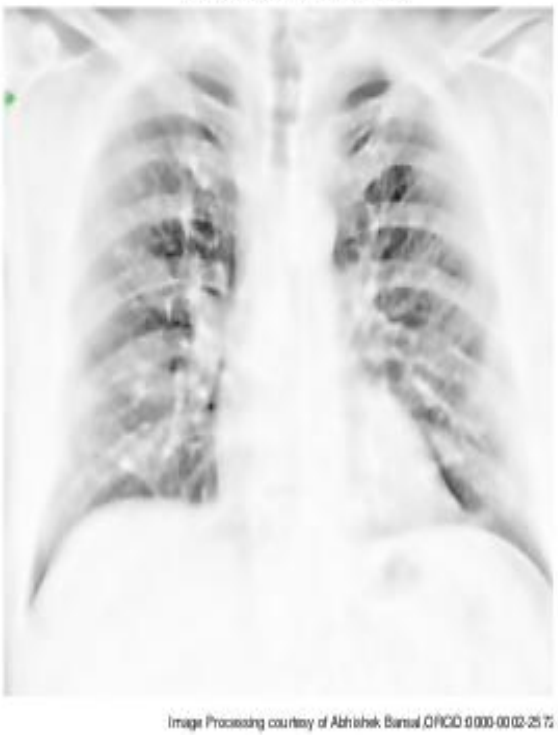
International Journal of Advanced Computing and Intelligent System (IJACIS)
Volume 1, Issue 1 (2023)
DOI: 10.66917/ijacis.a000003
https://msis-press.com/journals/ijacis



(a) Dehazing Algorithm



(b) Dehazing Algorithm



(c) Dehazing Algorithm



(d) Dehazing Algorithm

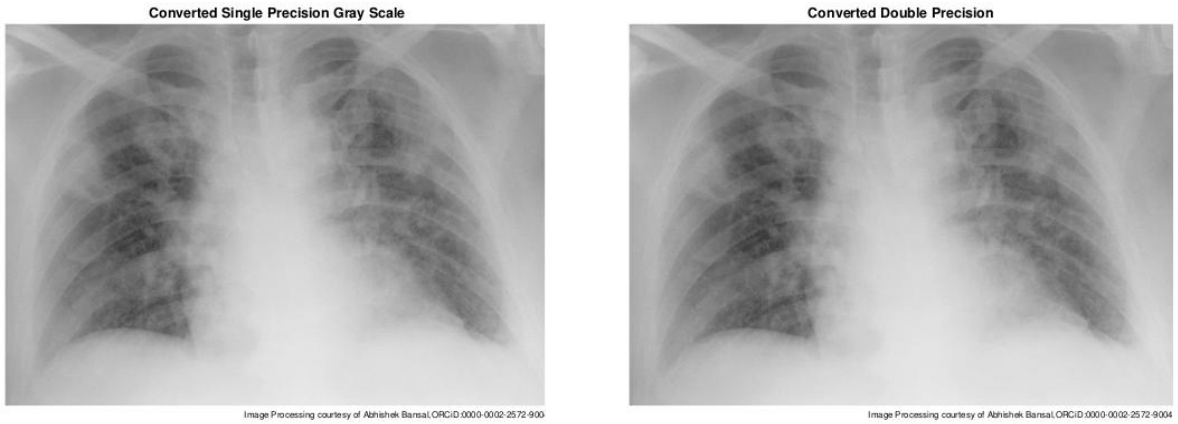
Fig. 45: Dehazing Algorithm

International Journal of Advanced Computing and Intelligent System (IJACIS)
Volume 1, Issue 1 (2023)
DOI: 10.66917/ijacis.a000003
https://msis-press.com/journals/ijacis

5. Results : Day 3, PA

5.1. X-Ray Converted

In this subsection, X-Ray(PA) of Day 3 is converted to single precision grayscale and double precision,on which all further image processings will be done. These are shown in Fig. 46.

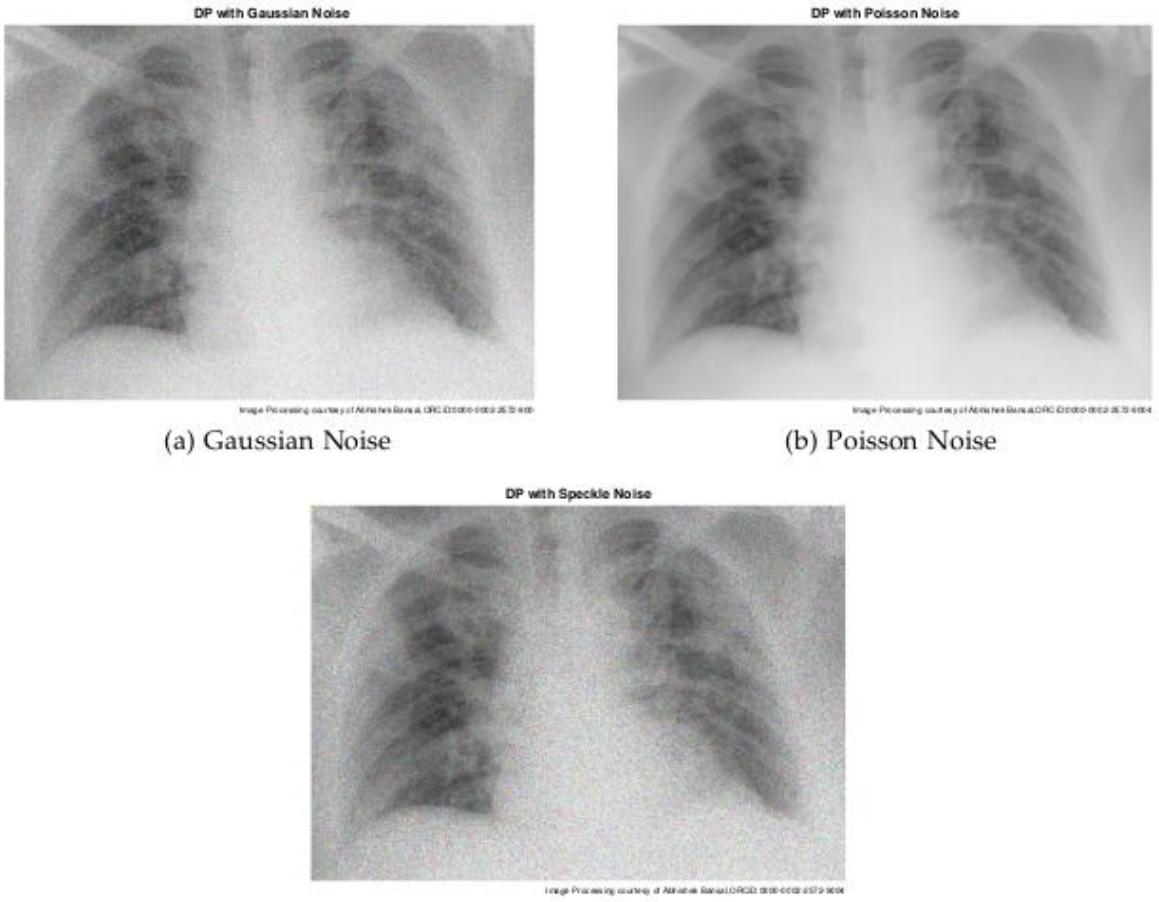


(a) Single Precision (b) Double Precision

Fig. 46: Converted to Single Precision & Double Precision,Day3

5.2. Double Precision Noise Addition

In this subsection, the double precision X-Ray of Day 3 (Fig 46(b)) of the previous subsection is subjected to noises namely Gaussian with variance 0.01, Poisson Noise and speckle noise with variance 0.05. These are shown in Fig. 47.



(a) Gaussian Noise

(b) Poisson Noise

(c) Speckle Noise

Fig. 47: Noises Added to Double Precision,Day3

539

540

541

542

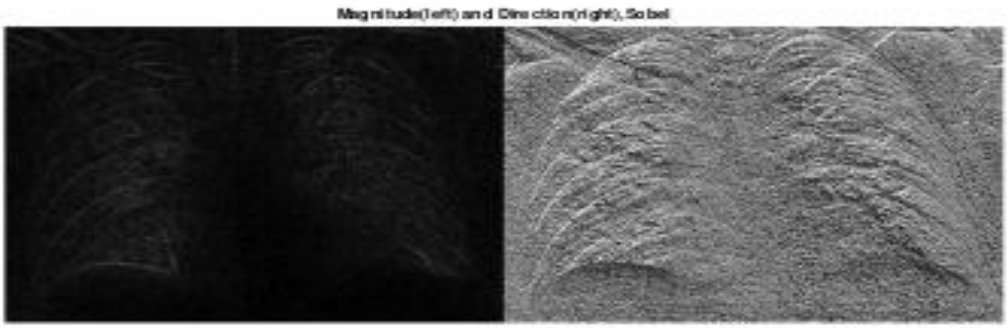
543 5.3. Gradient Magnitude and Direction

544 In this subsection, the gradient of the single precision X-Ray of Day 3 (Fig 46(a)) is

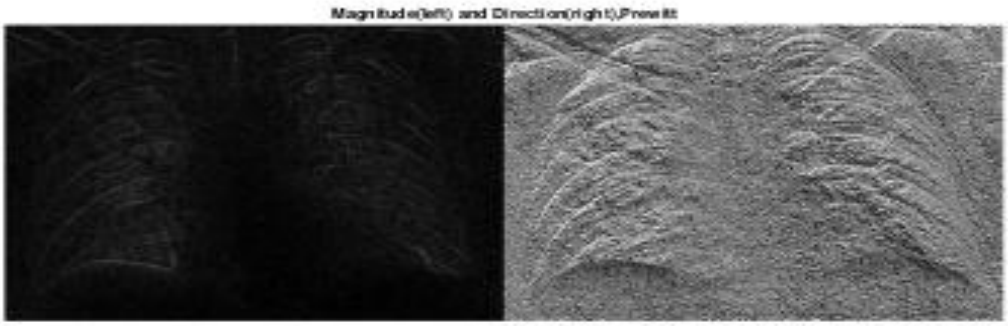
545 obtained and its magnitude and direction is plotted using methods of Sobel, Prewitt,

546 central difference and intermediate difference. These are shown in Fig. 48.

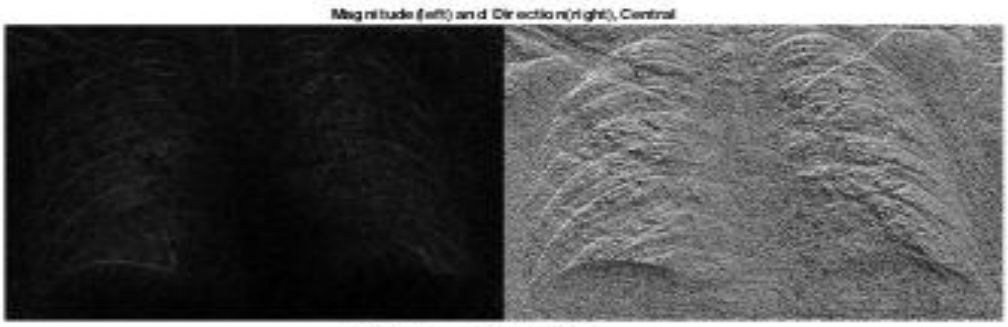
547



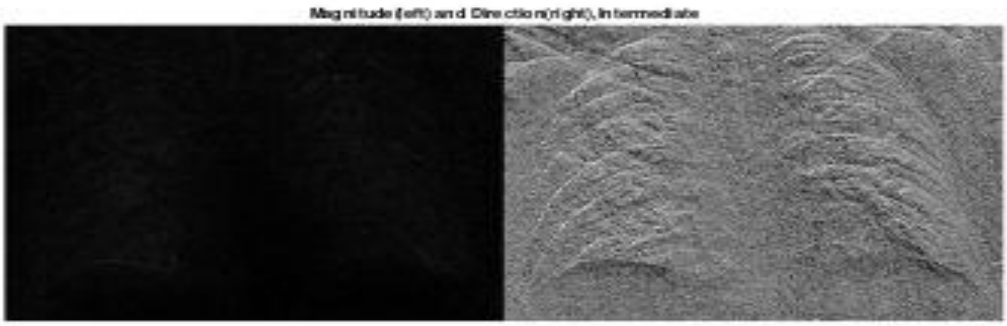
(a) Sobel Method



(b) Prewitt Method



(c) Central Difference



(d) Intermediate Difference

Fig. 48: X-Ray Gradient Magnitude and Direction,Day3

548

549

550

5.4. Directional Gradients

In this subsection, the directional gradient of the single precision X-Ray of Day 3 (Fig 46(a)) is plotted using methods of Sobel, Prewitt, central difference and intermediate difference. These are shown in Fig. 49.

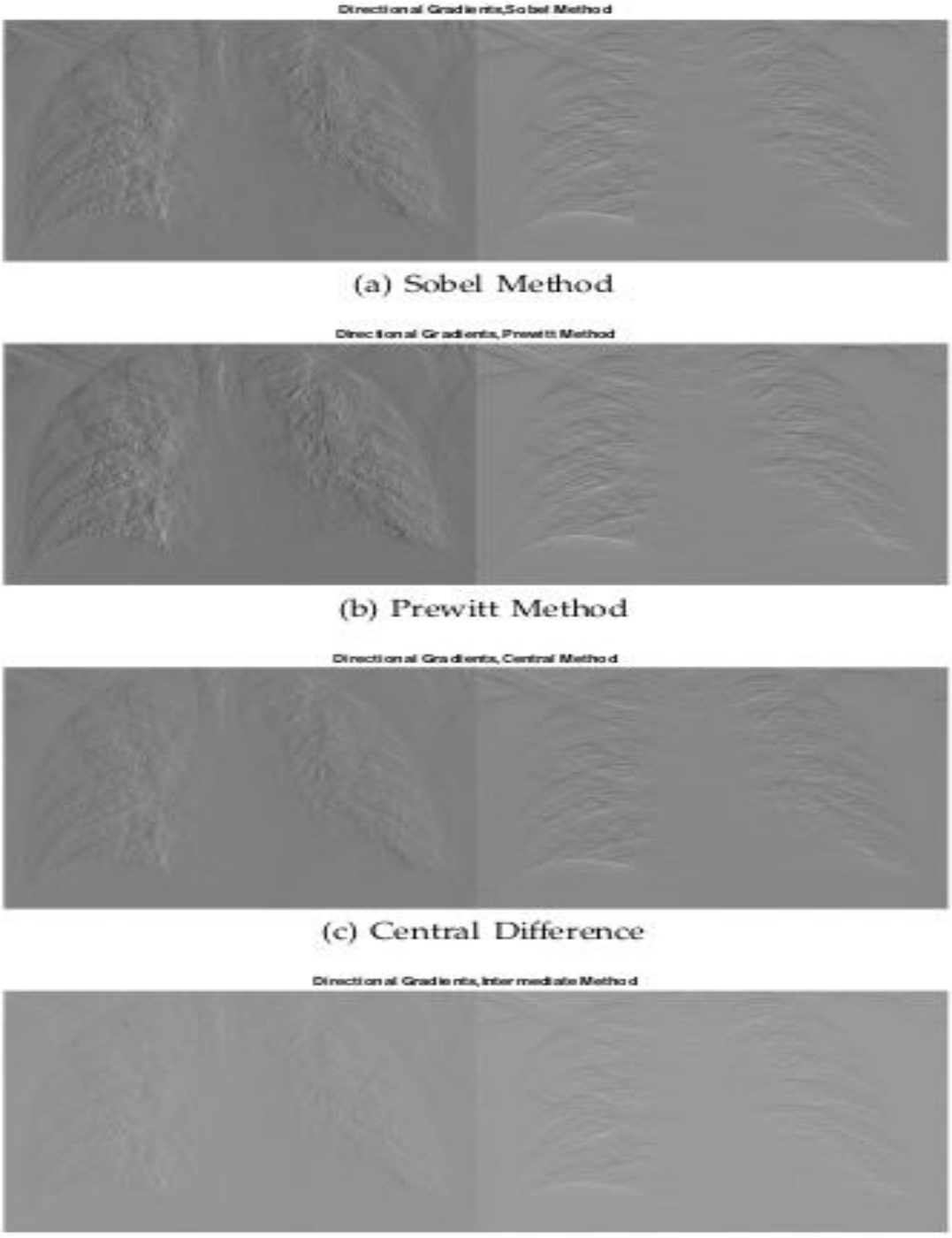
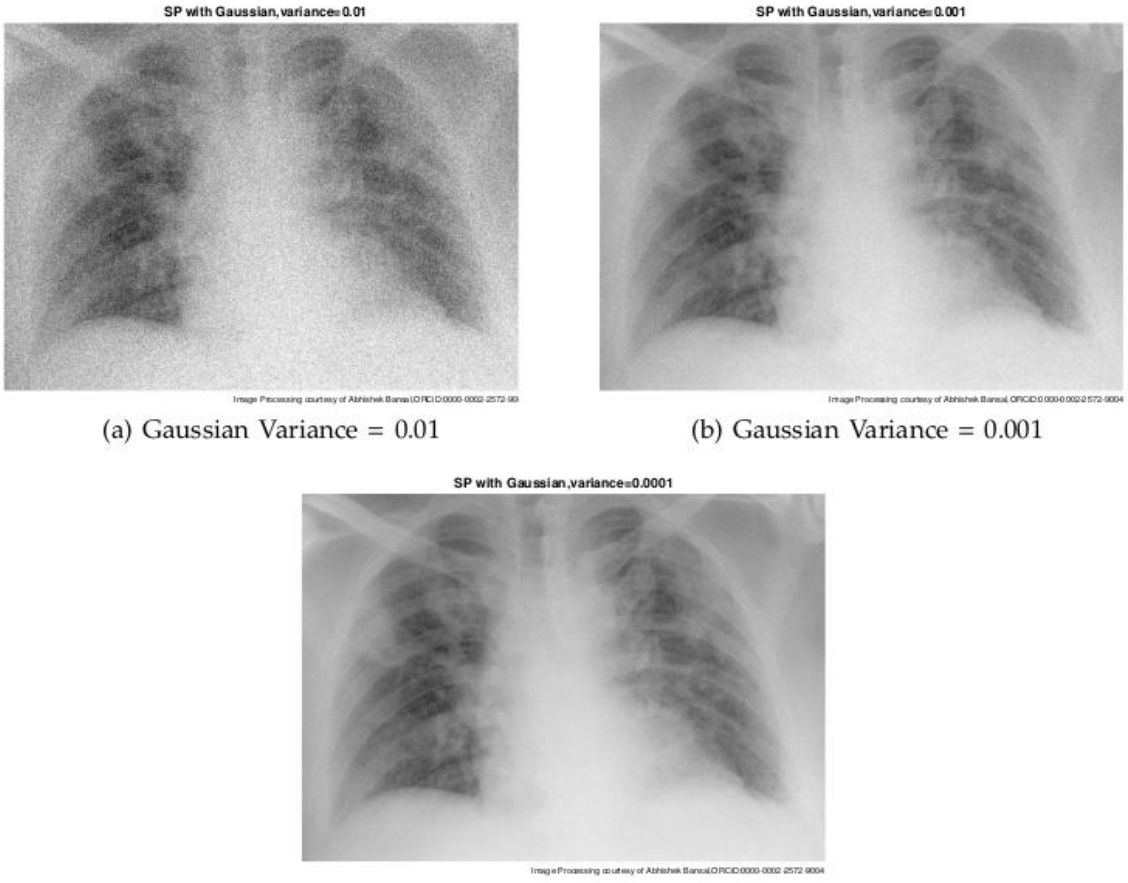


Fig. 49: Directional Gradients,Day3

5.5. Gaussian Noises & Sobel Gradient

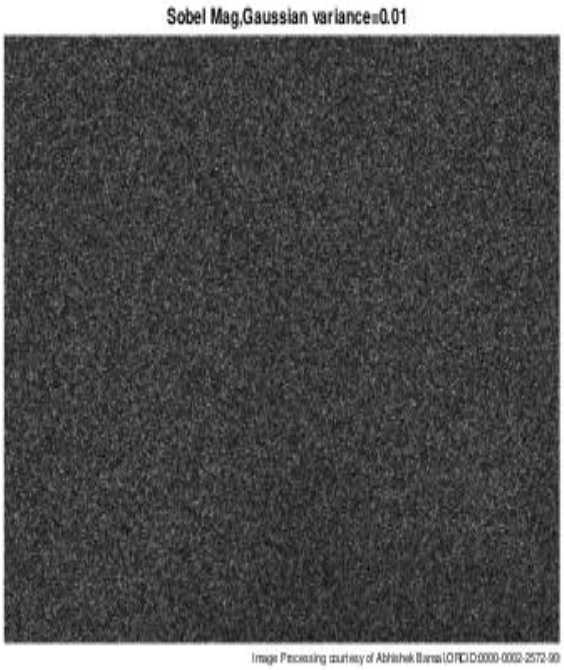
In this subsection, the single precision X-Ray of Day 3 (Fig 46(a)) is subjected to Gaussian noise with three variances of 0.01, 0.001 and 0.0001. These are shown in Fig. 50. The gradient magnitude of these noisy X-Rays are plotted using Sobel method, which are shown in Fig. 51. The figures of gradient magnitude of Fig. 50 are further smoothed using 2-D Gaussian smoothing. The Gaussian smoothing and central difference gradient are shown in Fig. 52. The Gaussian smoothing and intermediate difference gradient are shown in Fig. 53.



(a) Gaussian Variance = 0.01 (b) Gaussian Variance = 0.001

(c) Gaussian Variance = 0.0001

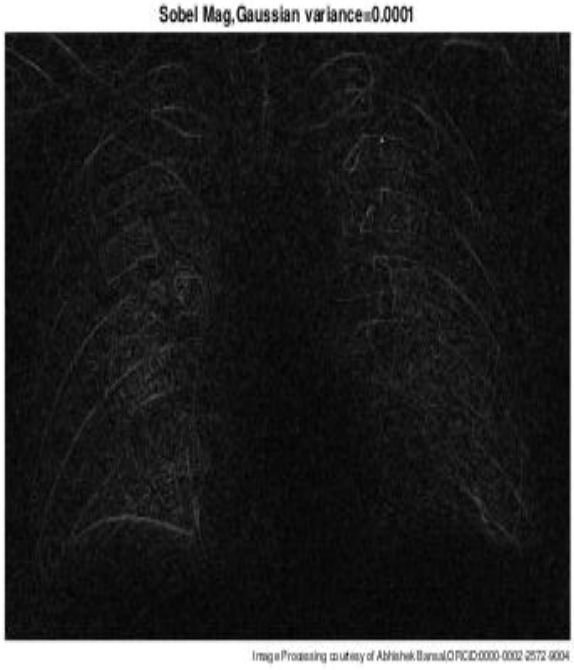
Fig. 50: Gaussian White Noise added to Image,Day3



(a) Gaussian Variance = 0.01



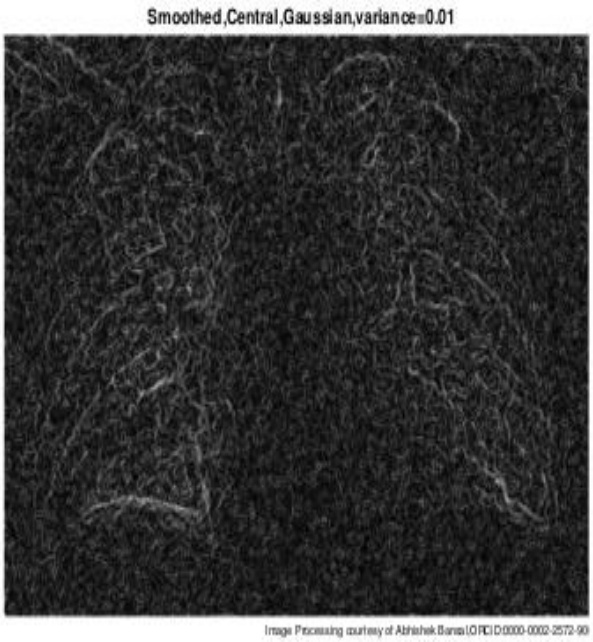
(b) Gaussian Variance = 0.001



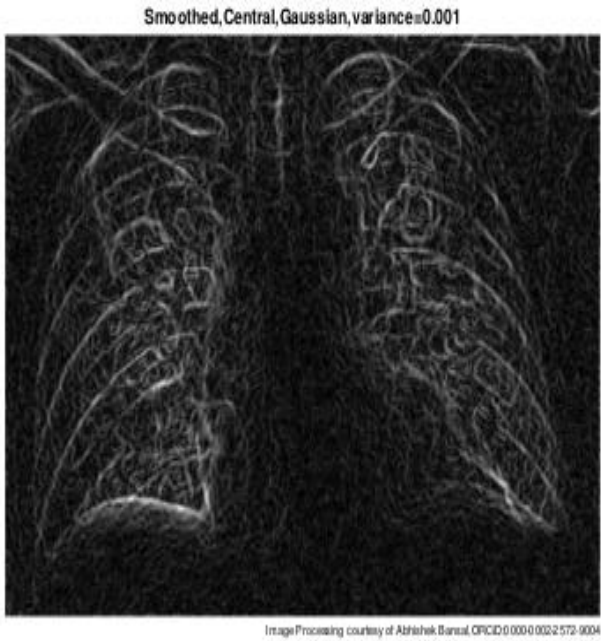
(c) Gaussian Variance = 0.0001

Fig. 51: Gradient of Noisy X-Ray using Sobel Method,Day3

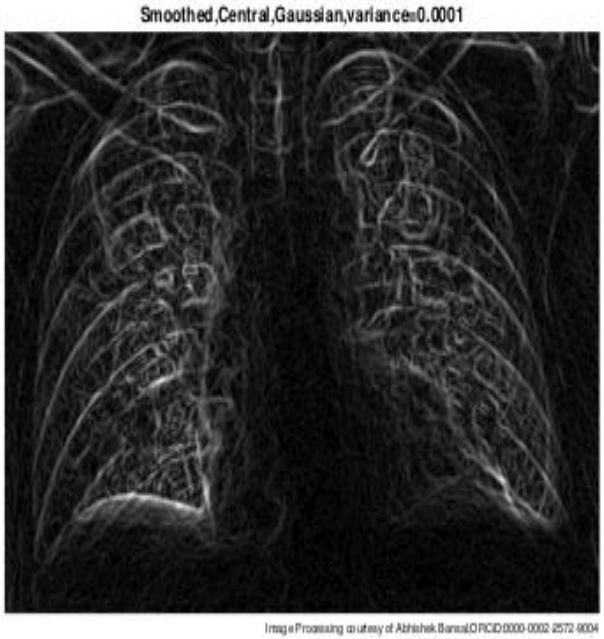
568



(a) Gaussian Variance = 0.01



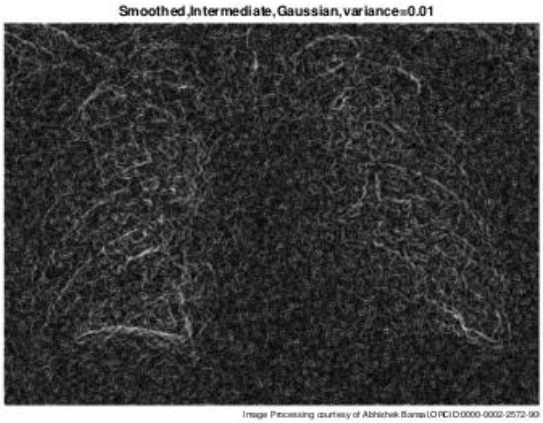
(b) Gaussian Variance = 0.001



(c) Gaussian Variance = 0.0001

Fig. 52: Gaussian smoothing & central difference gradient,Day3

569



(a) Gaussian Variance = 0.01



(b) Gaussian Variance = 0.001



(c) Gaussian Variance = 0.0001

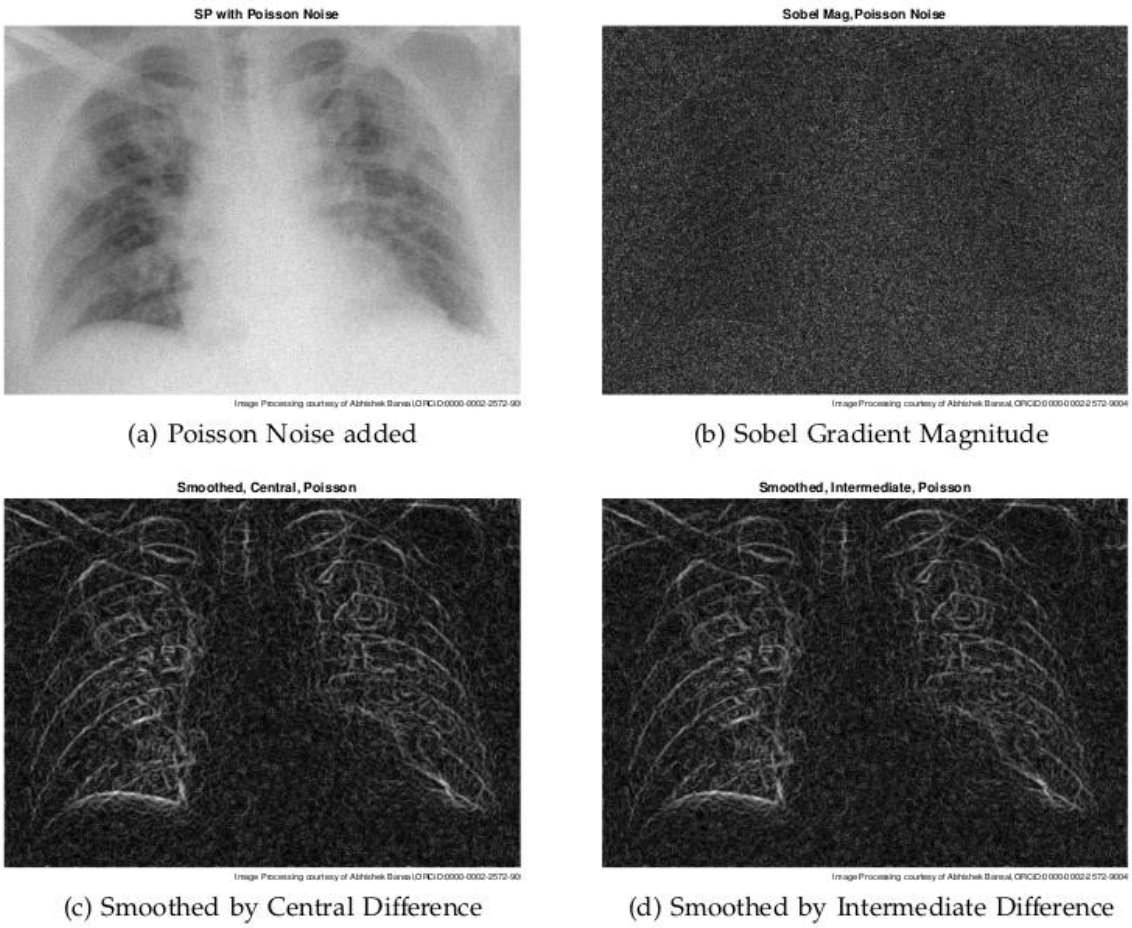
Fig. 53: Gaussian smoothing & intermediate difference gradient,Day3

570
571

572 5.6. Poisson Noise & Sobel Gradient

573 In this subsection, the single precision X-Ray of Day 3 (Fig 46(a)) is subjected to
574 Poisson Noise,Fig. 54(a). The gradient magnitude of Poisson noise X-Ray is plotted
575 using Sobel method, which are shown in Fig. 54(b). This is further smoothed using
576 2-D Gaussian smoothing and central difference gradient in Fig. 54(c); and 2-D Gaussian
577 smoothing and intermediate difference gradient in Fig. 54(d).

578



(a) Poisson Noise added (b) Sobel Gradient Magnitude

(c) Smoothed by Central Difference (d) Smoothed by Intermediate Difference

Fig. 54: Poisson Noise & Gradient Magnitude,Day3

579

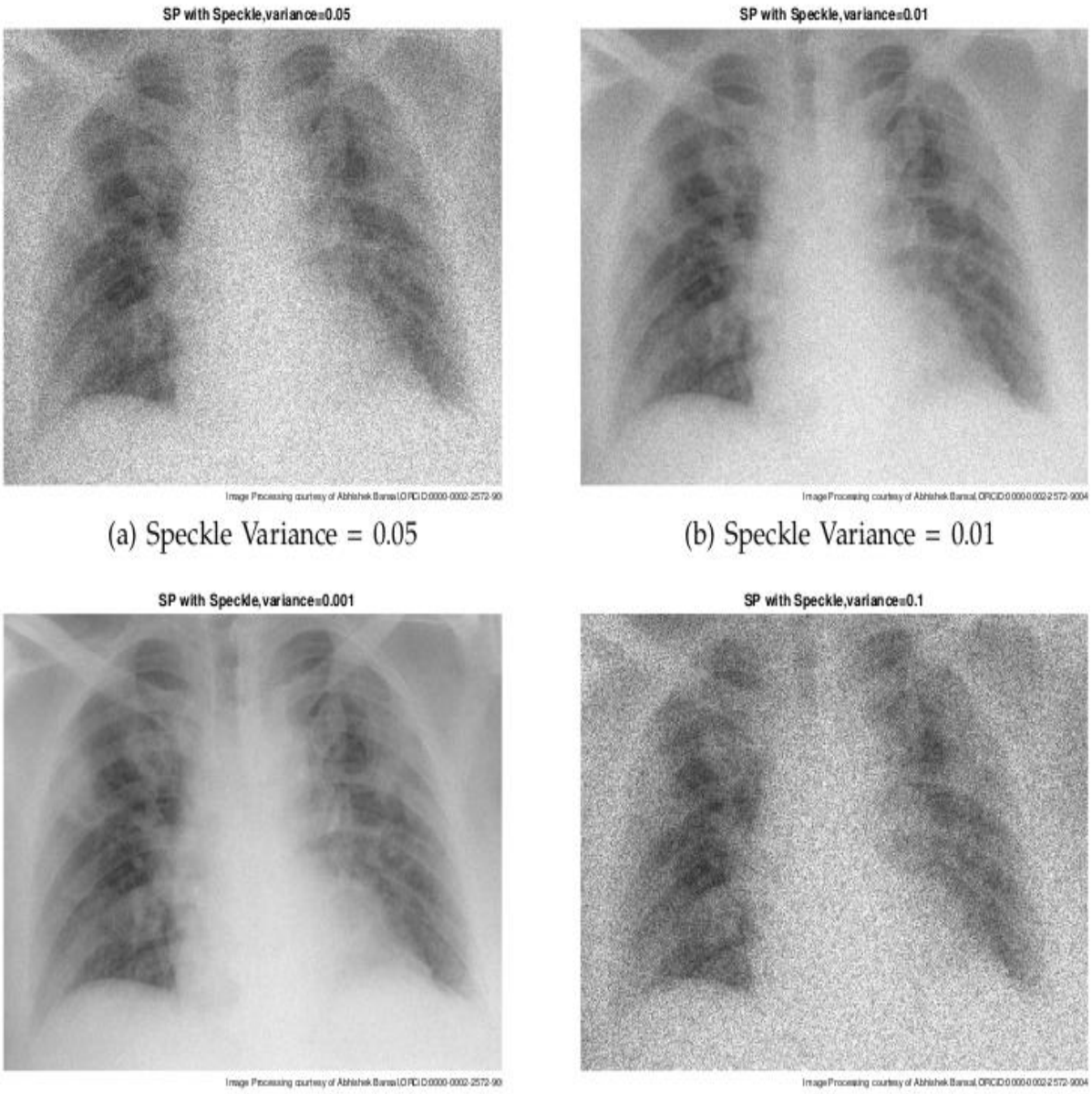
580

581 5.7. Speckle Noise & Sobel Gradient

582 In this subsection, the single precision X-Ray of Day 3 (Fig 46(a)) is subjected to
583 Speckle noise with four variances of 0.05, 0.01, 0.001 and 0.1. These are shown in
584 Fig. 55[a-d]. The gradient magnitude of these noisy X-Rays are plotted using Sobel
585 method, which are shown in Fig. 56. These are further smoothed using 2-D Gaussian
586 smoothing. The Gaussian smoothing and central difference gradient are shown in Fig.
587 57. The Gaussian smoothing and intermediate difference gradient are shown in Fig. 58.

588

589



(a) Speckle Variance = 0.05

(b) Speckle Variance = 0.01

(c) Speckle Variance = 0.001

(d) Speckle Variance = 0.1

Fig. 55: Speckle Noise added to Image,Day3

590

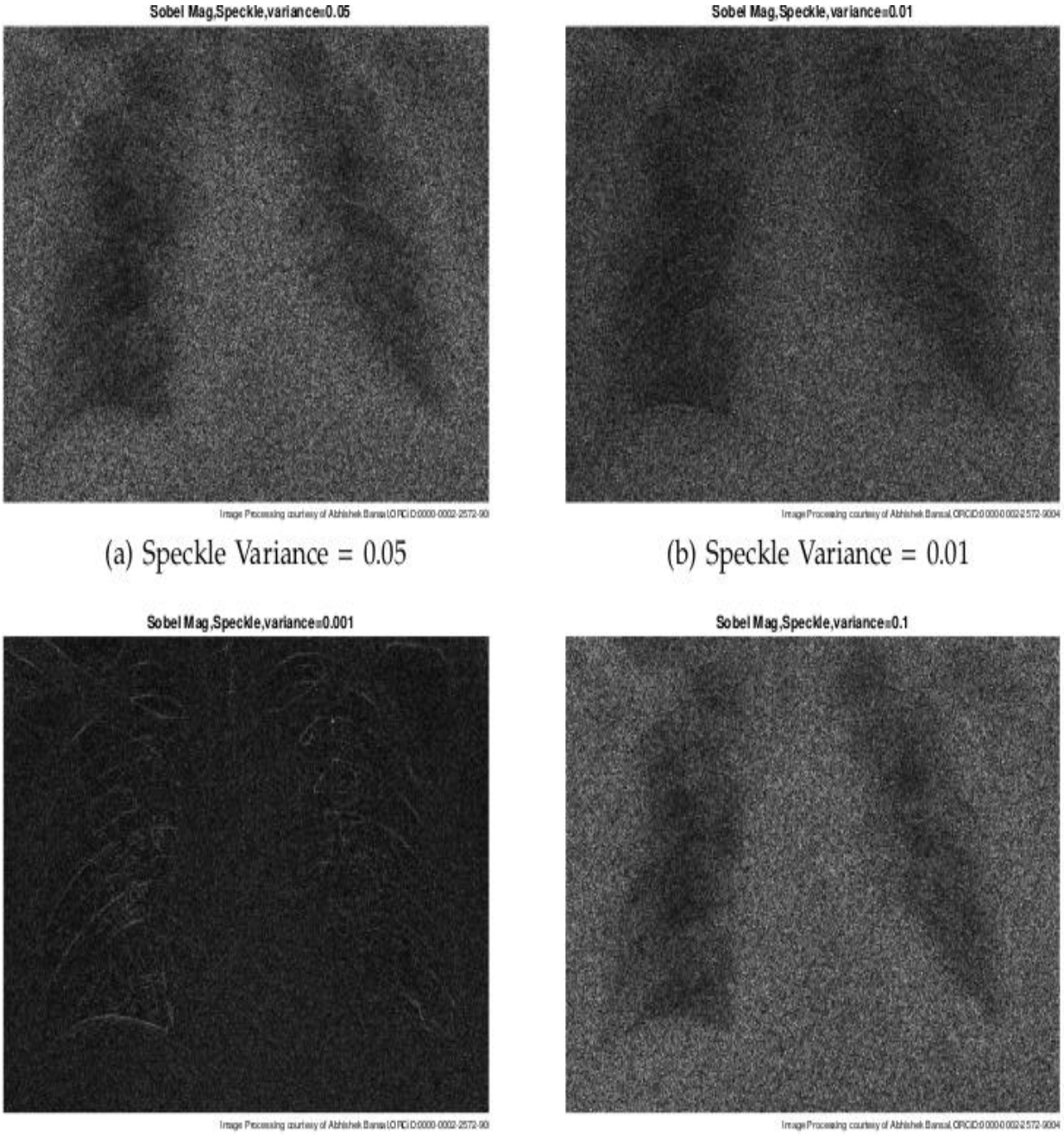
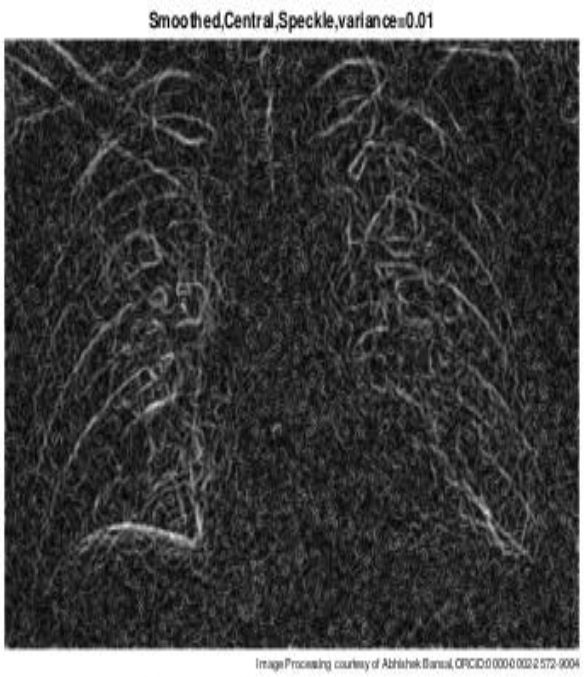


Fig. 56: Gradient of Noisy X-Ray using Sobel Method,Day3

591



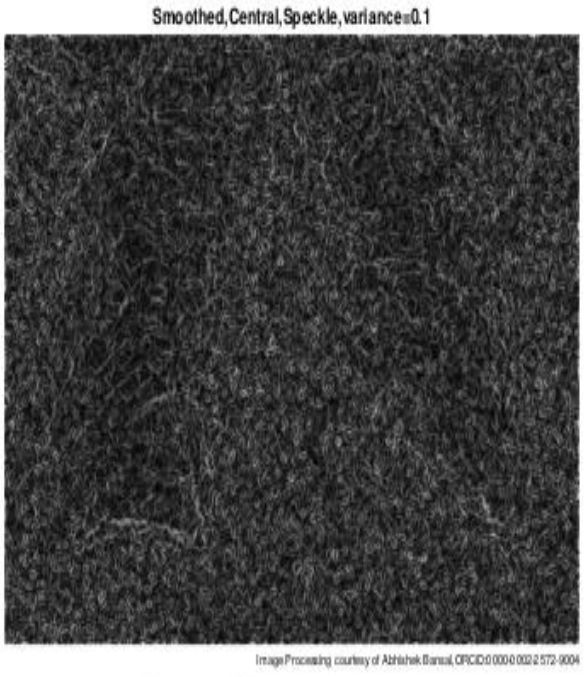
(a) Speckle Variance = 0.05



(b) Speckle Variance = 0.01



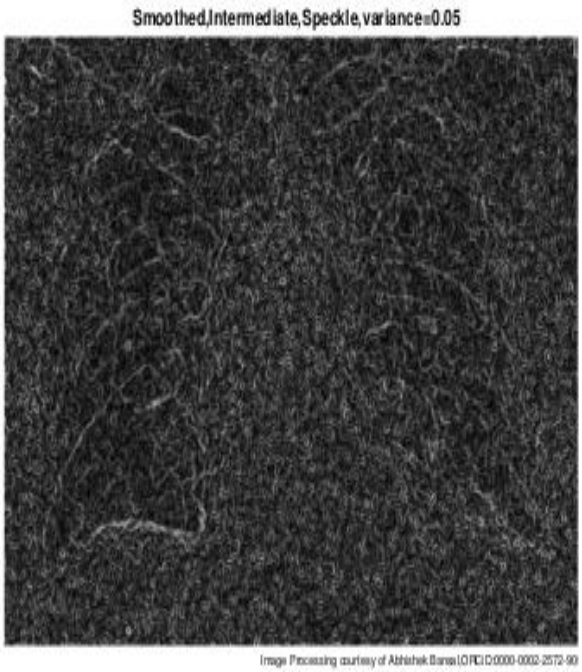
(c) Speckle Variance = 0.001



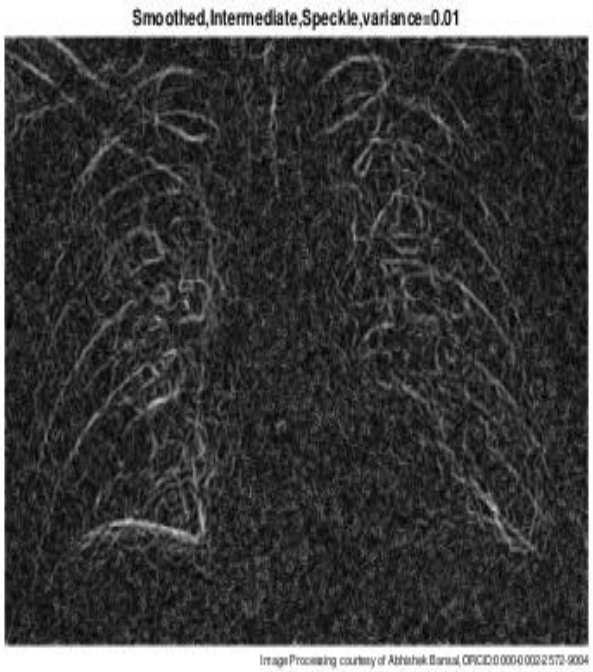
(d) Speckle Variance = 0.1

Fig. 57: Gaussian smoothing & central difference gradient,Day3

592



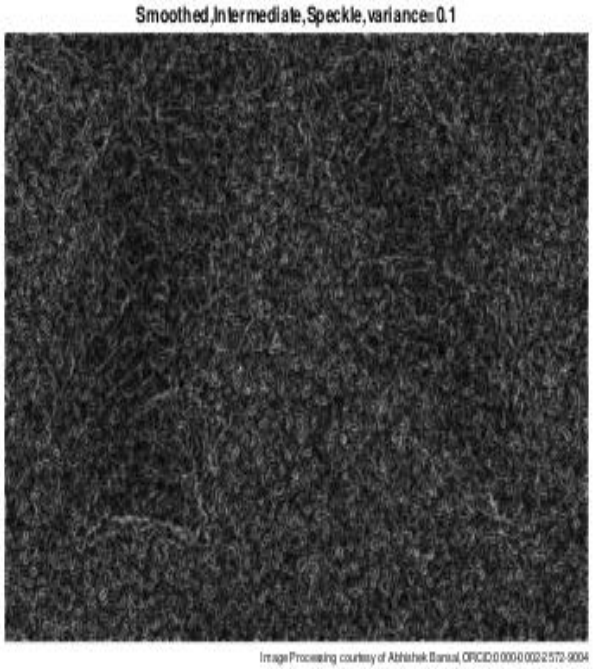
(a) Speckle Variance = 0.05



(b) Speckle Variance = 0.01



(c) Speckle Variance = 0.001



(d) Speckle Variance = 0.1

Fig. 58: Gaussian smoothing & intermediate difference gradient,Day3

International Journal of Advanced Computing and Intelligent System (IJACIS)
Volume 1, Issue 1 (2023)
DOI: 10.66917/ijacis.a000003
https://msis-press.com/journals/ijacis

5.8. Pixel Intensities & Contrast

In this subsection, the original X-Ray (without converting to single precision or double precision) is contrasted for study and analysis.

Let the center fit

$$z = \frac{(x - 127.5)}{74.05}$$

then from polynomial regression

$$y = 1911 \times z^9 + 949.3 \times z^8 - 1.239 \times 10^4 \times z^7 - 5847 \times z^6 + 2.778 \times 10^4 \times z^5 + 1.157 \times 10^4 \times z^4 - 2.885 \times 10^4 \times z^3 - 1.135 \times 10^4 \times z^2 + 1.716 \times 10^4 \times z + 1.064 \times 10^4$$

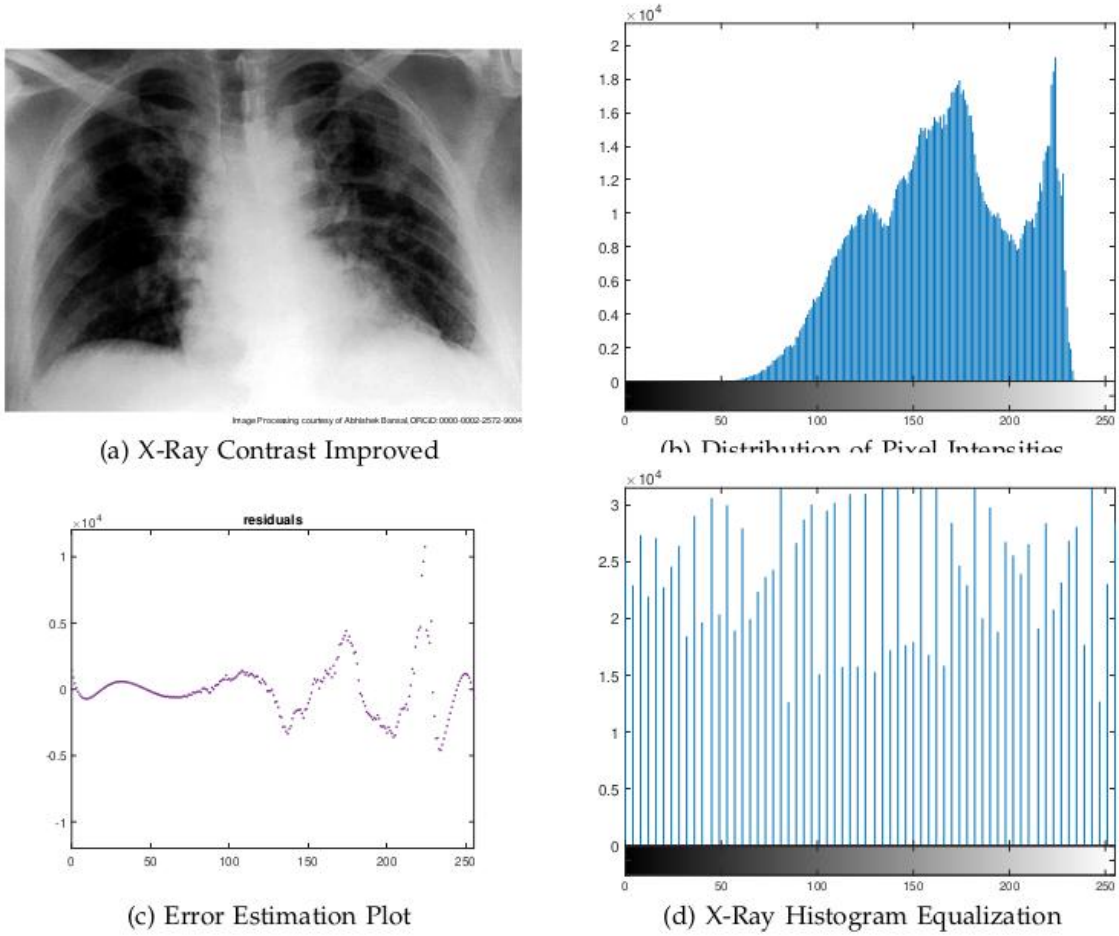
Let $\bar{y}$ be the mean of y, $\hat{y}$ the calculated values of y, then the coefficient of determination, R^2

$$R^2 = 1 - \frac{\sum_{i=1}^{n} (y_i - \hat{y})^2}{\sum_{i=1}^{n} (y_i - \bar{y})^2} = 0.8837$$

607

The measure of the goodness of fit given by norm of residuals is 3.244 × 104 . Here, the polynomial of degree 9 chosen here is the global which can be focused on the areas of interest (to be decided by infection part or researchers/doctors interest) and separate equations can be obtained for each particular area of interest. This gives insight in mathematical formulation and has been used in the Novel B-Mathematical Modeling of Respiratory System.

The Fig.59(a) shows that X-Ray contrast is improved for analysis when compared with Fig. 1(a). Fig. 59(b) shows the distribution of X-Ray pixel intensities. Fig. 59(c) shows the error estimation plot, which is the plot of the residuals. Fig. 59(d) shows the X-Ray histogram equalization which is the spreading of the intensity values over the full range.



(a) X-Ray Contrast Improved

(b) Distribution of Pixel Intensities

(c) Error Estimation Plot

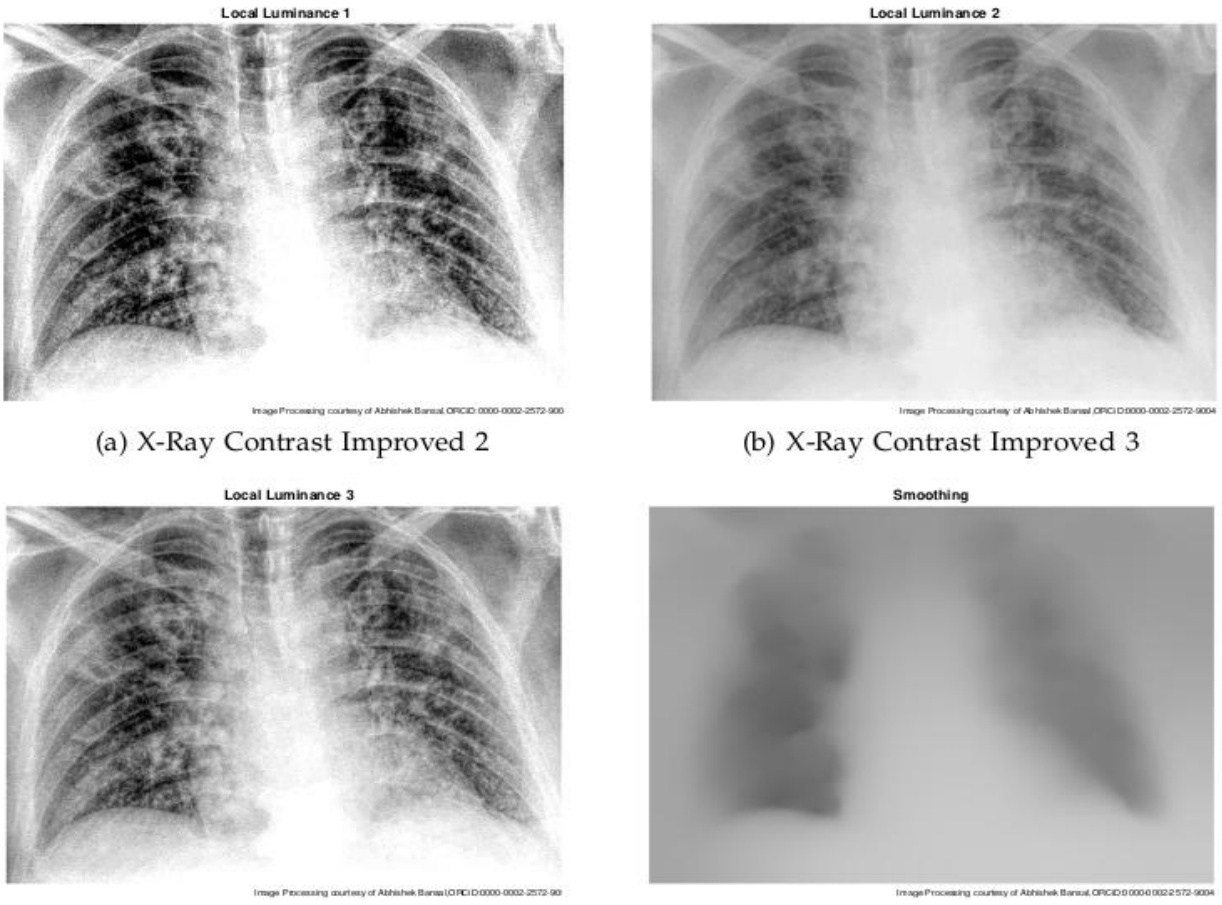
(d) X-Ray Histogram Equalization

Fig. 59: Distribution of Pixel Intensities in X-Ray,Day3

TABLE V: Data Statistics for Fig. 59(b)

	X	Y
min	0	0
max	255	1.929×10^4
mean	127.5	6111
median	127.5	5199
mode	0	0
std deviation	74.05	5956
range	255	1.929×10^4

In Fig. 60, X-Ray Contrast is improved with five local luminances. The original Fig. 46(a) X-Ray contrast is improved with four more local luminances by varying the intensity values at low and high intensities. These are shown in Fig 60(a), Fig. 60(b) and Fig. 60(c). In Fig. 60(d), the original Fig. 46(a) X-Ray is contrasted with fifth value of improvement but smoothing technique is applied after it.



(a) X-Ray Contrast Improved 2 (b) X-Ray Contrast Improved 3

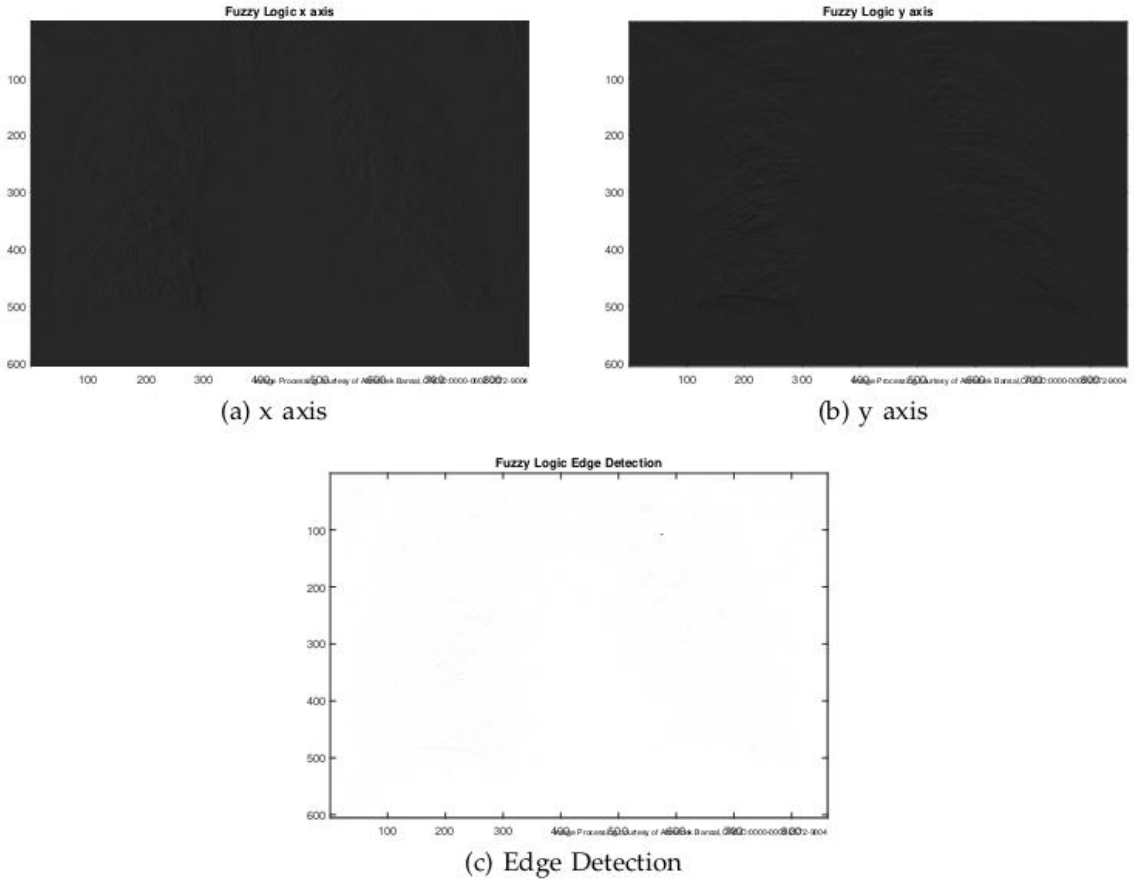
(c) X-Ray Contrast Improved 4 (d) X-Ray Contrast Improved & Smoothed

Fig. 60: X-Ray Contrast Improved with Five Local Luminances,Day3

5.9. Fuzzy Logic

In this subsection, the images obtained using fuzzy logic edge-detection algorithm and Fuzzy Inference System (FIS) are given. Two 2-D Convolution are performed. The x-axis of directional gradient is convolved with x-axis gradients of double-precision X-Ray obtained in Fig. 46(b) and the X-Ray gradient of fuzzy logic x-axis is given in Fig.

61(a). The y-axis of directional gradient is convolved with y-axis gradients of double-precision X-Ray obtained in Fig. 46(b) and the X-Ray gradient of fuzzy logic y-axis is given in Fig. 61(b). The edge detection is shown in Fig. 61(c).



(a) x axis (b) y axis

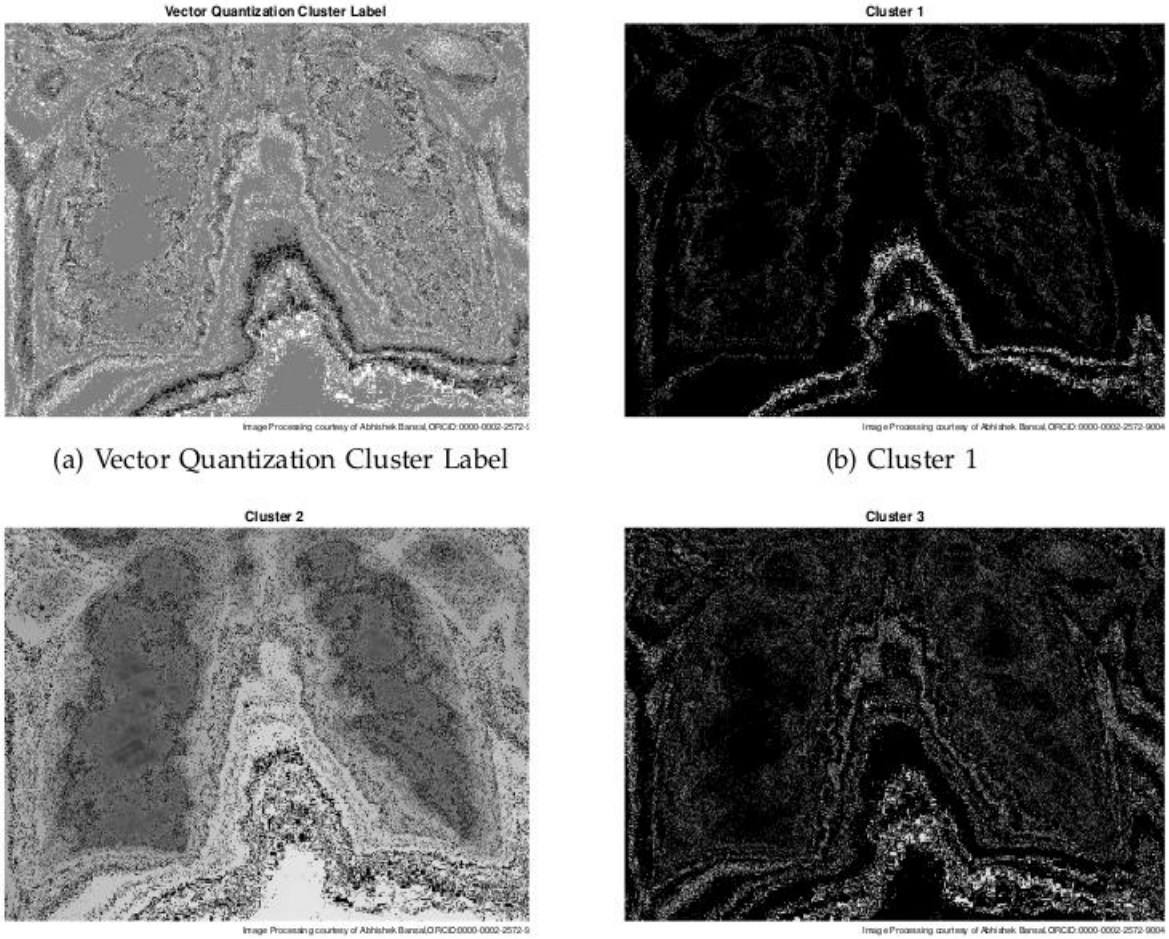
(c) Edge Detection

Fig. 61: Fuzzy Logic,Day3

5.10. K-means Clustering

In this subsection, the popular vector quantization technique of K-Means clustering is applied to X-Ray. In this technique, firstly CIE XYZ tristimulus technique is used to know the color information and thus, the information of luminosity layer 'L*', chromaticity-layer 'a*' and chromaticity-layer 'b*' is obtained. Then every pixel is clustered with its pixel label and partitioned into three clusters. The clustering obtained is shown in Fig. 62(a), Vector Quantization Cluster Label. And three clusters Cluster 1, Cluster 2 and Cluster 3 obtained are shown in Fig. 62(b), Fig. 62(c) and Fig. 62(d)

respectively.



(a) Vector Quantization Cluster Label (b) Cluster 1

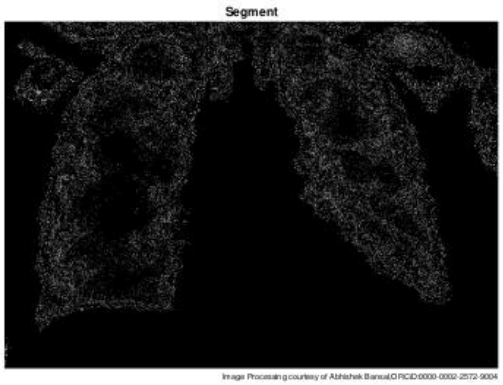
(c) Cluster 2 (d) Cluster 3

Fig. 62: Vector Quantization,K-means Clustering,Day3

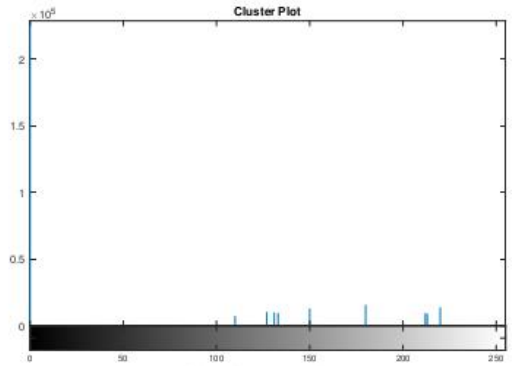
In Fig. 63(a), segmentation is applied and Fig. 63(b) and Fig. 63(c) shows respectively the cluster plot and the plot of error estimation, that is, the plot of residuals.

Moving in similar way as in the Subsection-8 and choosing same

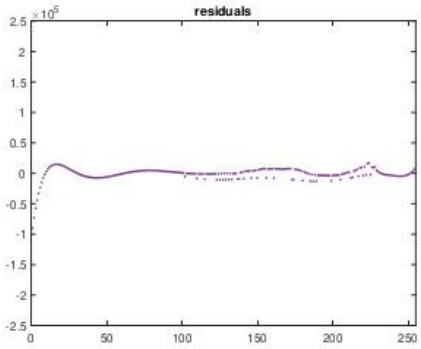
$$z = \frac{(x - 127.5)}{74.05}$$



(a) Segmentation



(b) Cluster Plot



(c) Cluster Plot Residuals

Fig. 63: Clustering Plot and Segment,Day3

665

666 we have,

$$y = -1.369 \times 10^4 \times z^9 + 1.246 \times 10^4 \times z^8 + 7.594 \times 10^4 \times z^7 - 6.079 \times 10^4 \times z^6 - 1.358 \times 10^5 \times z^5 + 9.016 \times 10^4 \times z^4 + 8.192 \times 10^4 \times z^3 - 4.42 \times 10^4 \times z^2 - 4723 \times z + 1.049 \times 10^4$$

667

668 $R^2 = 0.3119$ and Norm of Residuals $= 2.907 \times 10^5$

669 TABLE VI: Data Statistics for Fig. 63(b)

	X	Y
min	0	0
max	255	3.434×10^5
mean	127.5	6111
median	127.5	955.5
mode	0	0
std deviation	74.05	2.194×10^4
range	255	3.434×10^5

5.11. Morphological Segmentation

In this subsection, known morphological segmentation technique is applied on X-Rays. Three morphological openings are used. The morphological opening with structuring element of disk shaped with three different radius are shown in Fig. 64(a), Fig. 64(c) and Fig. 65(a). The background approximation images of X-Ray obtained after subtracting from the original image are shown in Fig. 64(b), Fig. 64(d) and Fig. 65(b).



(a) Morphological Opening 1



(b) Background Approximation Removed from Fig. 19(a)

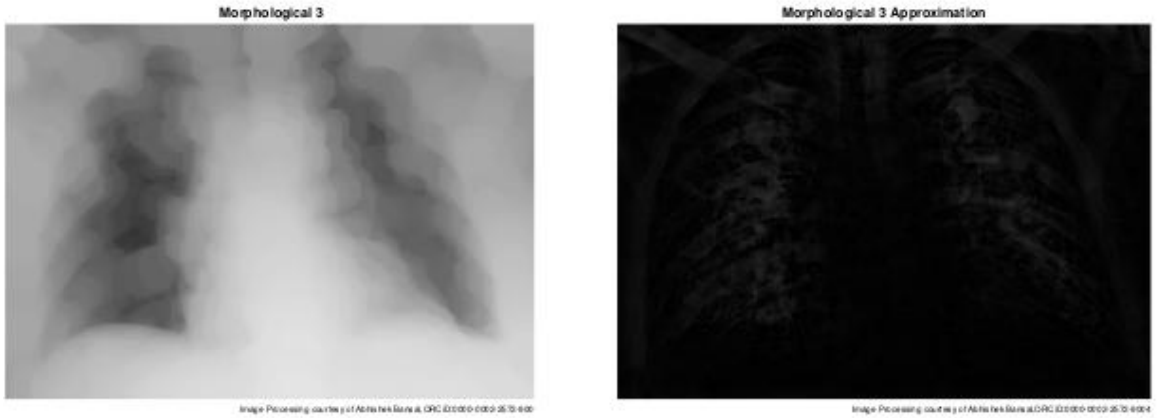


(c) [Morphological Opening 2



(d) Background Approximation Removed from Fig. 19(c)

Fig. 64: Morphological Segmentation,Day3



(a) Morphological Opening 3

(b) Background Approximation Removed from Fig. 20(a)

Fig. 65: Morphological Segmentation,Day3

679

680

681

682 5.12. Dehazing Algorithm

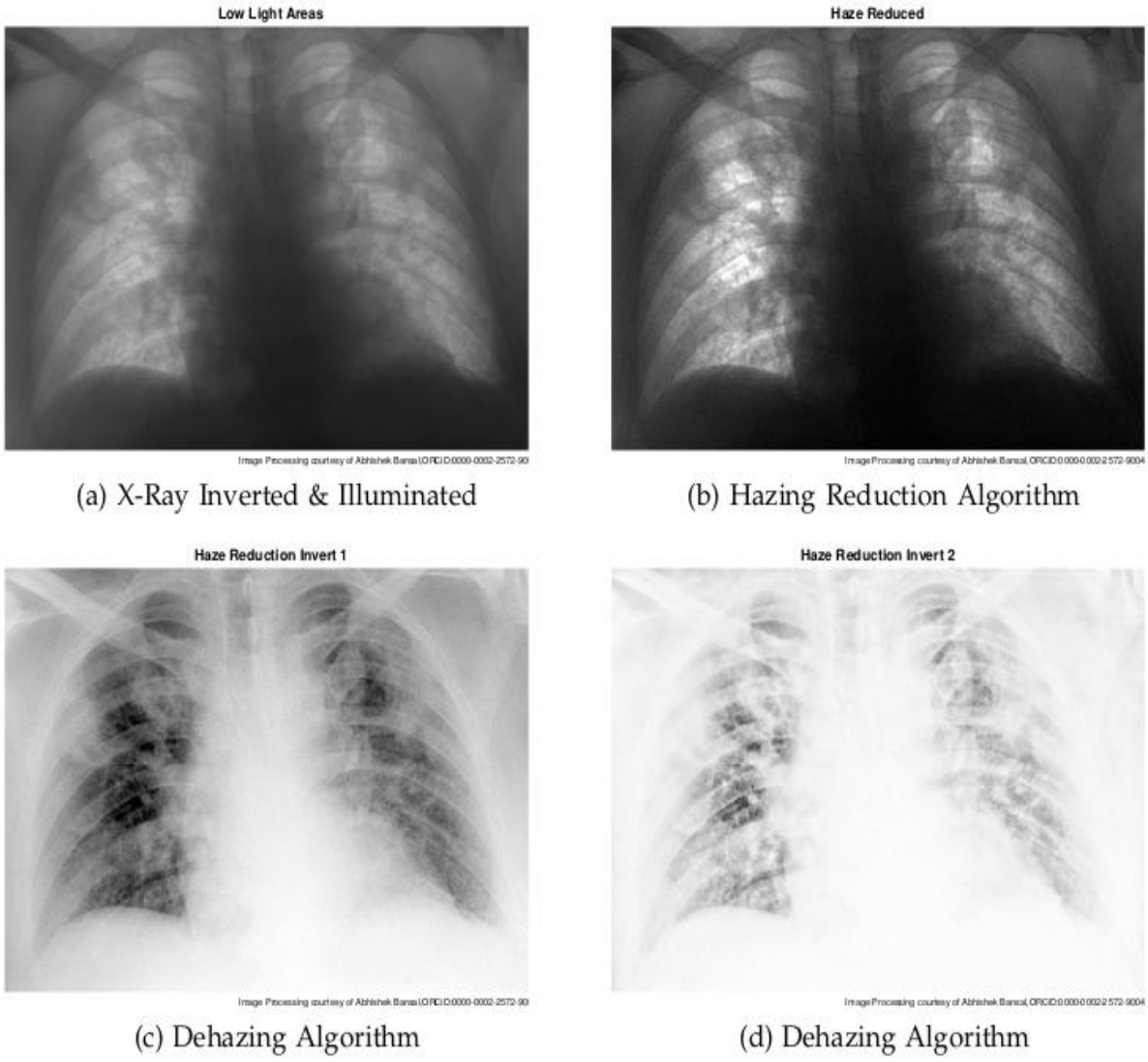
683 In Fig. 66(a), the original Fig. 46(a) X-Ray is inverted and the low-light areas and

684 focused and the new X-Ray is obtained.

685

686 The hazing obtained in Fig. 66(a) is reduced by hazing reduction algorithm.

687



(a) X-Ray Inverted & Illuminated

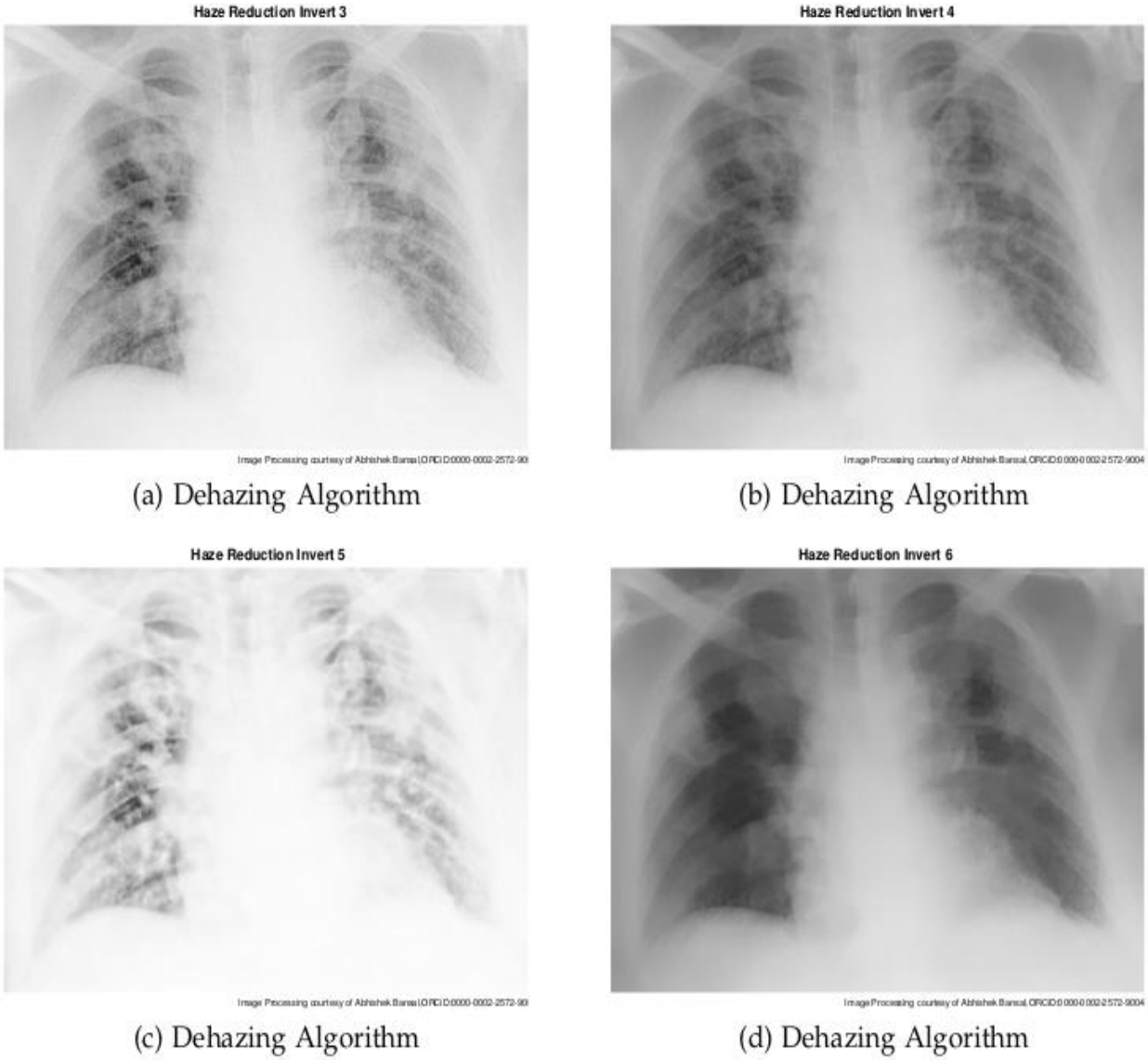
(b) Hazing Reduction Algorithm

(c) Dehazing Algorithm

(d) Dehazing Algorithm

Fig. 66: Dehazing Algorithm,Day3

On the new X-Ray of Fig. 66(b), dehazing algorithm is applied and its result is in Fig.66(c,d). Fig. 67[a-d] has four more such combinations on which dehazing algorithm is implemented.



(a) Dehazing Algorithm (b) Dehazing Algorithm

(c) Dehazing Algorithm (d) Dehazing Algorithm

Fig. 67: Dehazing Algorithm,Day3

694

695

696

697 **6. Results : Day 4, PA**

698

699 6.1. X-Ray Converted

700 In this subsection, X-Ray(PA) of Day 4 is converted to single precision gray-scale and

701 double precision, on which all further image processings will be done. These are shown

702 in Fig. 68.



(a) Single Precision (b) Double Precision

Fig. 68: Converted to Single Precision & Double Precision,Day4

703

704

705

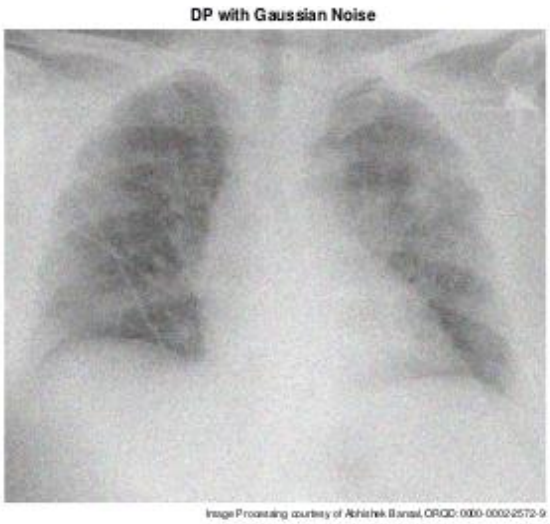
706 6.2. Double Precision Noise Addition

707 In this subsection, the double precision X-Ray of Day 4 (Fig 68(b)) of the previous

708 subsection is subjected to noises namely Gaussian with variance 0.01, Poisson Noise

709 and speckle noise with variance 0.05. These are shown in Fig. 69.

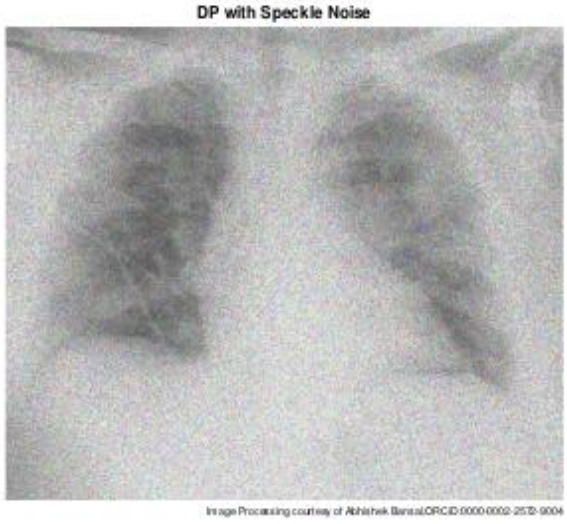
710



(a) Gaussian Noise



(b) Poisson Noise



(c) Speckle Noise

Fig. 69: Noises Added to Double Precision,Day4

711

712

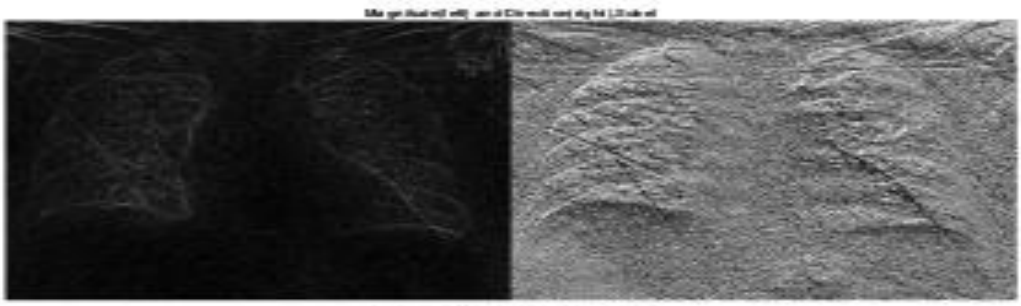
713 6.3. Gradient Magnitude and Direction

714 In this subsection, the gradient of the single precision X-Ray of Day 4 (Fig 68(a)) is

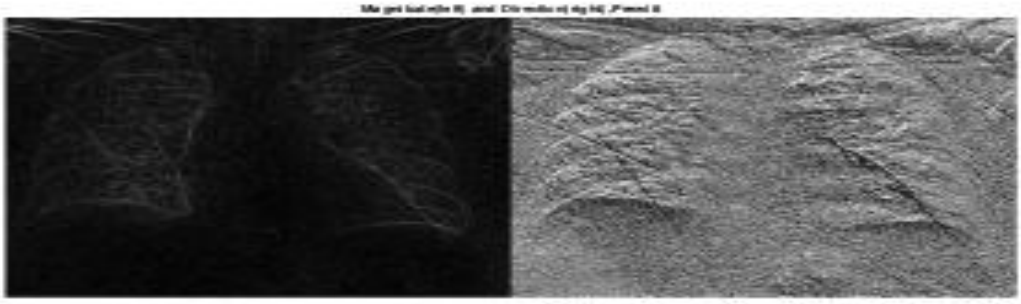
715 obtained and its magnitude and direction is plotted using methods of Sobel, Prewitt,

716 central difference and intermediate difference. These are shown in Fig. 70.

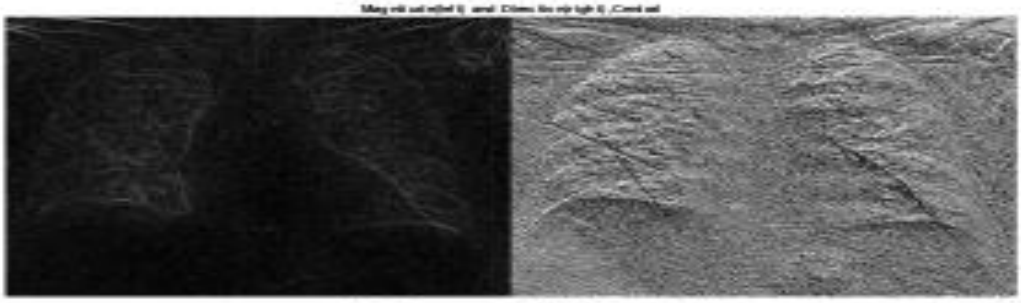
717



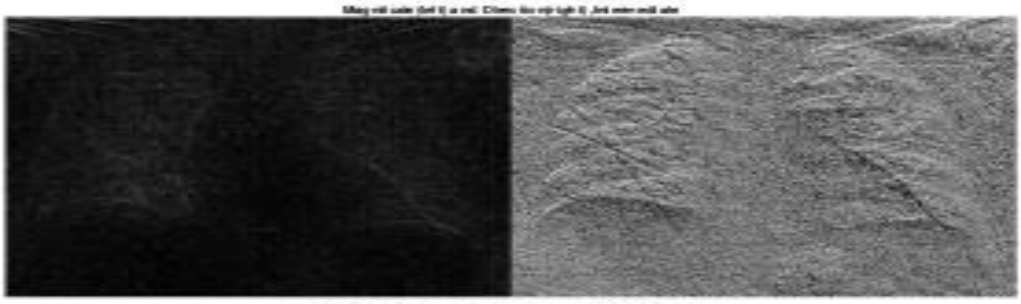
(a) Sobel Method



(b) Prewitt Method



(c) Central Difference



(d) Intermediate Difference

Fig. 70: X-Ray Gradient Magnitude and Direction,Day4

718

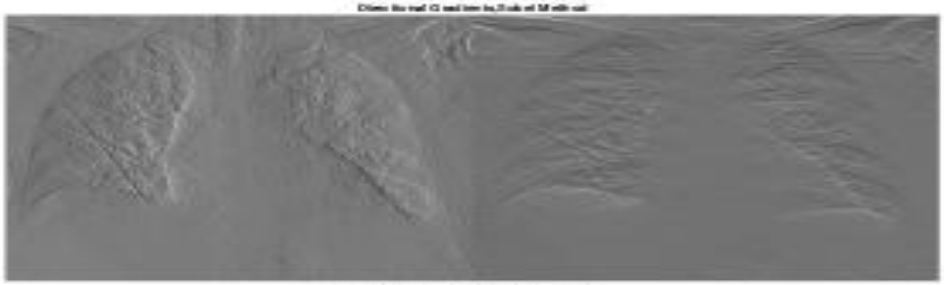
719

720

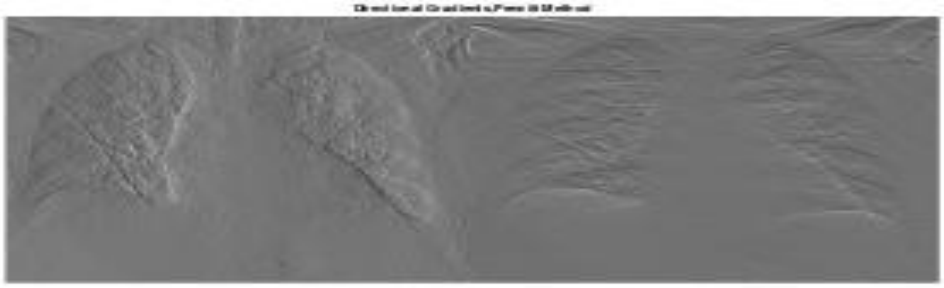
721 6.4. Directional Gradients

722 In this subsection, the directional gradient of the single precision X-Ray of Day 4 (Fig
723 68(a)) is plotted using methods of Sobel, Prewitt, central difference and intermediate
724 difference. These are shown in Fig. 71.

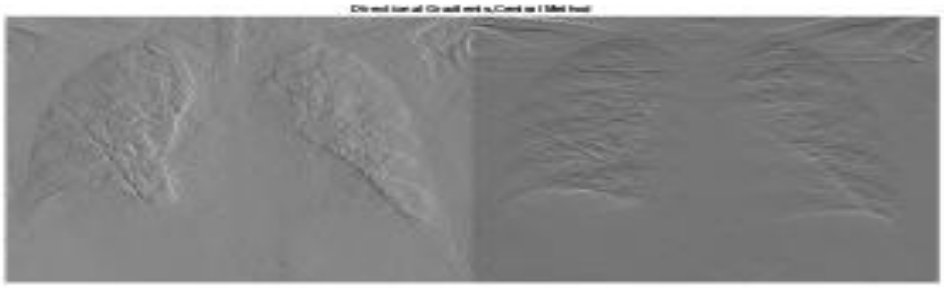
725



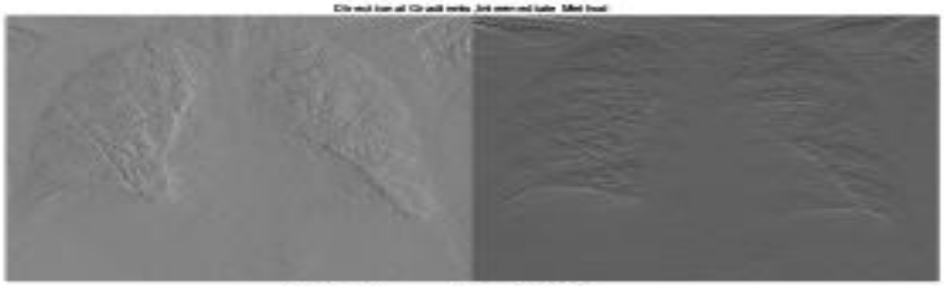
(a) Sobel Method



(b) Prewitt Method



(c) Central Difference

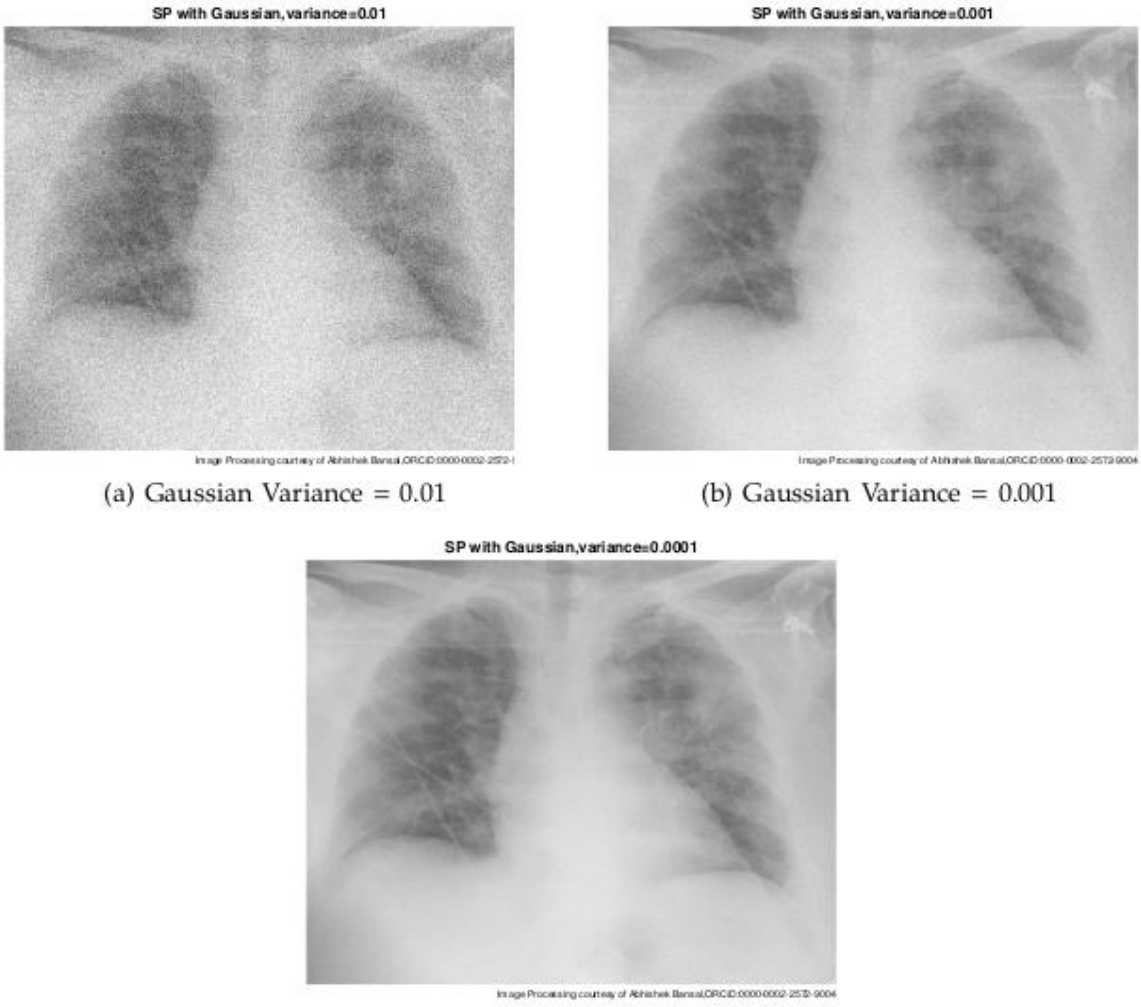


(d) Intermediate Difference

Fig. 71: Directional Gradients,Day4

6.5. Gaussian Noises & Sobel Gradient

In this subsection, the single precision X-Ray of Day 4 (Fig 68(a)) is subjected to Gaussian noise with three variances of 0.01, 0.001 and 0.0001. These are shown in Fig. 72. The gradient magnitude of these noisy X-Rays are plotted using Sobel method, which are shown in Fig. 73. The figures of gradient magnitude of Fig. 73 are further smoothed using 2-D Gaussian smoothing. The Gaussian smoothing and central difference gradient are shown in Fig. 74. The Gaussian smoothing and intermediate difference gradient are shown in Fig. 75.

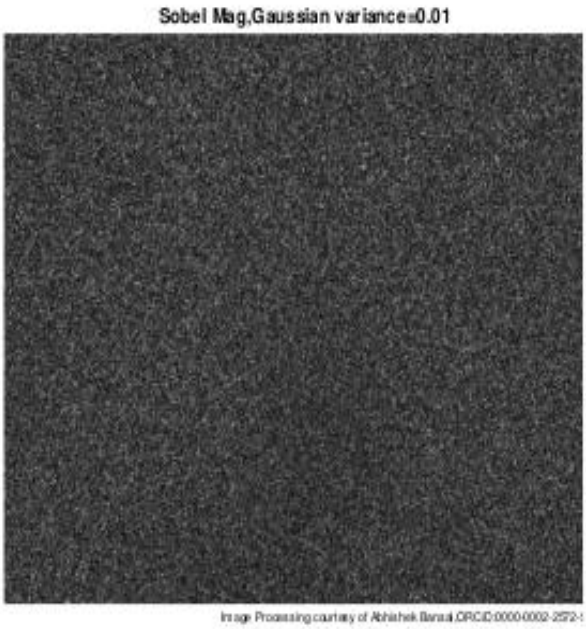


(a) Gaussian Variance = 0.01

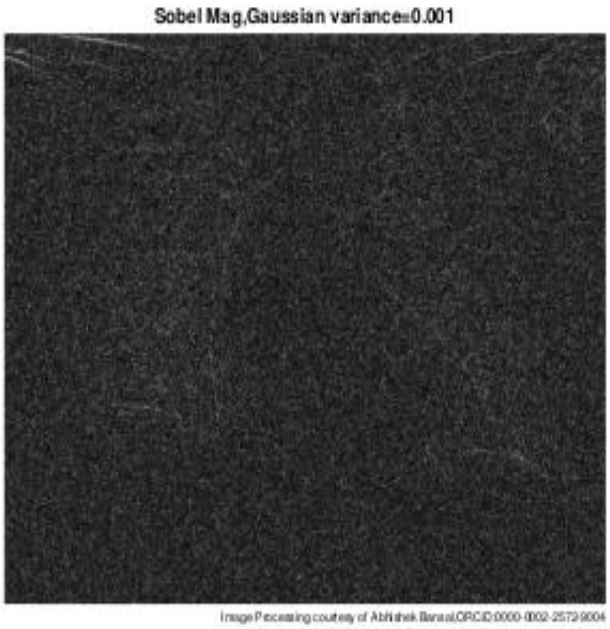
(b) Gaussian Variance = 0.001

(c) Gaussian Variance = 0.0001

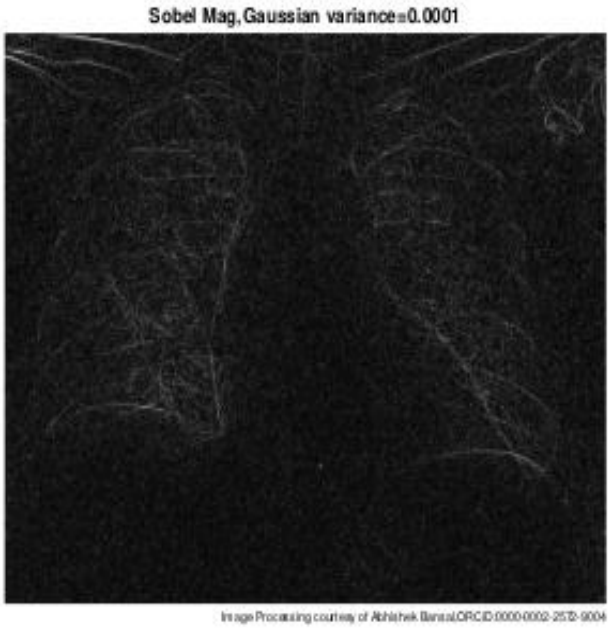
Fig. 72: Gaussian White Noise added to Image,Day4



(a) Gaussian Variance = 0.01



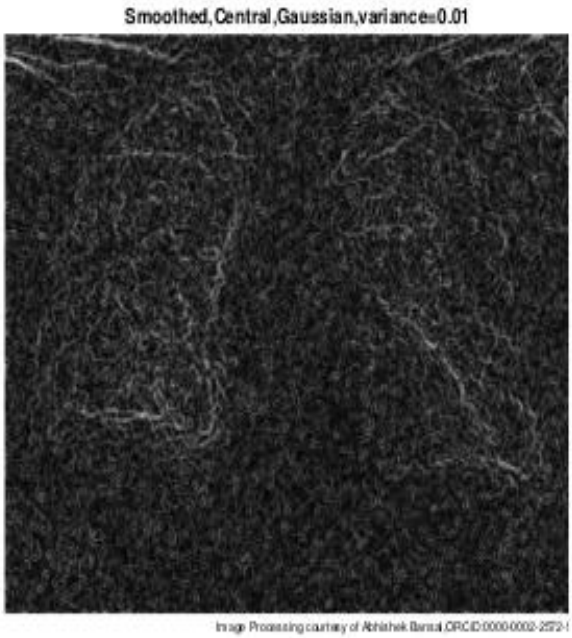
(b) Gaussian Variance = 0.001



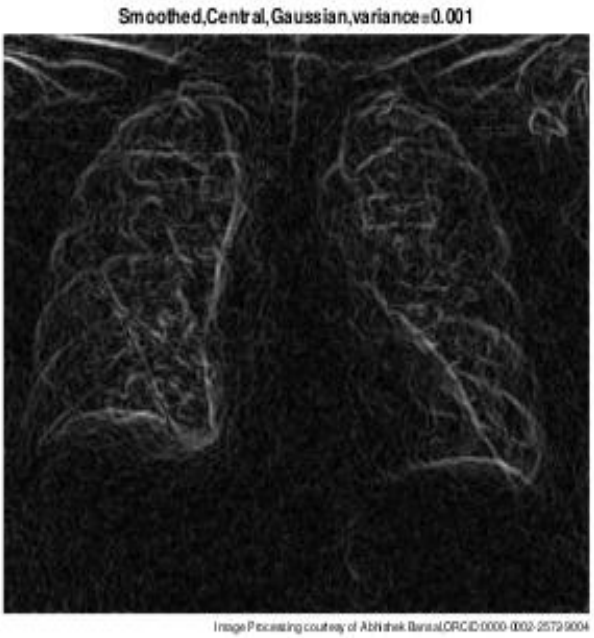
(c) Gaussian Variance = 0.0001

Fig. 73: Gradient of Noisy X-Ray using Sobel Method,Day4

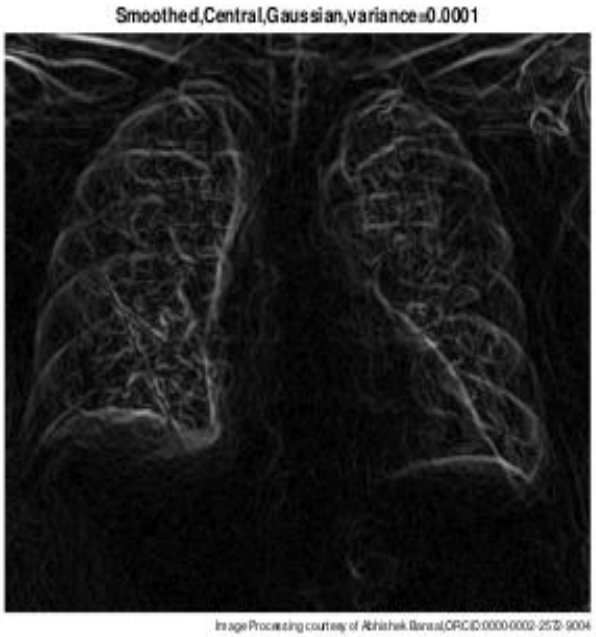
International Journal of Advanced Computing and Intelligent System (IJACIS)
Volume 1, Issue 1 (2023)
DOI: 10.66917/ijacis.a000003
https://msis-press.com/journals/ijacis



(a) Gaussian Variance = 0.01



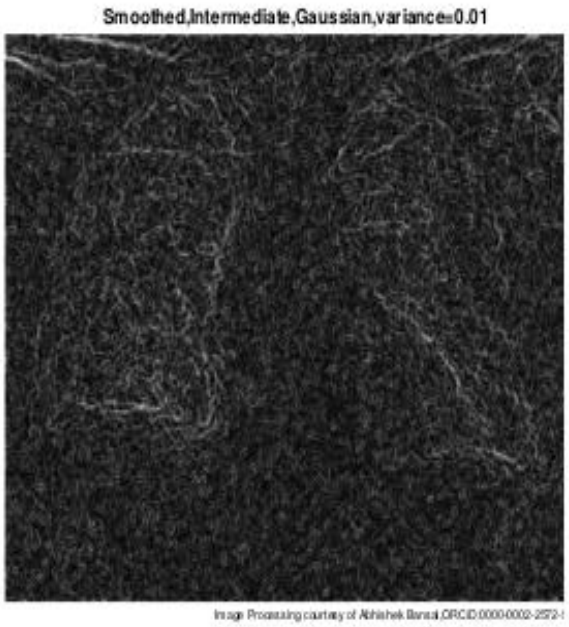
(b) Gaussian Variance = 0.001



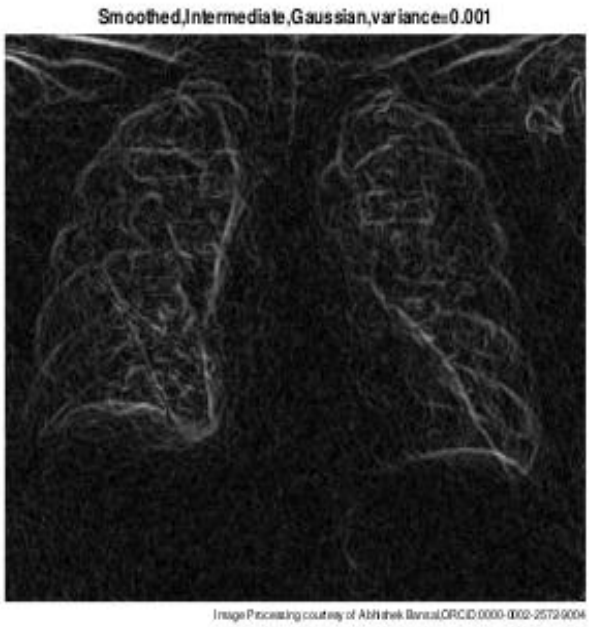
(c) Gaussian Variance = 0.0001

Fig. 74: Gaussian smoothing & central difference gradient,Day4

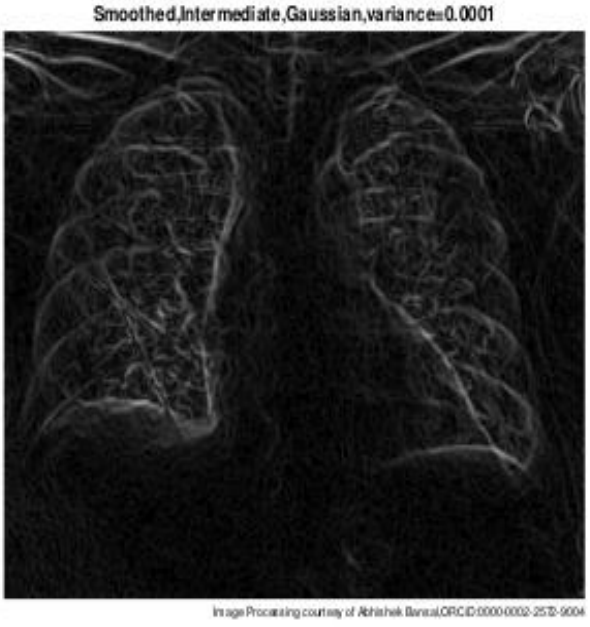
International Journal of Advanced Computing and Intelligent System (IJACIS)
Volume 1, Issue 1 (2023)
DOI: 10.66917/ijacis.a000003
https://msis-press.com/journals/ijacis



(a) Gaussian Variance = 0.01



(b) Gaussian Variance = 0.001



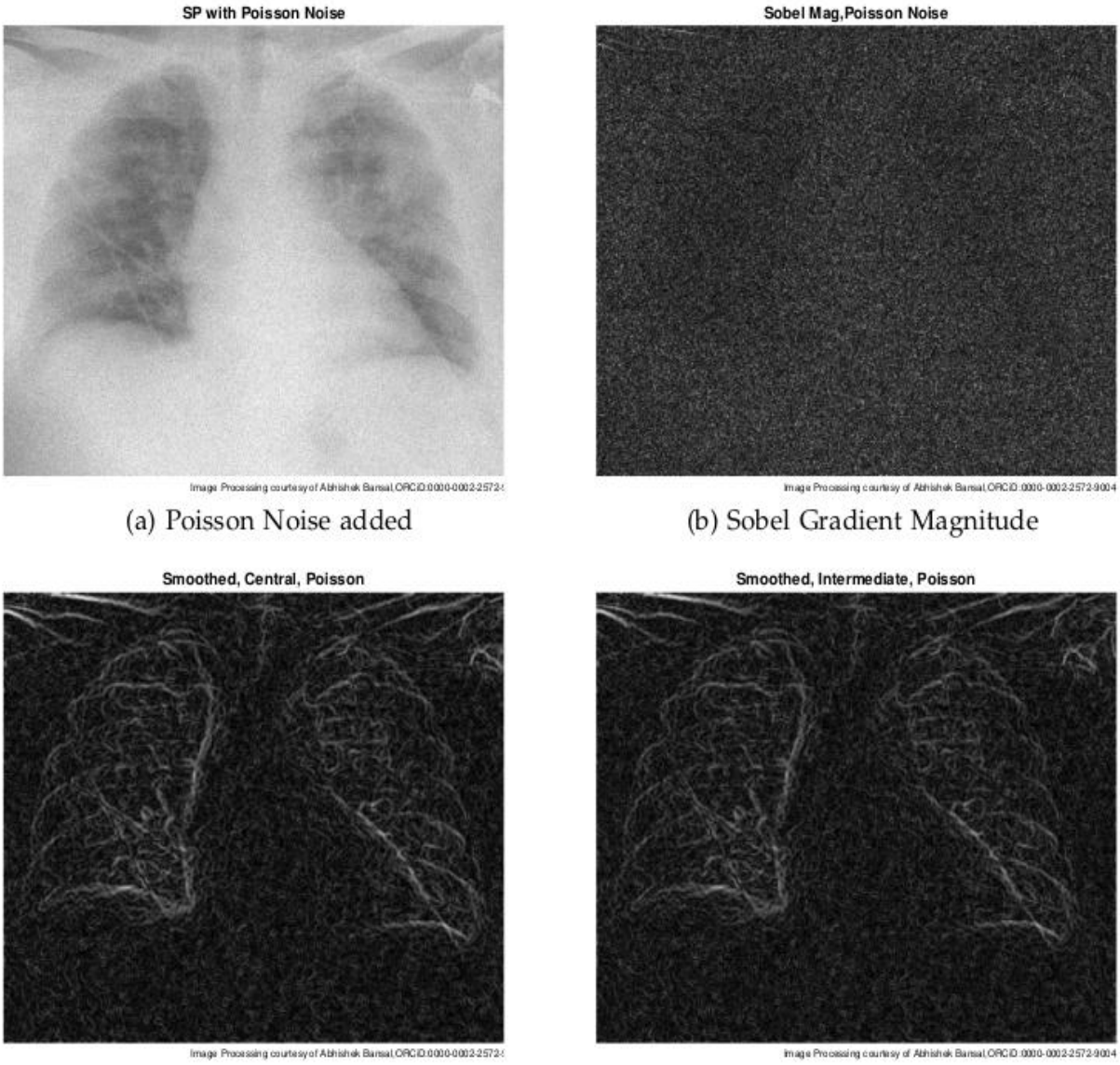
(c) Gaussian Variance = 0.0001

Fig. 75: Gaussian smoothing & intermediate difference gradient,Day4

International Journal of Advanced Computing and Intelligent System (IJACIS)
Volume 1, Issue 1 (2023)
DOI: 10.66917/ijacis.a000003
https://msis-press.com/journals/ijacis

6.6. Poisson Noise & Sobel Gradient

In this subsection, the single precision X-Ray of Day 4 (Fig 68(a)) is subjected to Poisson Noise,Fig. 76(a). The gradient magnitude of Poisson noise X-Ray is plotted using Sobel method, which are shown in Fig. 76(b). This is further smoothed using 2-D Gaussian smoothing and central difference gradient in Fig. 76(c); and 2-D Gaussian smoothing and intermediate difference gradient in Fig. 76(d).



(a) Poisson Noise added

(b) Sobel Gradient Magnitude

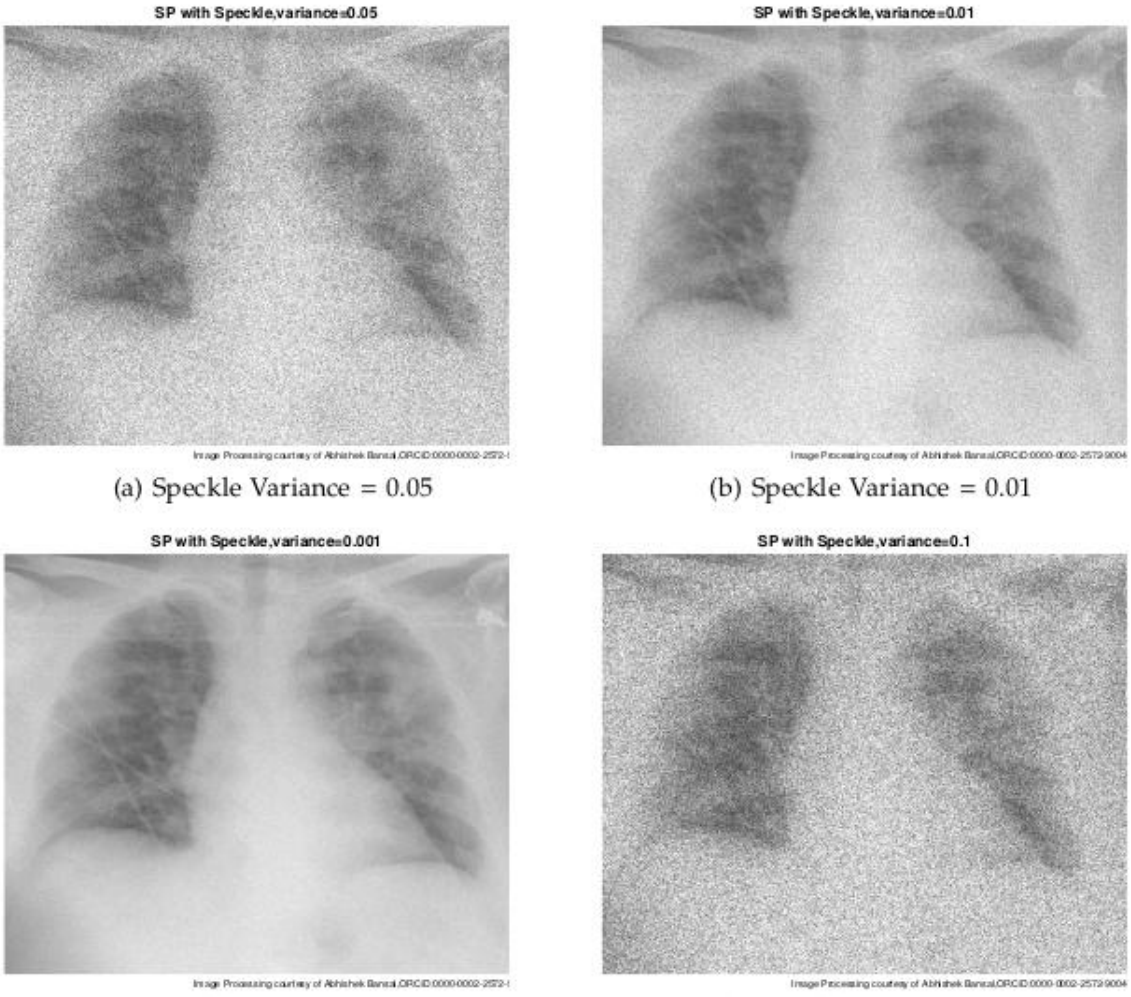
(c) Smoothed by Central Difference

(d) Smoothed by Intermediate Difference

Fig. 76: Poisson Noise & Gradient Magnitude,Day4

6.7. Speckle Noise & Sobel Gradient

In this subsection, the single precision X-Ray of Day 4 (Fig 68(a)) is subjected to Speckle noise with four variances of 0.05, 0.01, 0.001 and 0.1. These are shown in Fig. 77[a-d]. The gradient magnitude of these noisy X-Rays are plotted using Sobel method, which are shown in Fig. 78. These are further smoothed using 2-D Gaussian smoothing. The Gaussian smoothing and central difference gradient are shown in Fig. 79. The Gaussian smoothing and intermediate difference gradient are shown in Fig. 80.



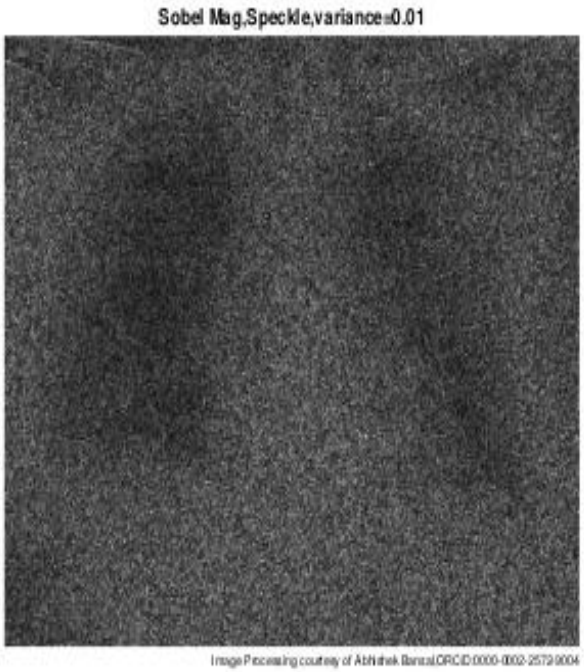
(a) Speckle Variance = 0.05 (b) Speckle Variance = 0.01

(c) Speckle Variance = 0.001 (d) Speckle Variance = 0.1

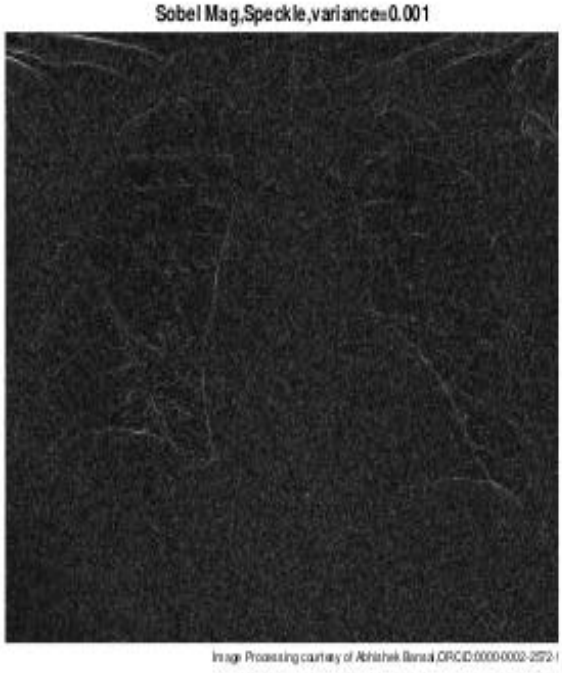
Fig. 77: Speckle Noise added to Image,Day4



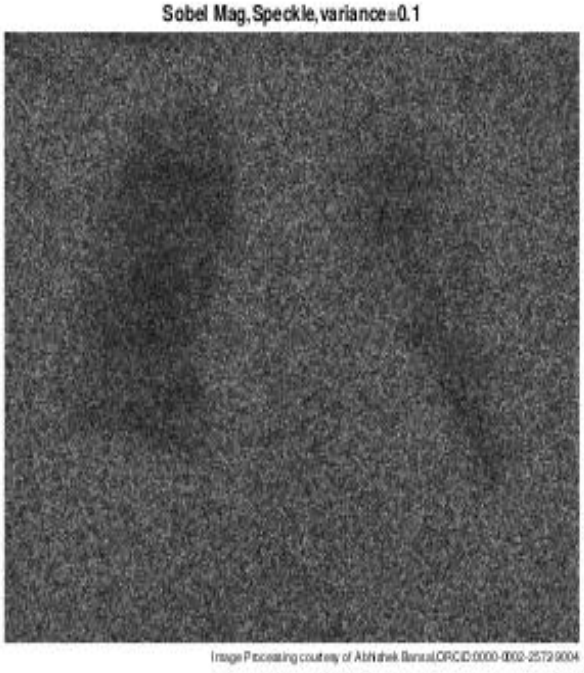
(a) Speckle Variance = 0.05



(b) Speckle Variance = 0.01



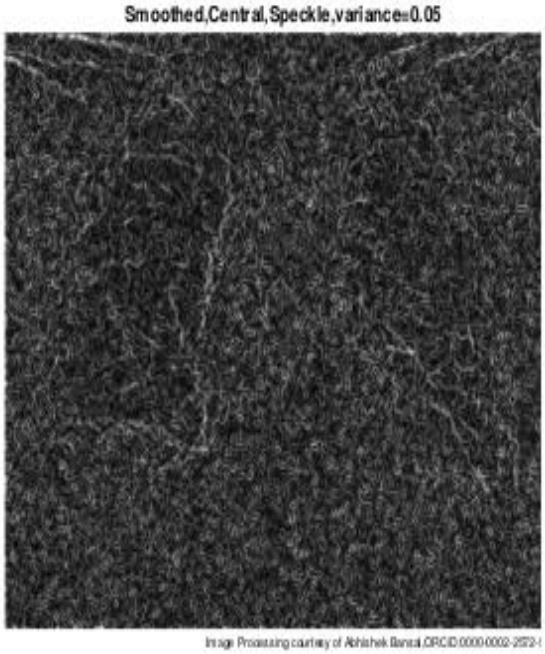
(c) Speckle Variance = 0.001



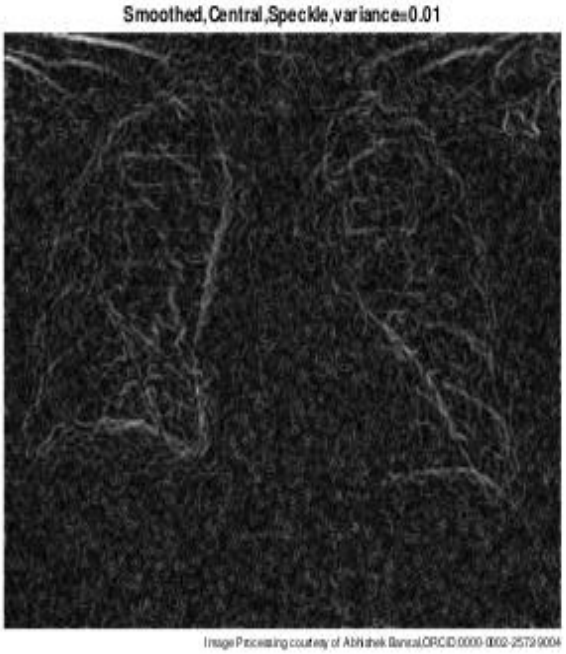
(d) Speckle Variance = 0.1

Fig. 78: Gradient of Noisy X-Ray using Sobel Method,Day4

International Journal of Advanced Computing and Intelligent System (IJACIS)
Volume 1, Issue 1 (2023)
DOI: 10.66917/ijacis.a000003
https://msis-press.com/journals/ijacis



(a) Speckle Variance = 0.05



(b) Speckle Variance = 0.01



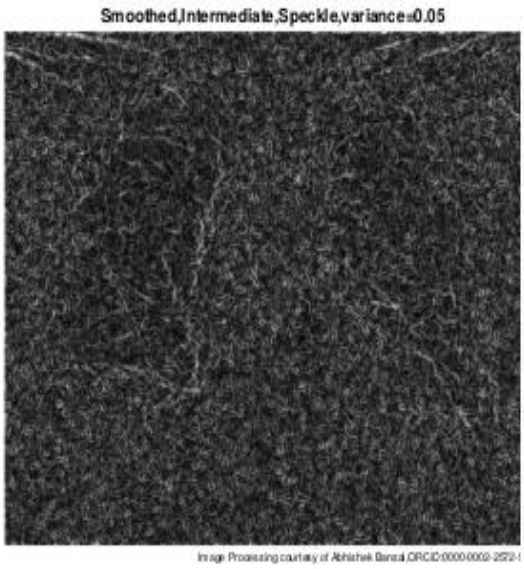
(c) Speckle Variance = 0.001



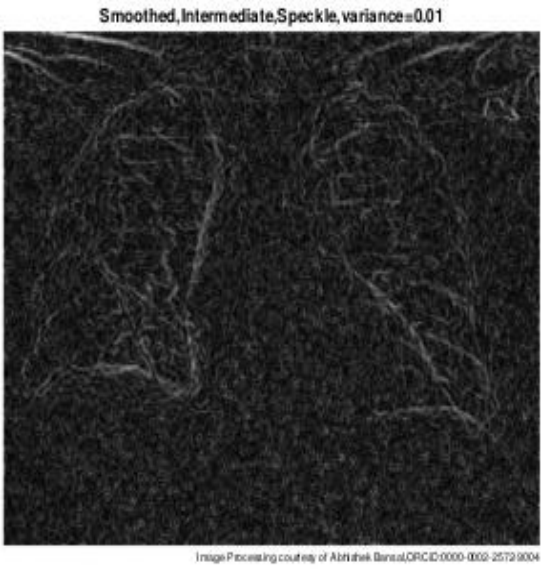
(d) Speckle Variance = 0.1

Fig. 79: Gaussian smoothing & central difference gradient,Day4

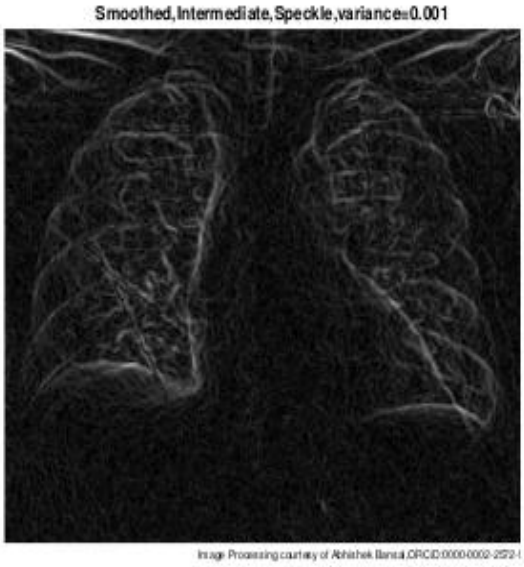
International Journal of Advanced Computing and Intelligent System (IJACIS)
Volume 1, Issue 1 (2023)
DOI: 10.66917/ijacis.a000003
https://msis-press.com/journals/ijacis



(a) Speckle Variance = 0.05



(b) Speckle Variance = 0.01



(c) Speckle Variance = 0.001



(d) Speckle Variance = 0.1

Fig. 80: Gaussian smoothing & intermediate difference gradient,Day4

International Journal of Advanced Computing and Intelligent System (IJACIS)
Volume 1, Issue 1 (2023)
DOI: 10.66917/ijacis.a000003
https://msis-press.com/journals/ijacis

765 6.8. Pixel Intensities & Contrast

766 In this subsection, the original X-Ray (without converting to single precision or double
767 precision) is contrasted for study and analysis.

768 Let the center fit

$$z = \frac{(x - 137.5)}{74.05}$$

771 then from polynomial regression

$$y = -456.5 \times z^9 + 2091 \times z^8 + 5796 \times z^7 - 9125 \times z^6 - 1.939 \times 10^4 \times z^5 + 6667 \times z^4 + 1.607 \times 10^4 \times z^3 + 5324 \times z^2 + 7713 \times z + 4413$$

772

773 Let $\bar{y}$ be the mean of y, $\hat{y}$ the calculated values of y, then the coefficient of determination,

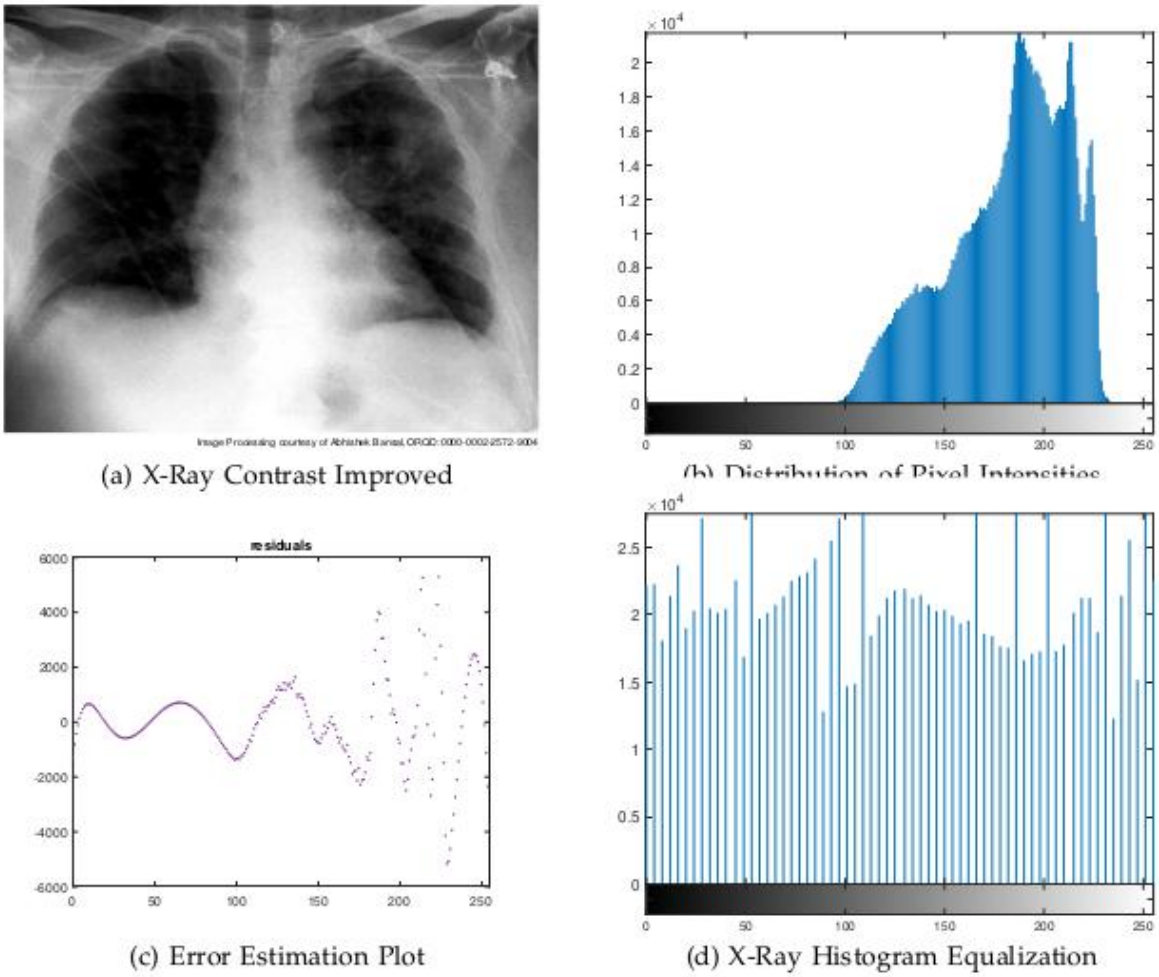
$$R^2 = 1 - \frac{\sum_{i=1}^{n}(y_i - \hat{y})^2}{\sum_{i=1}^{n}(y_i - \bar{y})^2} = 0.9513$$

776

777 The measure of the goodness of fit given by norm of residuals is 2.42×10^4. Here,
778 the polynomial of degree 9 chosen here is the global which can be focused on the areas
779 of interest (to be decided by infection part or researchers/doctors interest) and separate
780 equations can be obtained for each particular area of interest. This gives insight in
781 mathematical formulation and has been used in the Novel B-Mathematical Modeling
782 of Respiratory System.

783 TABLE VII: Data Statistics for Fig. 81(b)

	X	Y
min	0	0
max	255	2.192×10^4
mean	137.5	5360
median	137.5	616.5
mode	0	0
std deviation	74.05	6870
range	255	2.192×10^4



(a) X-Ray Contrast Improved

(b) Distribution of Pixel Intensities

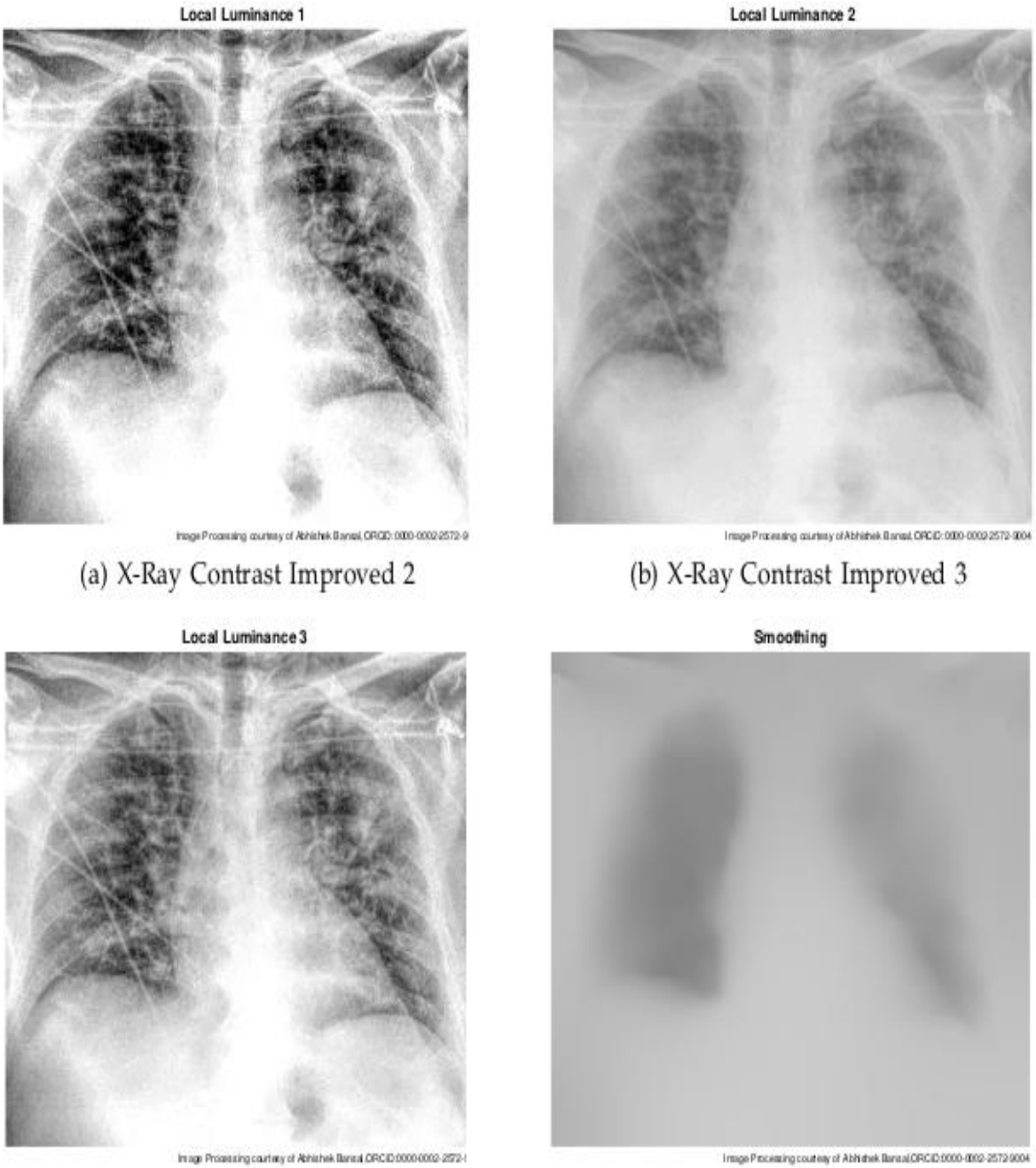
(c) Error Estimation Plot

(d) X-Ray Histogram Equalization

Fig. 81: Distribution of Pixel Intensities in X-Ray,Day4

The Fig.81(a) shows that X-Ray contrast is improved for analysis when compared with Fig. 1(a). Fig. 81(b) shows the distribution of X-Ray pixel intensities. Fig. 81(c) shows the error estimation plot, which is the plot of the residuals. Fig. 81(d) shows the X-Ray histogram equalization which is the spreading of the intensity values over the full range.

In Fig. 82, X-Ray Contrast is improved with five local luminances. The original Fig. 68(a) X-Ray contrast is improved with four more local luminances by varying the intensity values at low and high intensities. These are shown in Fig 82(a), Fig. 82(b) and Fig. 82(c). In Fig. 82(d), the original Fig. 68(a) X-Ray is contrasted with fifth value of improvement but smoothing technique is applied after it.



(a) X-Ray Contrast Improved 2

(b) X-Ray Contrast Improved 3

(c) X-Ray Contrast Improved 4

(d) X-Ray Contrast Improved & Smoothed

Fig. 82: X-Ray Contrast Improved with Five Local Luminances,Day4

803

804

805

806

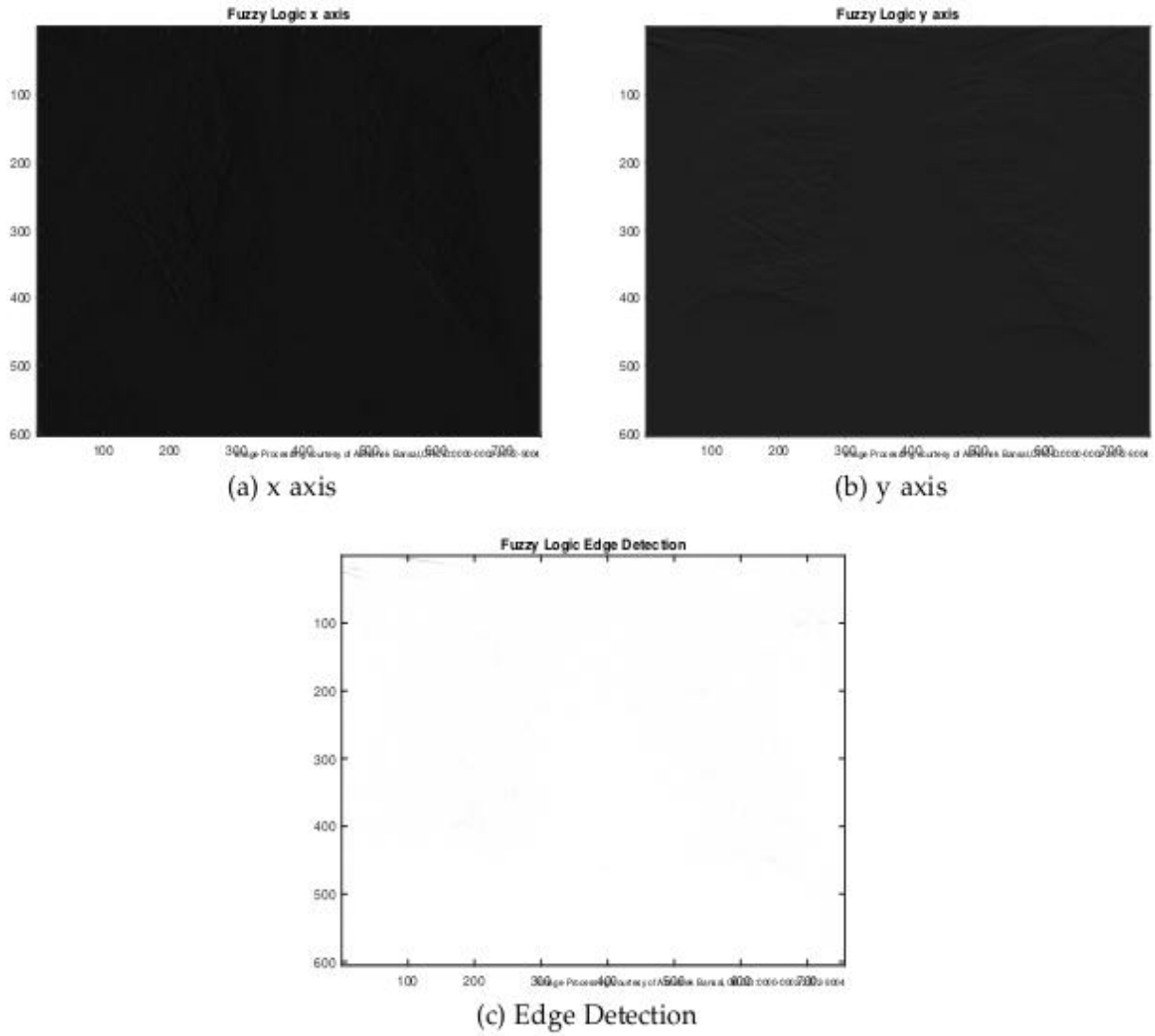
807

808

809

6.9. Fuzzy Logic

In this subsection, the images obtained using fuzzy logic edge-detection algorithm and Fuzzy Inference System (FIS) are given. Two 2-D Convolution are performed. The x-axis of directional gradient is convolved with x-axis gradients of double-precision X-Ray obtained in Fig. 68(b) and the X-Ray gradient of fuzzy logic x-axis is given in Fig. 83(a). The y-axis of directional gradient is convolved with y-axis gradients of double-precision X-Ray obtained in Fig. 68(b) and the X-Ray gradient of fuzzy logic y-axis is given in Fig. 83(b). The edge detection is shown in Fig. 83(c).



(a) x axis

(b) y axis

(c) Edge Detection

Fig. 83: Fuzzy Logic,Day4

836

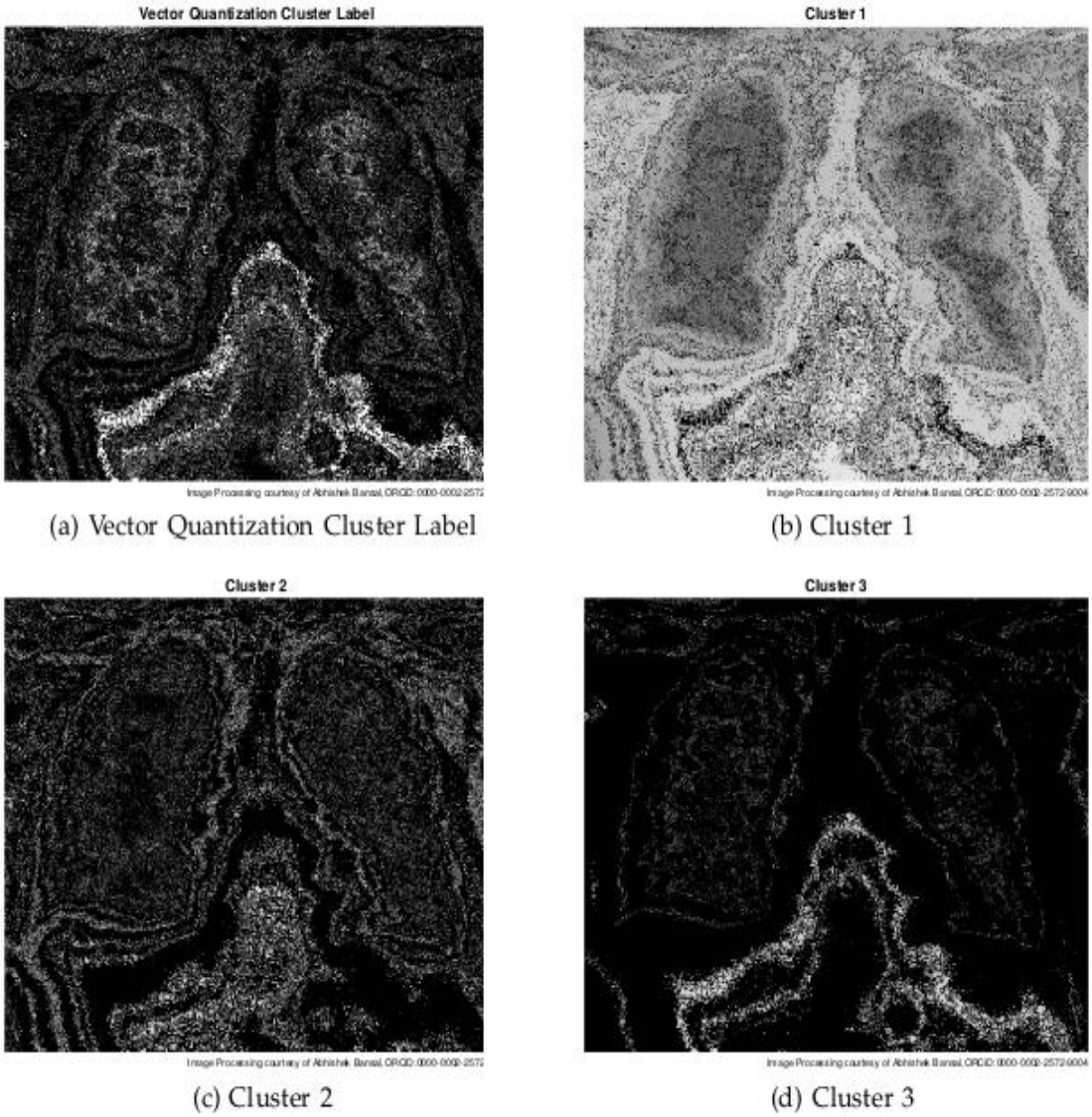
837

838

839 6.10. K-means Clustering

840 In this subsection, the popular vector quantization technique of K-Means cluster-
841 ing is applied to X-Ray. In this technique, firstly CIE XYZ tristimulus technique is
842 used to know the color information and thus, the information of luminosity layer
843 'L*', chromaticity-layer 'a*' and chromaticity-layer 'b*' is obtained. Then every pixel is
844 clustered with its pixel label and partitioned into three clusters. The clustering obtained
845 is shown in Fig. 84(a), Vector Quantization Cluster Label. And three clusters Cluster
846 1, Cluster 2 and Cluster 3 obtained are shown in Fig. 84(b), Fig. 84(c) and Fig. 84(d)

847 respectively.



(a) Vector Quantization Cluster Label (b) Cluster 1

(c) Cluster 2 (d) Cluster 3

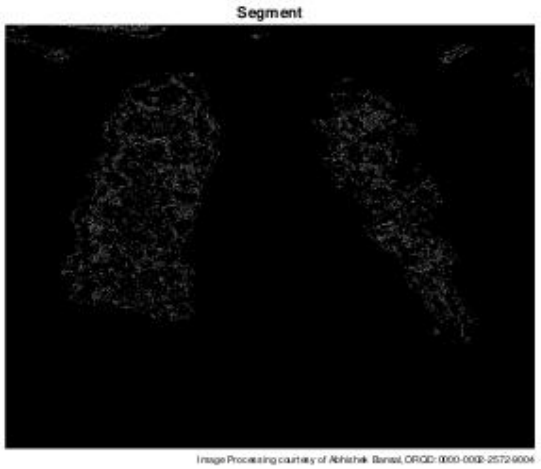
Fig. 84: Vector Quantization,K-means Clustering,Day4

848

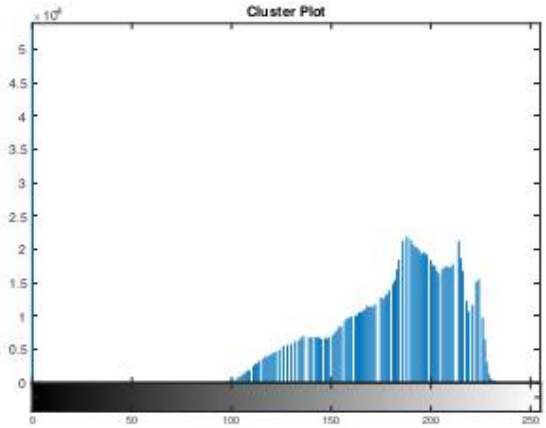
849

850 In Fig. 85(a), segmentation is applied and Fig. 85(b) and Fig. 85(c) shows respectively

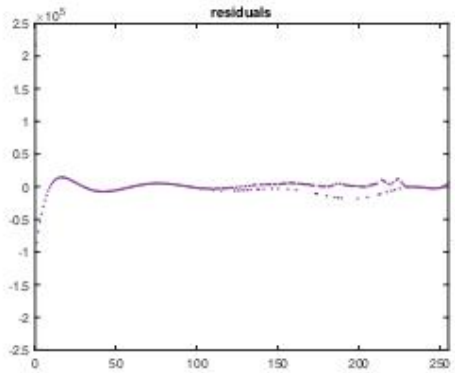
851 the cluster plot and the plot of error estimation, that is, the plot of residuals.



(a) Segmentation



(b) Cluster Plot



(c) Cluster Plot Residuals

Fig. 85: Clustering Plot and Segment,Day4

Moving in similar way as in the Subsection-8 and choosing same

$$z = \frac{(x - 137.5)}{74.05}$$

we have,

$$y = -1.465 \times 10^4 \times z^9 + 1.29 \times 10^4 \times z^8 + 8.51 \times 10^4 \times z^7 - 6.144 \times 10^4 \times z^6 - 1.632 \times 10^5 \times z^5 + 8.416 \times 10^4 \times z^4 + 1.101 \times 10^5 \times z^3 - 3.07 \times 10^4 \times z^2 - 1.052 \times 10^4 \times z + 5573$$

$R^2 = 0.3442$

and Norm of Residuals = 2.704×10^5

TABLE VIII: Data Statistics for Fig. 85(b)

	X	Y
min	0	0
max	255	3.225×10^5
mean	137.5	5360
median	137.5	0
mode	0	0
std deviation	74.05	2.091×10^4
range	255	3.225×10^5

6.11. Morphological Segmentation

In this subsection, known morphological segmentation technique is applied on X-Rays. Three morphological openings are used. The morphological opening with structuring element of disk shaped with three different radius are shown in Fig. 86(a), Fig. 86(c) and Fig. 87(a). The background approximation images of X-Ray obtained after subtracting from the original image are shown in Fig. 86(b), Fig. 86(d) and Fig. 87(b).



(a) Morphological Opening 1



(b) Background Approximation Removed from Fig. 19(a)



(c) [Morphological Opening 2



(d) Background Approximation Removed from Fig. 19(c)

Fig. 86: Morphological Segmentation,Day4



(a) Morphological Opening 3



(b) Background Approximation Removed from Fig. 20(a)

Fig. 87: Morphological Segmentation,Day4

International Journal of Advanced Computing and Intelligent System (IJACIS)
Volume 1, Issue 1 (2023)
DOI: 10.66917/ijacis.a000003
https://msis-press.com/journals/ijacis

886

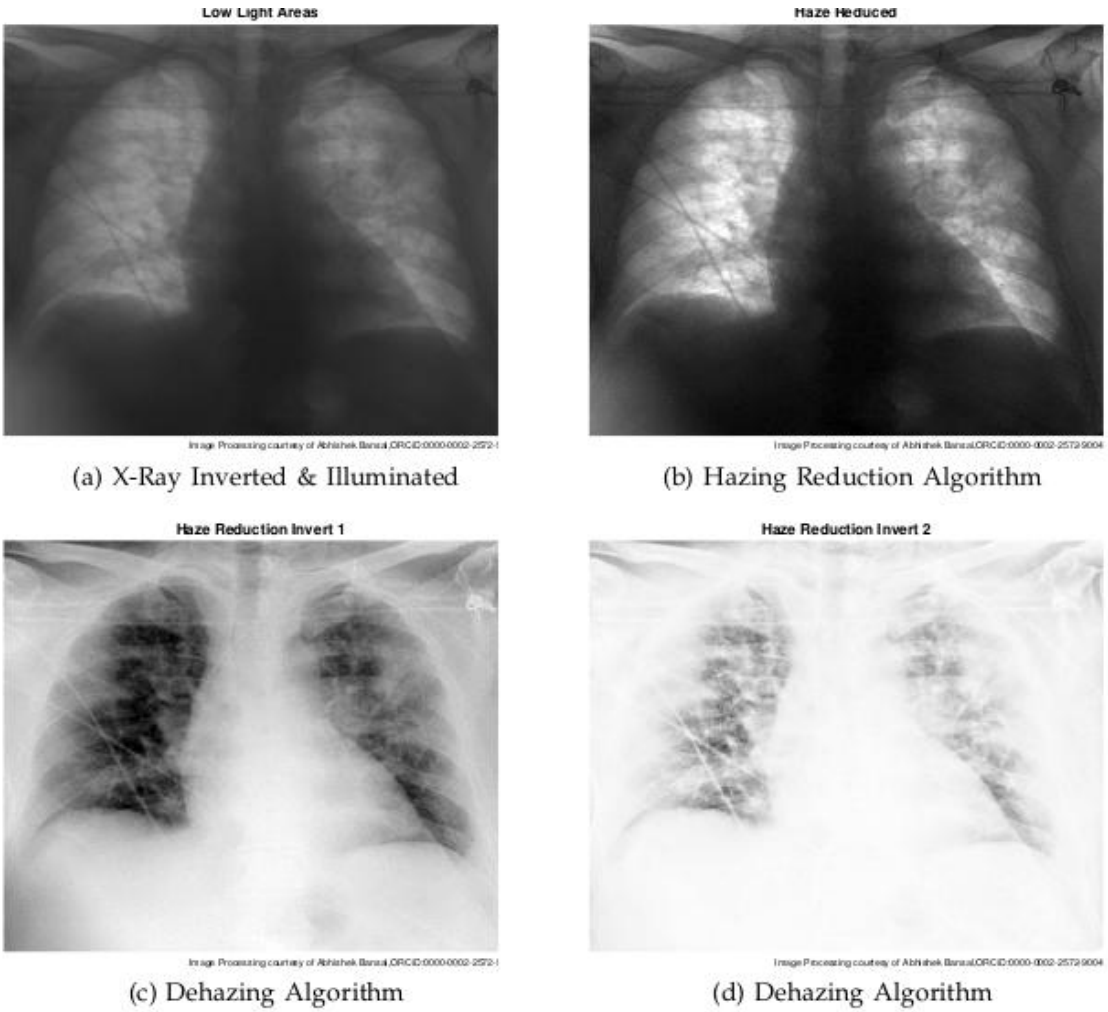
887 6.12. Dehazing Algorithm

888 In Fig. 88(a), the original Fig. 68(a) X-Ray is inverted and the low-light areas and

889 focused and the new X-Ray is obtained. The hazing obtained in Fig. 88(a) is reduced

890 by hazing reduction algorithm.

891



(a) X-Ray Inverted & Illuminated (b) Hazing Reduction Algorithm

(c) Dehazing Algorithm (d) Dehazing Algorithm

Fig. 88: Dehazing Algorithm,Day4

892

893

894 On the new X-Ray of Fig. 88(b), dehazing algorithm is applied and its result is in Fig.

895 88(c,d). Fig. 89[a-d] has four more such combinations on which dehazing algorithm is

896 implemented.

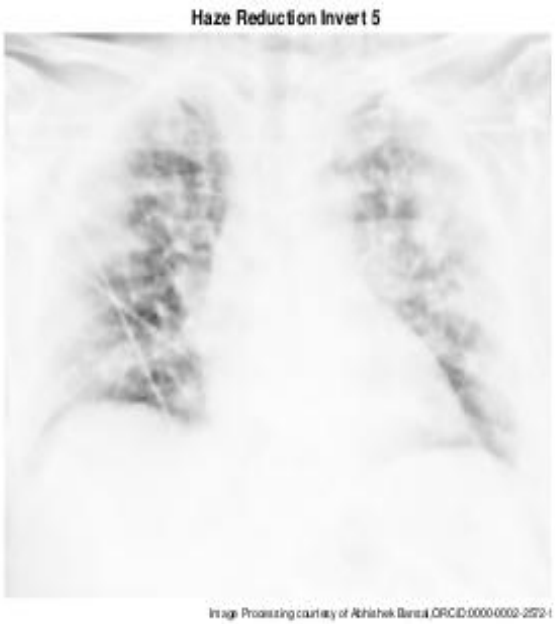
897



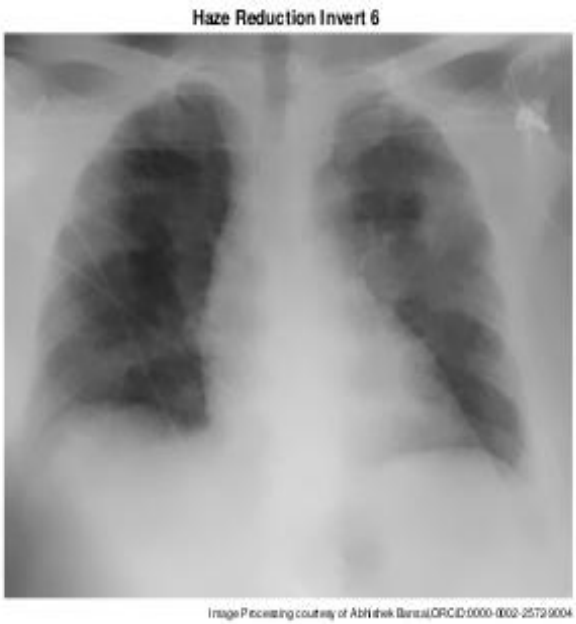
(a) Dehazing Algorithm



(b) Dehazing Algorithm



(c) Dehazing Algorithm



(d) Dehazing Algorithm

Fig. 89: Dehazing Algorithm,Day4

898

899

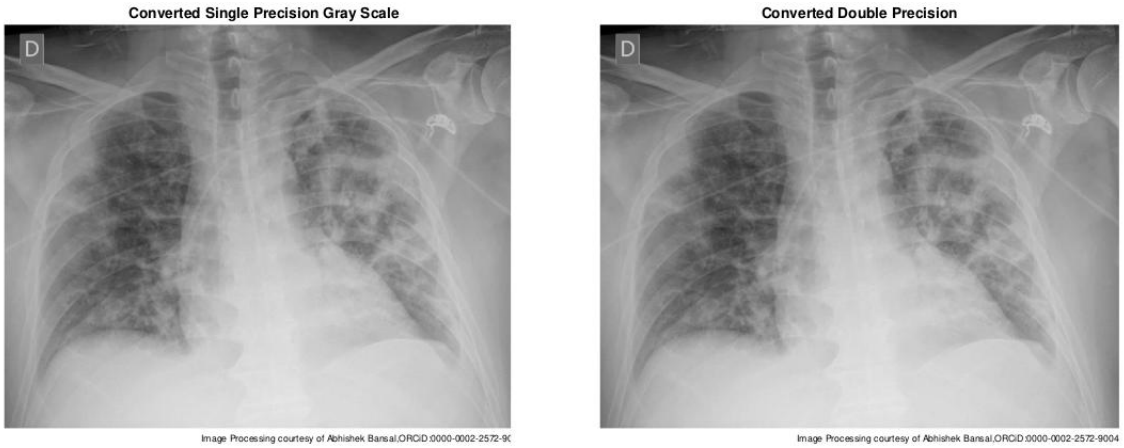
900

901

7. Results : Day 6, PA

7.1. X-Ray Converted

In this subsection, X-Ray(PA) of Day 6 is converted to single precision grayscale and double precision, on which all further image processings will be done. These are shown in Fig. 90.

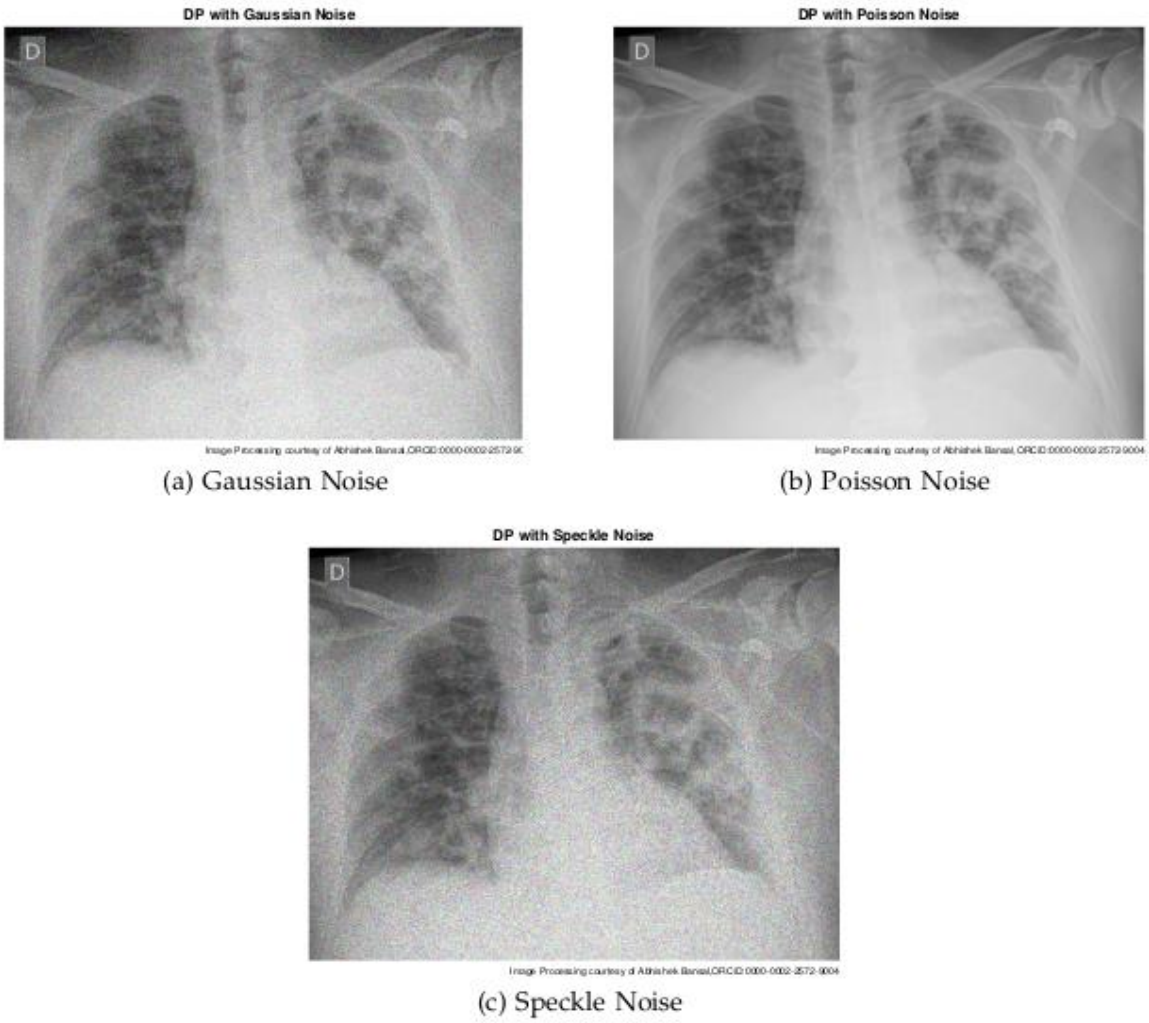


(a) Single Precision (b) Double Precision

Fig. 90: Converted to Single Precision & Double Precision,Day6

7.2. Double Precision Noise Addition

In this subsection, the double precision X-Ray of Day 6 (Fig 90(b)) of the previous subsection is subjected to noises namely Gaussian with variance 0.01, Poisson Noise and speckle noise with variance 0.05. These are shown in Fig. 91.



(a) Gaussian Noise

(b) Poisson Noise

(c) Speckle Noise

Fig. 91: Noises Added to Double Precision,Day6

915

916

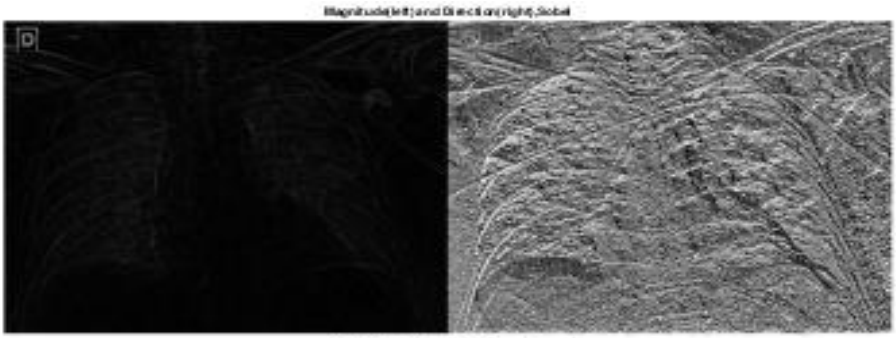
917

918 7.3. Gradient Magnitude and Direction

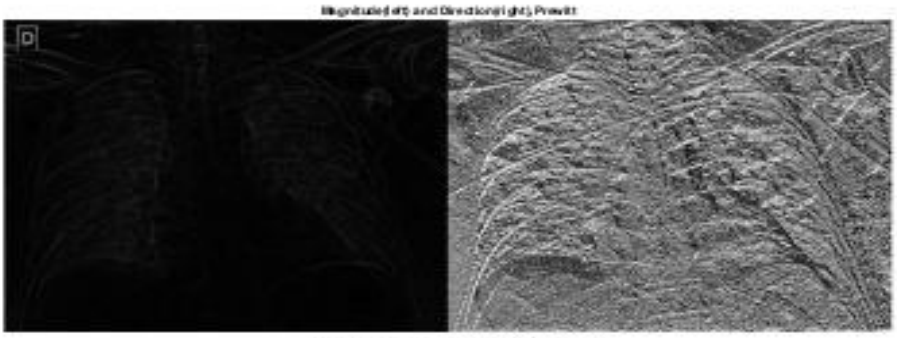
919 In this subsection, the gradient of the single precision X-Ray of Day 6 (Fig 90(a)) is

920 obtained and its magnitude and direction is plotted using methods of Sobel, Prewitt,

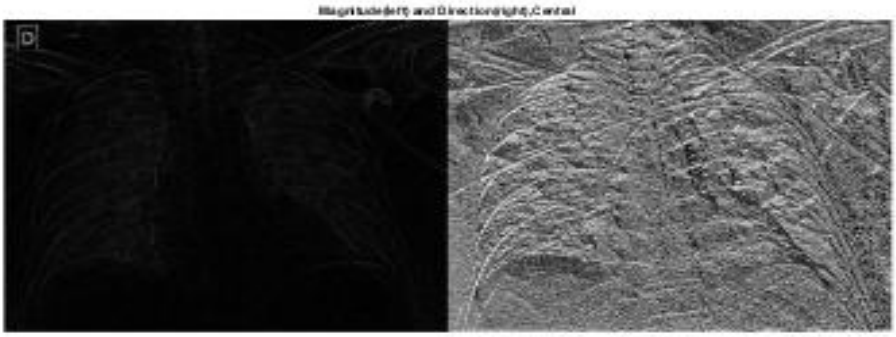
921 central difference and intermediate difference. These are shown in Fig. 92.



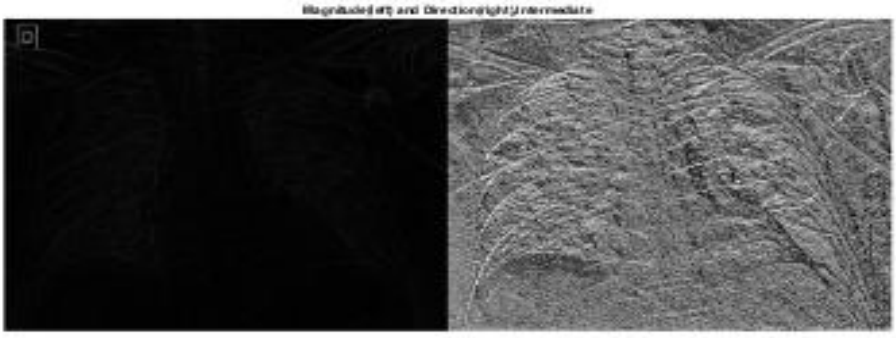
(a) Sobel Method



(b) Prewitt Method



(c) Central Difference



(d) Intermediate Difference

Fig. 92: X-Ray Gradient Magnitude and Direction,Day6

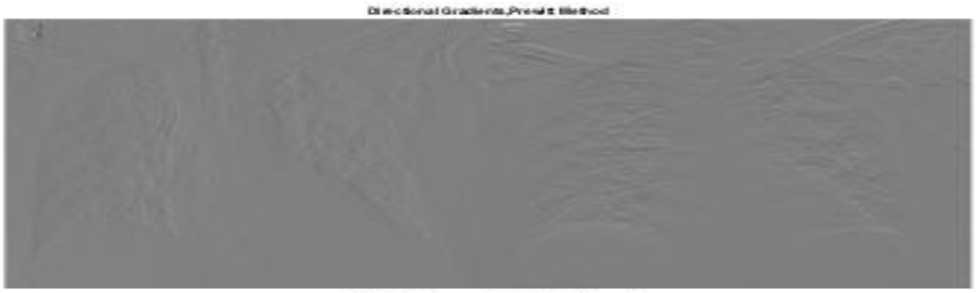
International Journal of Advanced Computing and Intelligent System (IJACIS)
Volume 1, Issue 1 (2023)
DOI: 10.66917/ijacis.a000003
https://msis-press.com/journals/ijacis

7.4. Directional Gradients

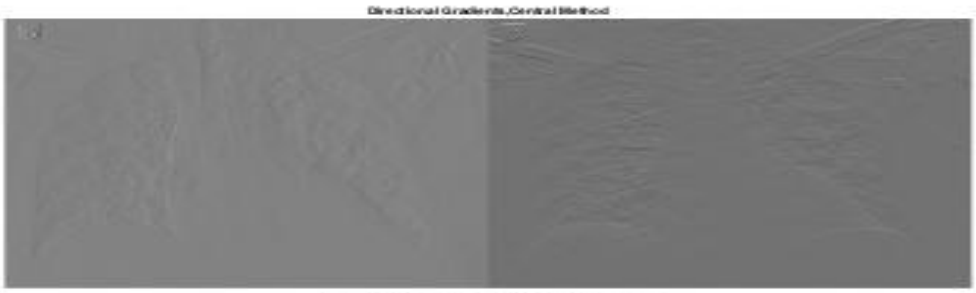
In this subsection, the directional gradient of the single precision X-Ray of Day 6 (Fig 90(a)) is plotted using methods of Sobel, Prewitt, central difference and intermediate difference. These are shown in Fig. 93.



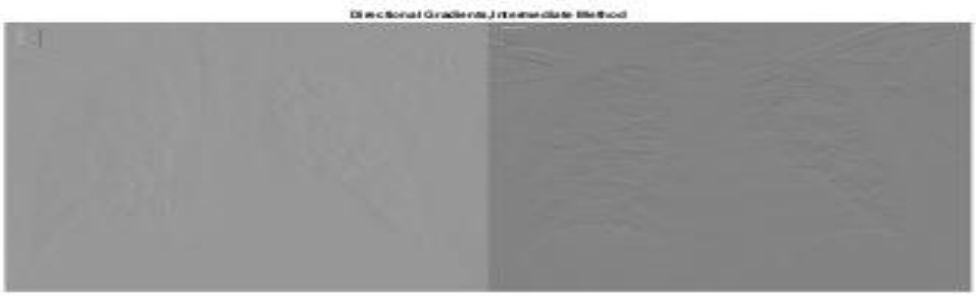
(a) Sobel Method



(b) Prewitt Method



(c) Central Difference

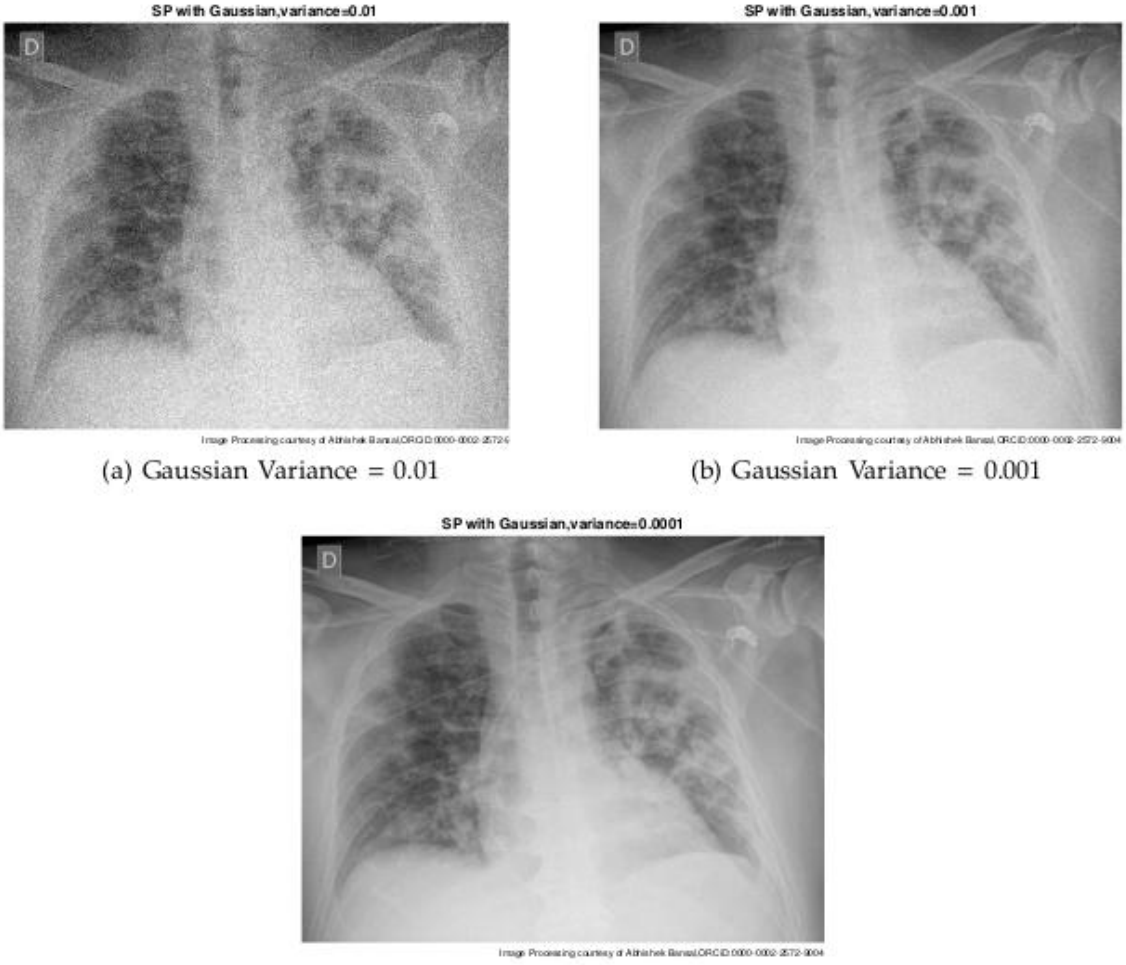


(d) Intermediate Difference

Fig. 93: Directional Gradients,Day6

7.5. Gaussian Noises & Sobel Gradient

In this subsection, the single precision X-Ray of Day 6 (Fig 90(a)) is subjected to Gaussian noise with three variances of 0.01, 0.001 and 0.0001. These are shown in Fig. 94. The gradient magnitude of these noisy X-Rays are plotted using Sobel method, which are shown in Fig. 95. The figures of gradient magnitude of Fig. 95 are further smoothed using 2-D Gaussian smoothing. The Gaussian smoothing and central difference gradient are shown in Fig. 96. The Gaussian smoothing and intermediate difference gradient are shown in Fig. 97.



(a) Gaussian Variance = 0.01

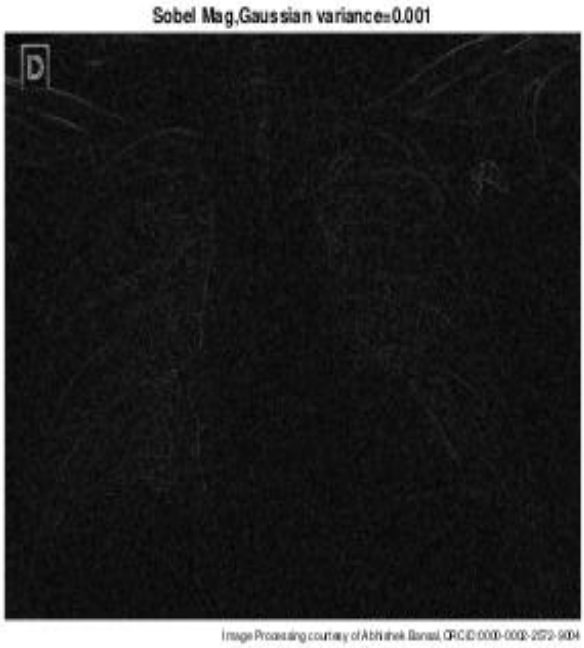
(b) Gaussian Variance = 0.001

(c) Gaussian Variance = 0.0001

Fig. 94: Gaussian White Noise added to Image,Day6



(a) Gaussian Variance = 0.01



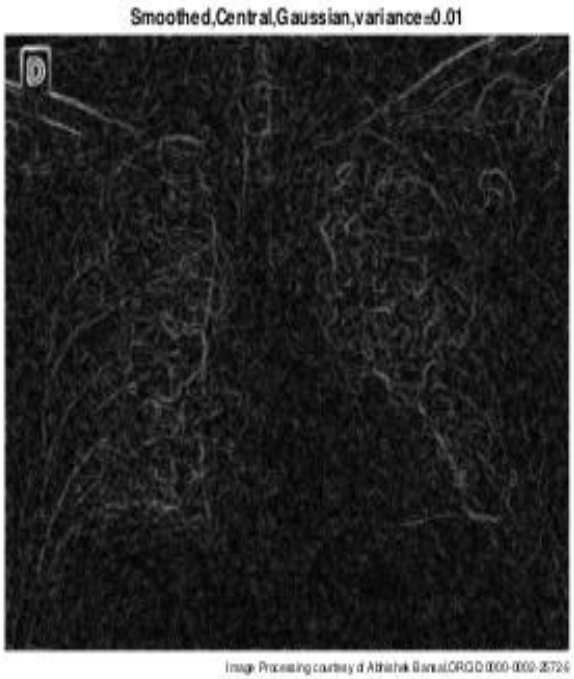
(b) Gaussian Variance = 0.001



(c) Gaussian Variance = 0.0001

Fig. 95: Gradient of Noisy X-Ray using Sobel Method,Day6

946



(a) Gaussian Variance = 0.01



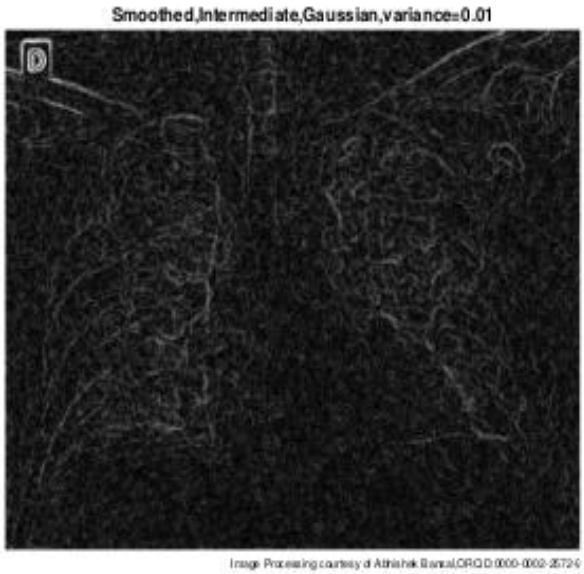
(b) Gaussian Variance = 0.001



(c) Gaussian Variance = 0.0001

Fig. 96: Gaussian smoothing & central difference gradient,Day6

International Journal of Advanced Computing and Intelligent System (IJACIS)
Volume 1, Issue 1 (2023)
DOI: 10.66917/ijacis.a000003
https://msis-press.com/journals/ijacis



(a) Gaussian Variance = 0.01



(b) Gaussian Variance = 0.001



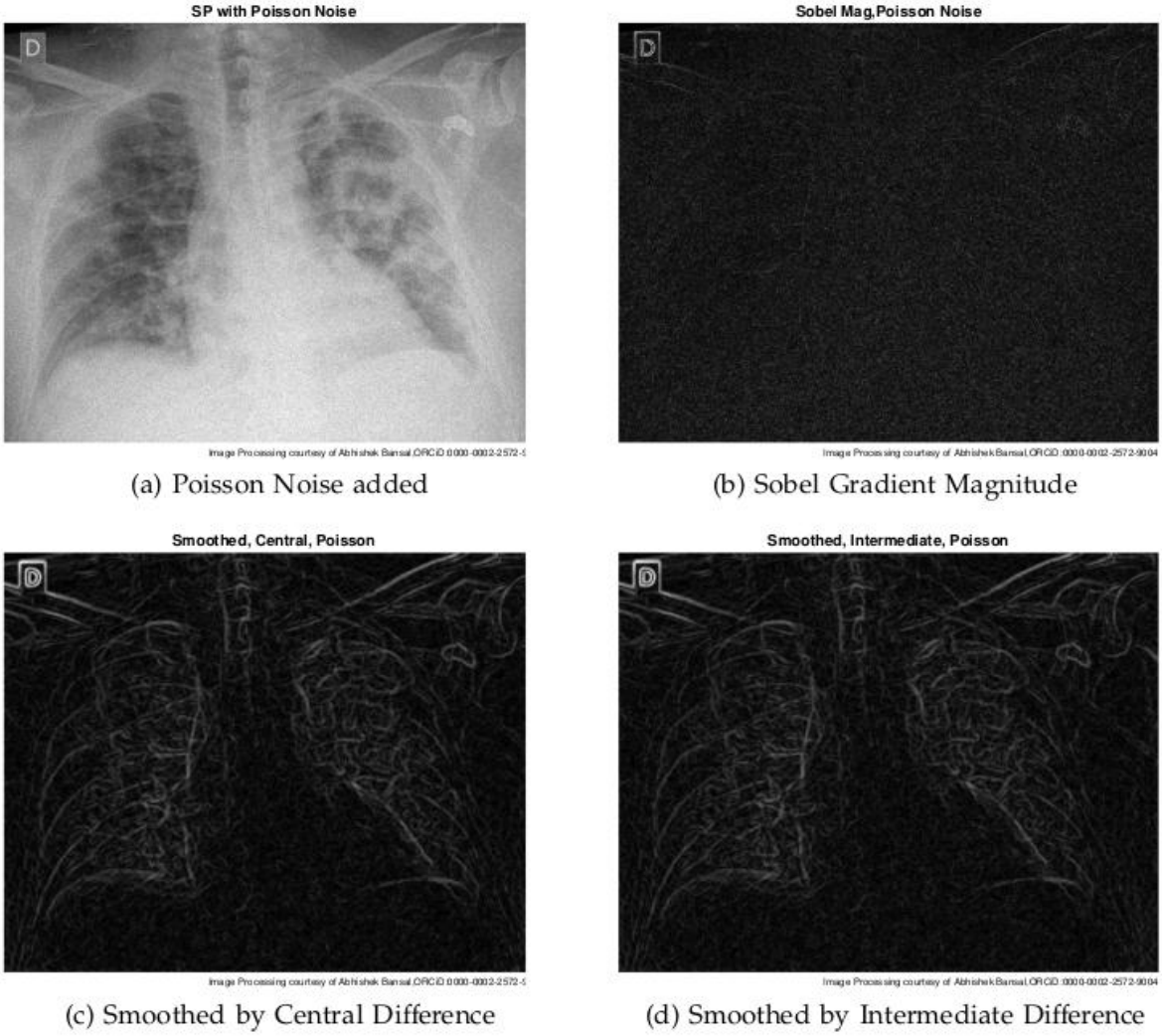
(c) Gaussian Variance = 0.0001

Fig. 97: Gaussian smoothing & intermediate difference gradient,Day6

948

7.6. Poisson Noise & Sobel Gradient

In this subsection, the single precision X-Ray of Day 6 (Fig 90(a)) is subjected to Poisson Noise,Fig. 98(a). The gradient magnitude of Poisson noise X-Ray is plotted using Sobel method, which are shown in Fig. 98(b). This is further smoothed using 2-D Gaussian smoothing and central difference gradient in Fig. 98(c); and 2-D Gaussian smoothing and intermediate difference gradient in Fig. 98(d).



(a) Poisson Noise added (b) Sobel Gradient Magnitude

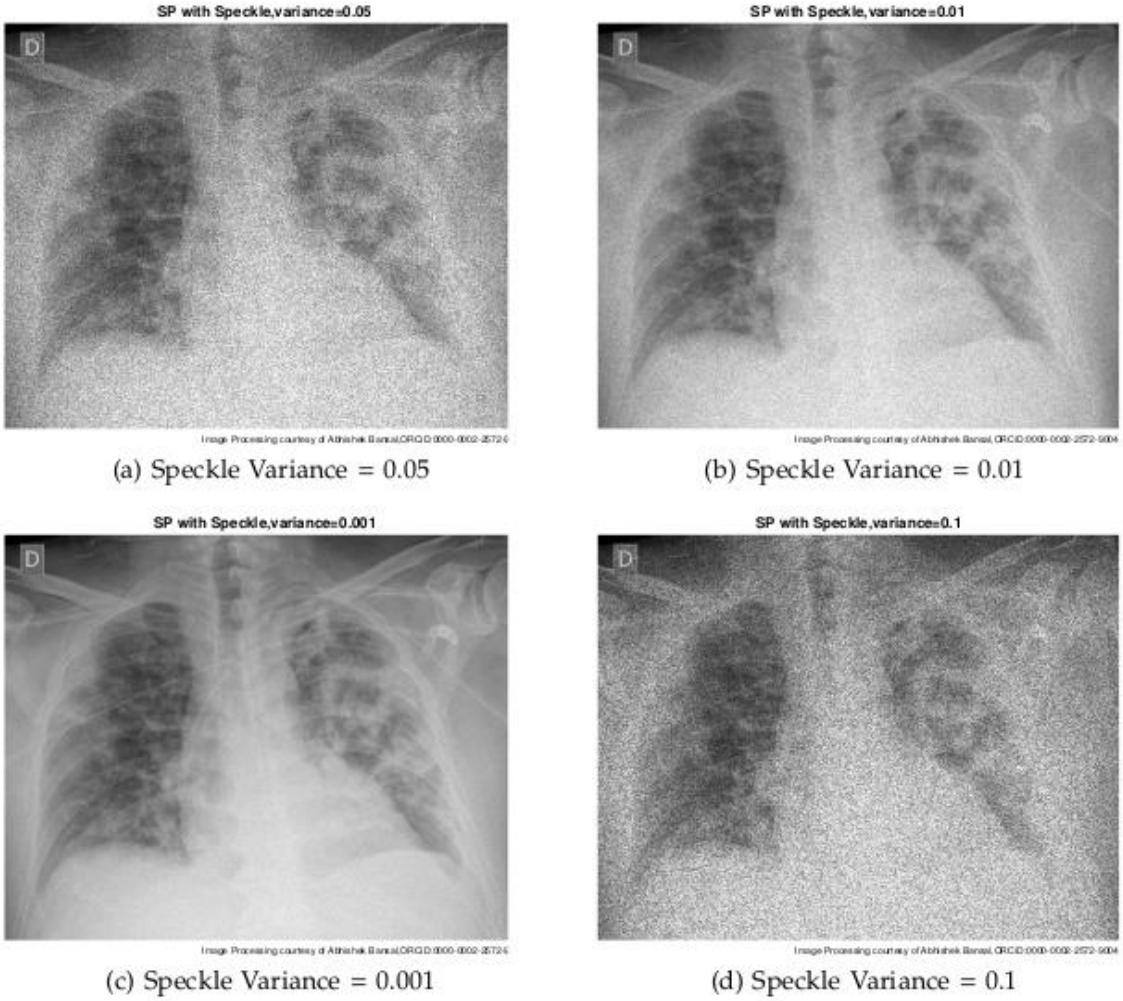
(c) Smoothed by Central Difference (d) Smoothed by Intermediate Difference

Fig. 98: Poisson Noise & Gradient Magnitude,Day6

7.7. Speckle Noise & Sobel Gradient

In this subsection, the single precision X-Ray of Day 6 (Fig 90(a)) is subjected to Speckle noise with four variances of 0.05, 0.01, 0.001 and 0.1. These are shown in Fig.

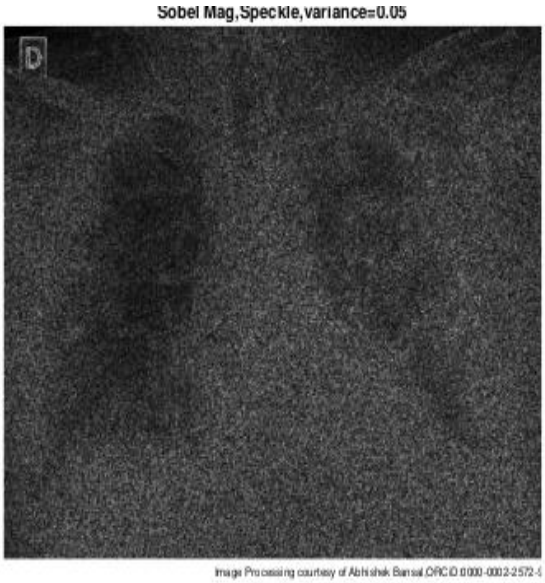
99[a-d]. The gradient magnitude of these noisy X-Rays are plotted using Sobel method, which are shown in Fig. 100. These are further smoothed using 2-D Gaussian smoothing. The Gaussian smoothing and central difference gradient are shown in Fig. 101. The Gaussian smoothing and intermediate difference gradient are shown in Fig. 102.



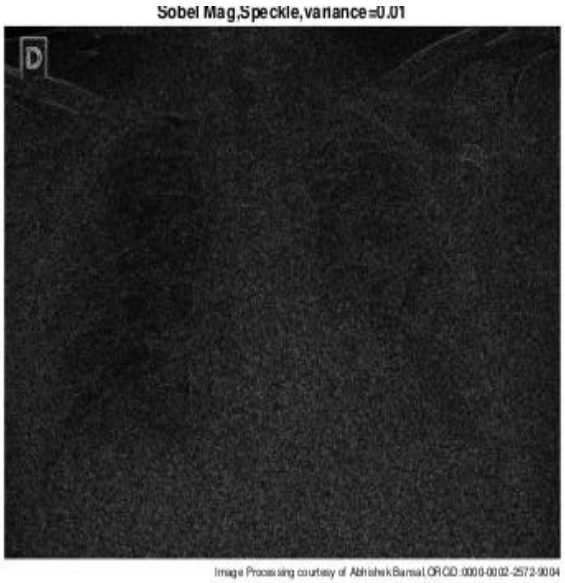
(a) Speckle Variance = 0.05 (b) Speckle Variance = 0.01

(c) Speckle Variance = 0.001 (d) Speckle Variance = 0.1

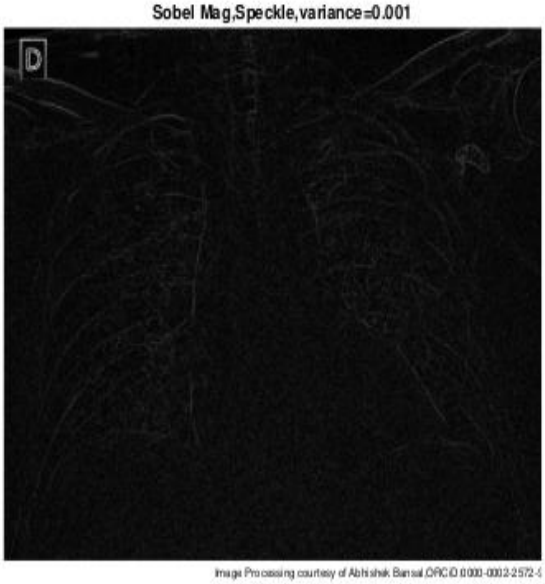
Fig. 99: Speckle Noise added to Image,Day6



(a) Speckle Variance = 0.05



(b) Speckle Variance = 0.01



(c) Speckle Variance = 0.001

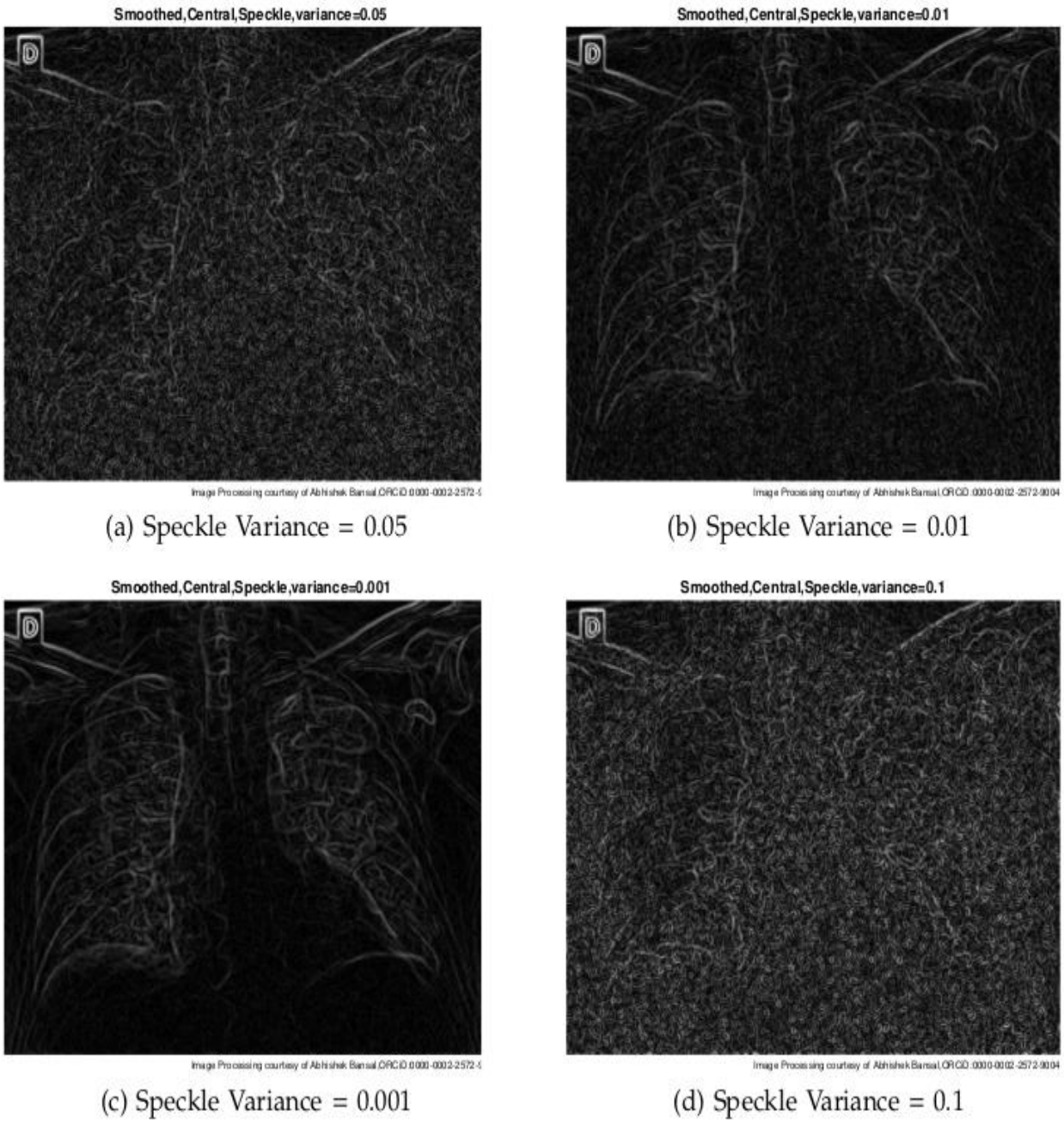


(d) Speckle Variance = 0.1

Fig. 100: Gradient of Noisy X-Ray using Sobel Method,Day6

968

969



(a) Speckle Variance = 0.05

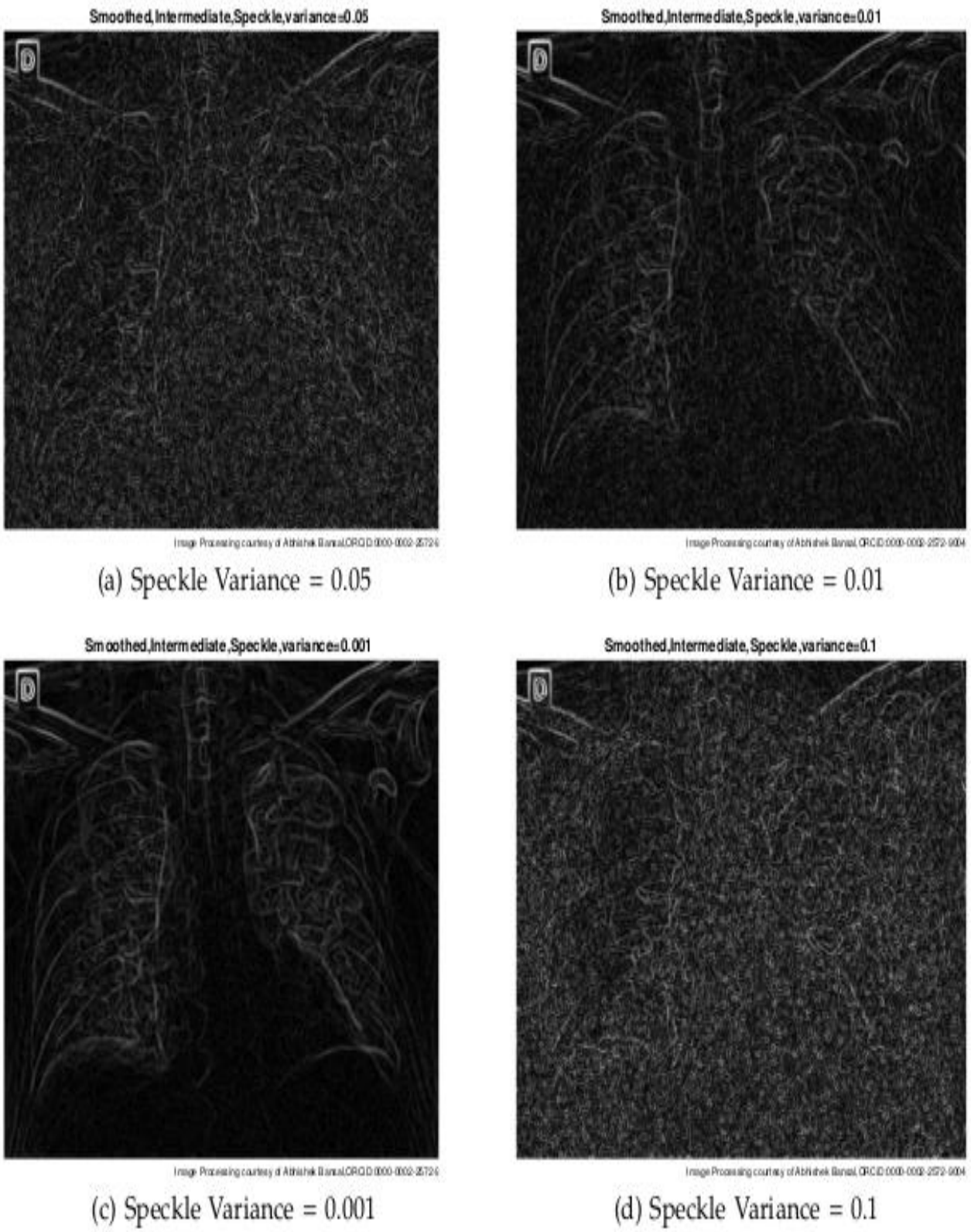
(b) Speckle Variance = 0.01

(c) Speckle Variance = 0.001

(d) Speckle Variance = 0.1

Fig. 101: Gaussian smoothing & central difference gradient,Day6

International Journal of Advanced Computing and Intelligent System (IJACIS)
Volume 1, Issue 1 (2023)
DOI: 10.66917/ijacis.a000003
https://msis-press.com/journals/ijacis



(a) Speckle Variance = 0.05

(b) Speckle Variance = 0.01

(c) Speckle Variance = 0.001

(d) Speckle Variance = 0.1

Fig. 102: Gaussian smoothing & intermediate difference gradient,Day6

International Journal of Advanced Computing and Intelligent System (IJACIS)
Volume 1, Issue 1 (2023)
DOI: 10.66917/ijacis.a000003
https://msis-press.com/journals/ijacis

7.8. Pixel Intensities & Contrast

In this subsection, the original X-Ray (without converting to single precision or double precision) is contrasted for study and analysis.

Let the center fit

$$z = \frac{(x - 147.5)}{74.05}$$

then from polynomial regression

$$y = 2242 \times z^9 + 1964 \times z^8 - 1.405 \times 10^4 \times z^7 - 1.145 \times 10^4 \times z^6 + 2.975 \times 10^4 \times z^5 + 2.194 \times 10^4 \times z^4 - 2.698 \times 10^4 \times z^3 - 1.881 \times 10^4 \times z^2 + 1.266 \times 10^4 \times z + 1.133 \times 10^4$$

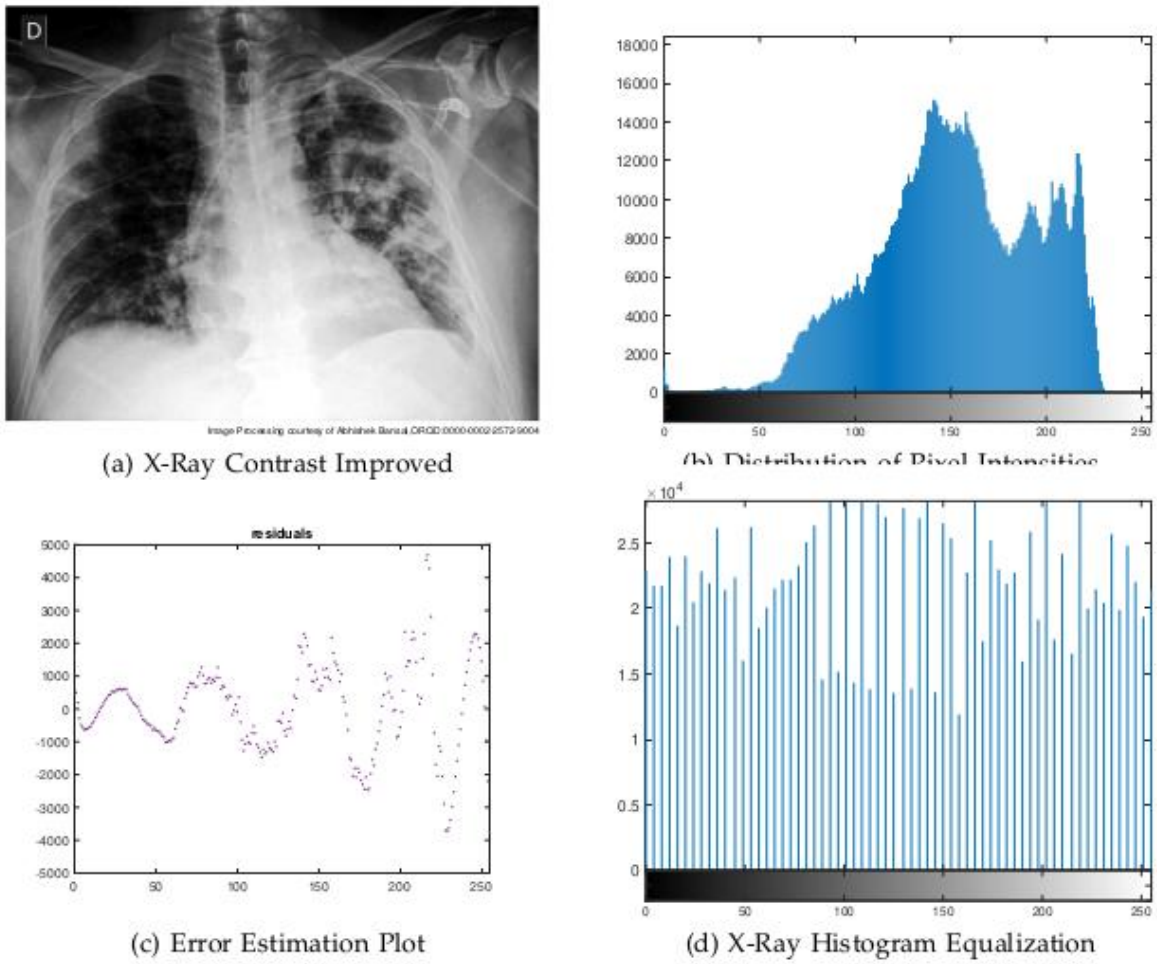
Let $\bar{y}$ be the mean of y, $\hat{y}$ the calculated values of y, then the coefficient of determination

$$R^2 = 1 - \frac{\sum_{i=1}^{n}(y_i - \hat{y})^2}{\sum_{i=1}^{n}(y_i - \bar{y})^2} = 0.9248$$

The measure of the goodness of fit given by norm of residuals is 2.145×10^4 . Here, the polynomial of degree 9 chosen here is the global which can be focused on the areas of interest (to be decided by infection part or researchers/doctors interest) and separate equations can be obtained for each particular area of interest. This gives insight in mathematical formulation and has been used in the Novel B-Mathematical Modeling of Respiratory System.

TABLE IX: Data Statistics for Fig. 103 (b)

	X	Y
min	0	0
max	255	1.516×10^4
mean	147.5	5516
median	147.5	4980
mode	0	0
std deviation	74.05	4898
range	255	1.516×10^4



(a) X-Ray Contrast Improved

(b) Distribution of Pixel Intensities

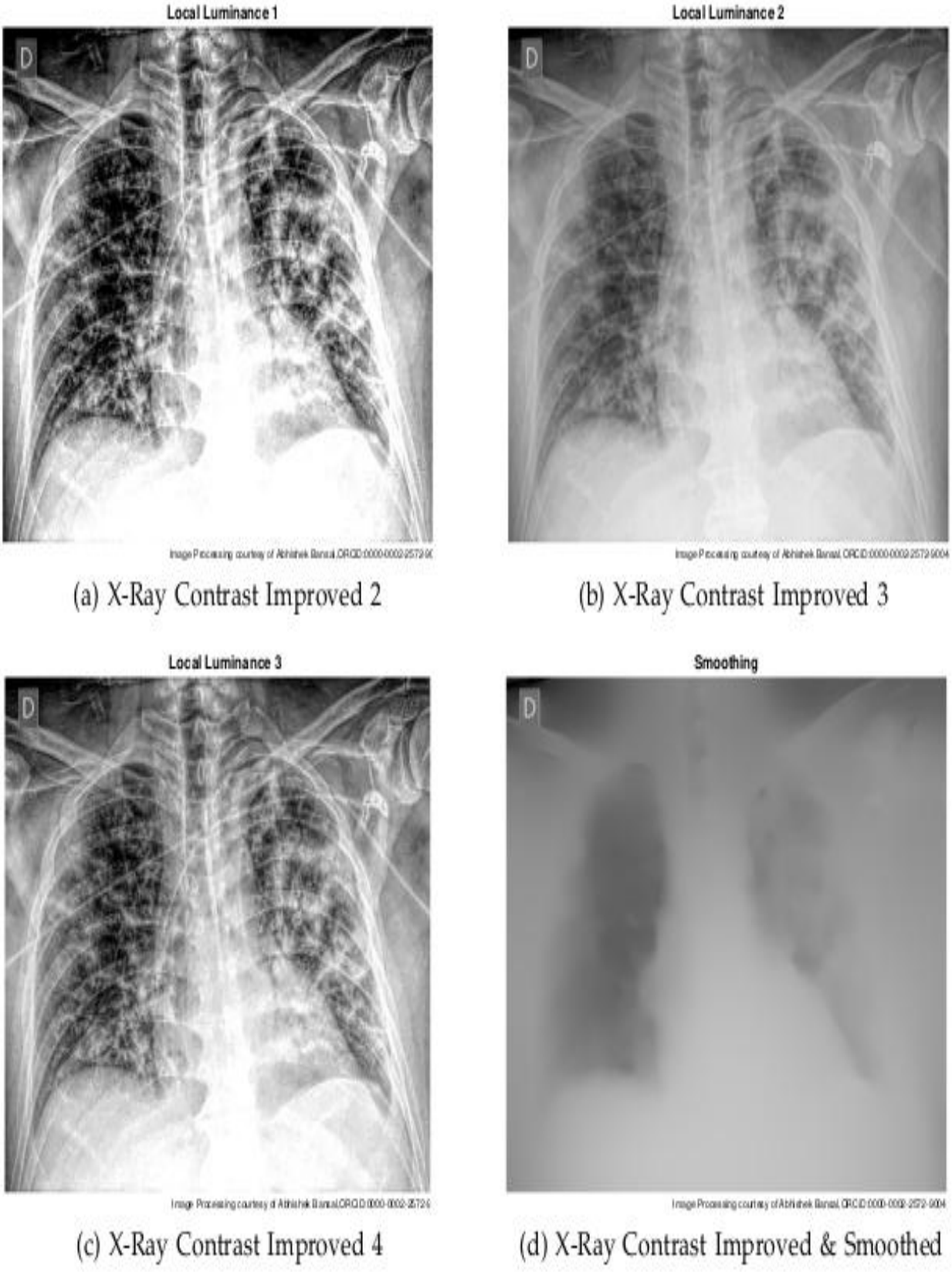
(c) Error Estimation Plot

(d) X-Ray Histogram Equalization

Fig. 103: Distribution of Pixel Intensities in X-Ray,Day6

The Fig.103(a) shows that X-Ray contrast is improved for analysis when compared with Fig. 1(a). Fig. 103(b) shows the distribution of X-Ray pixel intensities. Fig. 103(c) shows the error estimation plot, which is the plot of the residuals. Fig. 103(d) shows the X-Ray histogram equalization which is the spreading of the intensity values over the full range.

In Fig. 104, X-Ray Contrast is improved with five local luminances. The original Fig. 90(a) X-Ray contrast is improved with four more local luminances by varying the intensity values at low and high intensities. These are shown in Fig 104(a), Fig. 104(b) and Fig. 104(c). In Fig. 104(d), the original Fig. 90(a) X-Ray is contrasted with fifth value of improvement but smoothing technique is applied after it.



(a) X-Ray Contrast Improved 2

(b) X-Ray Contrast Improved 3

(c) X-Ray Contrast Improved 4

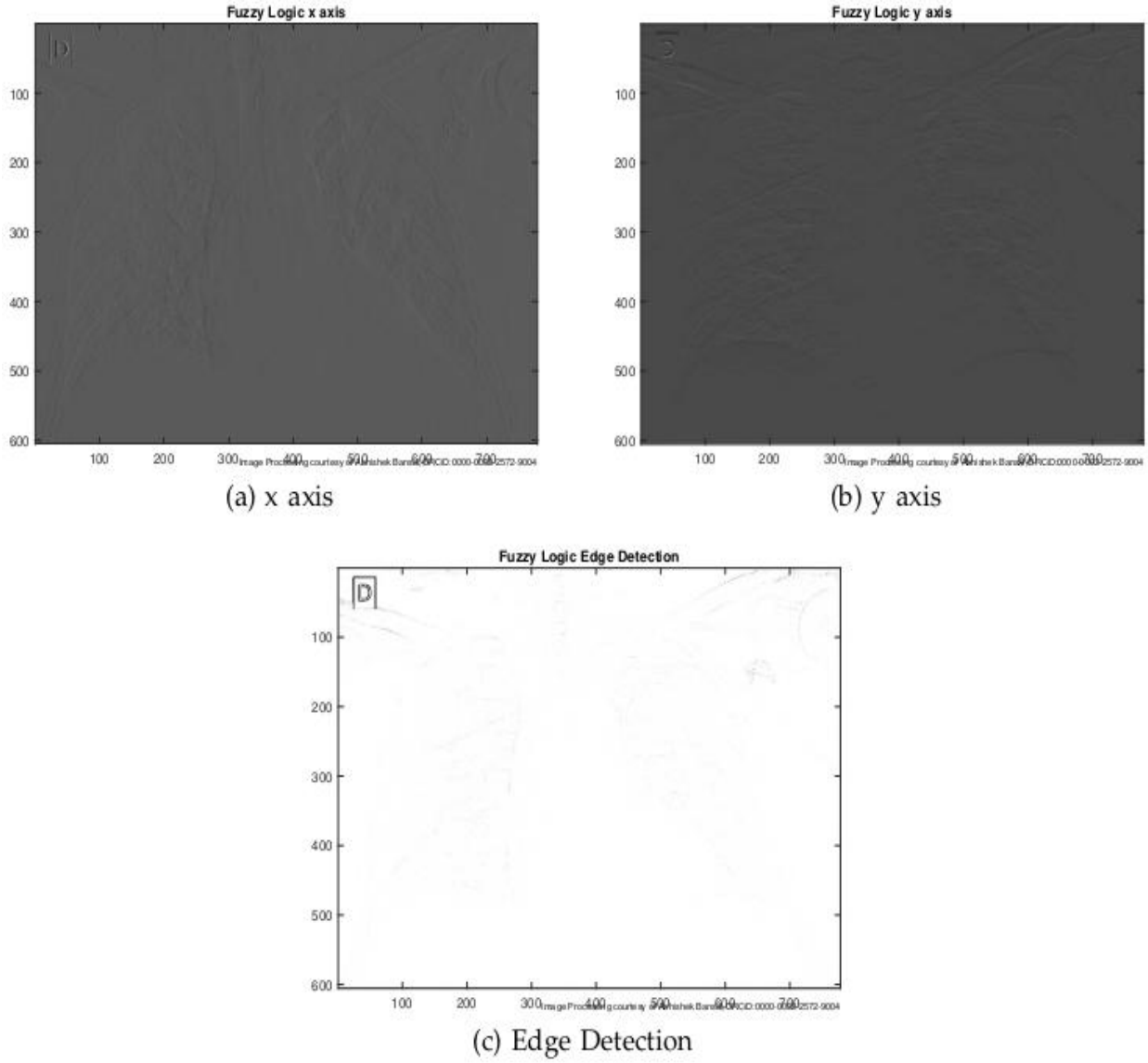
(d) X-Ray Contrast Improved & Smoothed

Fig. 104: X-Ray Contrast Improved with Five Local Luminances,Day6

International Journal of Advanced Computing and Intelligent System (IJACIS)
Volume 1, Issue 1 (2023)
DOI: 10.66917/ijacis.a000003
https://msis-press.com/journals/ijacis

7.9. Fuzzy Logic

In this subsection, the images obtained using fuzzy logic edge-detection algorithm and Fuzzy Inference System (FIS) are given. Two 2-D Convolution are performed. The x-axis of directional gradient is convolved with x-axis gradients of double-precision X-Ray obtained in Fig. 90(b) and the X-Ray gradient of fuzzy logic x-axis is given in Fig. 105(a). The y-axis of directional gradient is convolved with y-axis gradients of double-precision X-Ray obtained in Fig. 90(b) and the X-Ray gradient of fuzzy logic y-axis is given in Fig. 105(b). The edge detection is shown in Fig. 105(c).



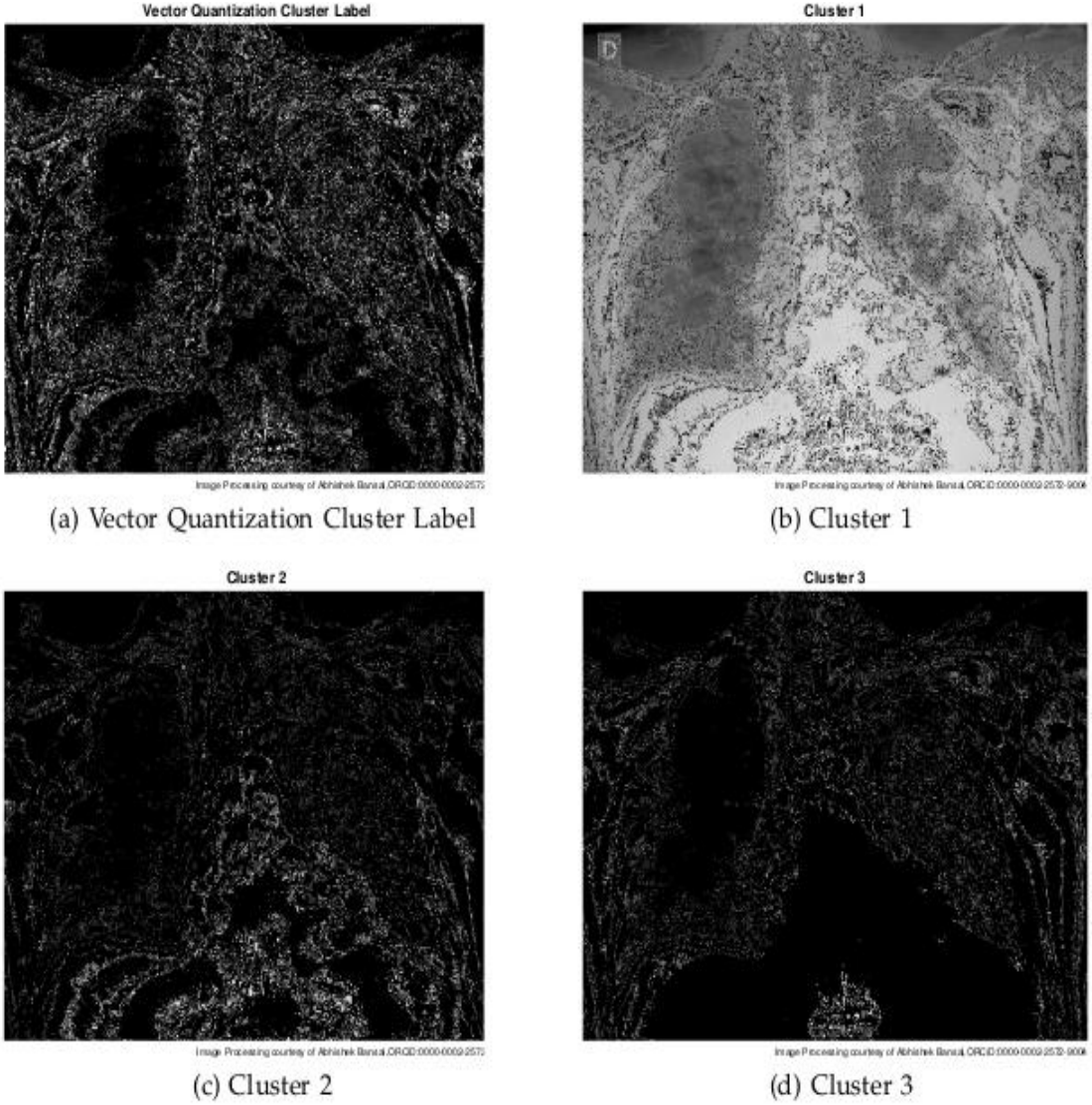
(a) x axis (b) y axis

(c) Edge Detection

Fig. 105: Fuzzy Logic,Day6

7.10. K-means Clustering

In this subsection, the popular vector quantization technique of K-Means clustering is applied to X-Ray. In this technique, firstly CIE XYZ tristimulus technique is used to know the color information and thus, the information of luminosity layer 'L*', chromaticity-layer 'a*' and chromaticity-layer 'b*' is obtained. Then every pixel is clustered with its pixel label and partitioned into three clusters. The clustering obtained is shown in Fig. 106(a), Vector Quantization Cluster Label. And three clusters Cluster 1, Cluster 2 and Cluster 3 obtained are shown in Fig. 106(b), Fig. 106(c) and Fig. 106(d) respectively.

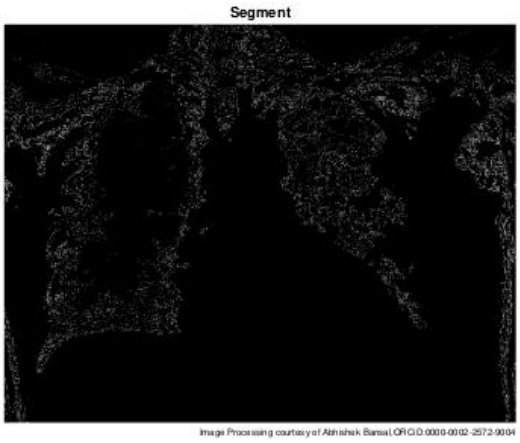


(a) Vector Quantization Cluster Label (b) Cluster 1

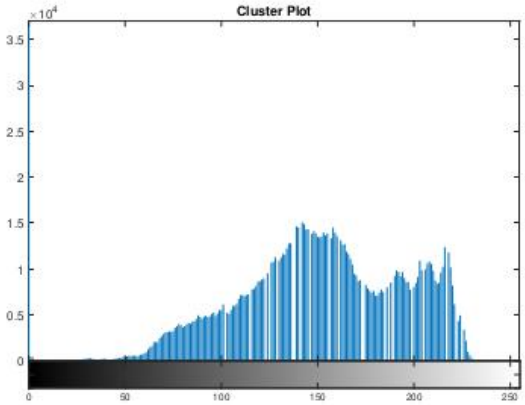
(c) Cluster 2 (d) Cluster 3

Fig. 106: Vector Quantization,K-means Clustering,Day6

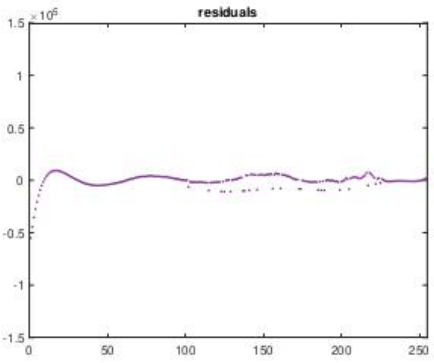
In Fig. 107(a), segmentation is applied and Fig. 107(b) and Fig. 107(c) shows respectively the cluster plot and the plot of error estimation, that is, the plot of residuals.



(a) Segmentation



(b) Cluster Plot



(c) Cluster Plot Residuals

Fig. 107: Clustering Plot and Segment,Day6

1029

1030 Moving in similar way as in the Subsection-8 and choosing same

$$z = \frac{(x - 147.5)}{74.05}$$

1033

1034 we have,

$$y = -7238 \times z^9 + 8947 \times z^8 + 3.917 \times 10^4 \times z^7 - 4.471 \times 10^4 \times z^6 - 7.035 \times 10^4 \times z^5 + 6.906 \times 10^4 \times z^4 + 4.169 \times 10^4 \times z^3 - 3.767 \times 10^4 \times z^2 - 1211 \times z + 1.086 \times 10^4$$

1035

1036 $R^2 = 0.3247$

1037 and Norm of Residuals = 1.806×10^5

1038 TABLE X: Data Statistics for Fig. 107(b)

	X	Y
min	0	0
max	255	2.108×10^5
mean	147.5	5516
median	147.5	3735
mode	0	0
std deviation	74.05	1.376×10^4
range	255	2.108×10^5

7.11. Morphological Segmentation

In this subsection, known morphological segmentation technique is applied on X-Rays. Three morphological openings are used.

The morphological opening with structuring element of disk shaped with three different radius are shown in Fig. 108(a), Fig.108(c) and Fig. 109(a). The background approximation images of X-Ray obtained after subtracting from the original image are shown in Fig. 108(b), Fig. 108(d) and Fig. 109(b).



(a) Morphological Opening 1



(b) Background Approximation Removed from Fig. 19(a)



(c) [Morphological Opening 2



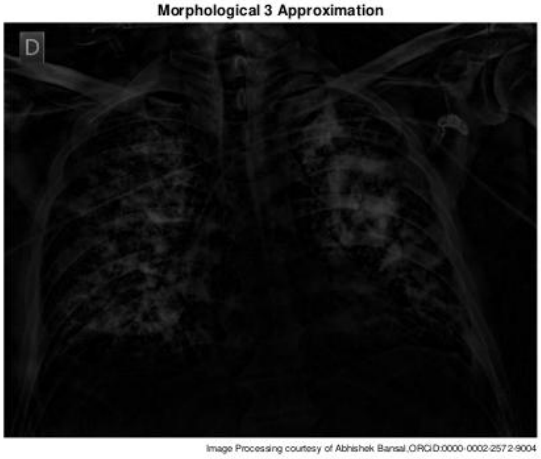
(d) Background Approximation Removed from Fig. 19(c)

Fig. 108: Morphological Segmentation,Day6

1064



(a) Morphological Opening 3



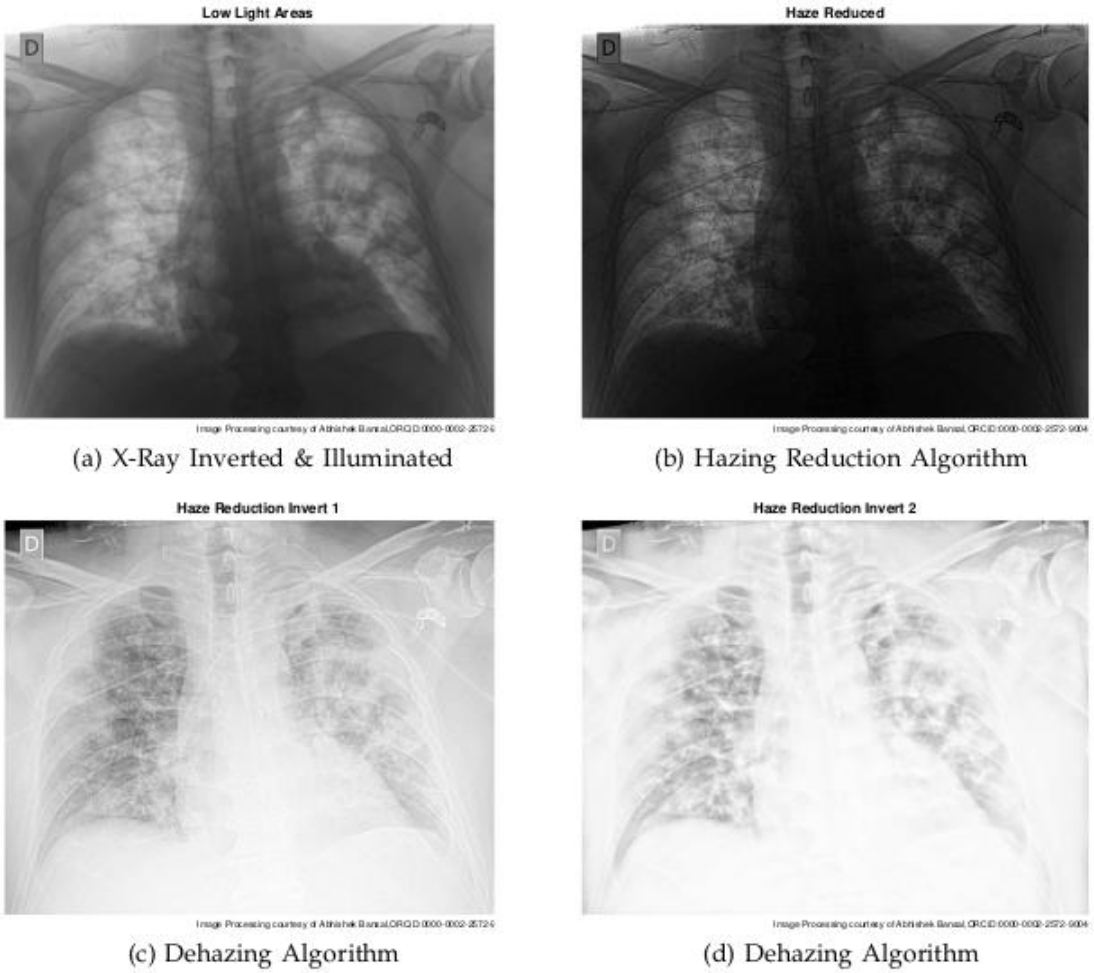
(b) Background Approximation Removed from Fig. 20(a)

Fig. 109: Morphological Segmentation,Day6

1065

7.12. Dehazing Algorithm

In Fig. 110(a), the original Fig. 90(a) X-Ray is inverted and the low-light areas and focused and the new X-Ray is obtained. The hazing obtained in Fig. 110(a) is reduced by hazing reduction algorithm.

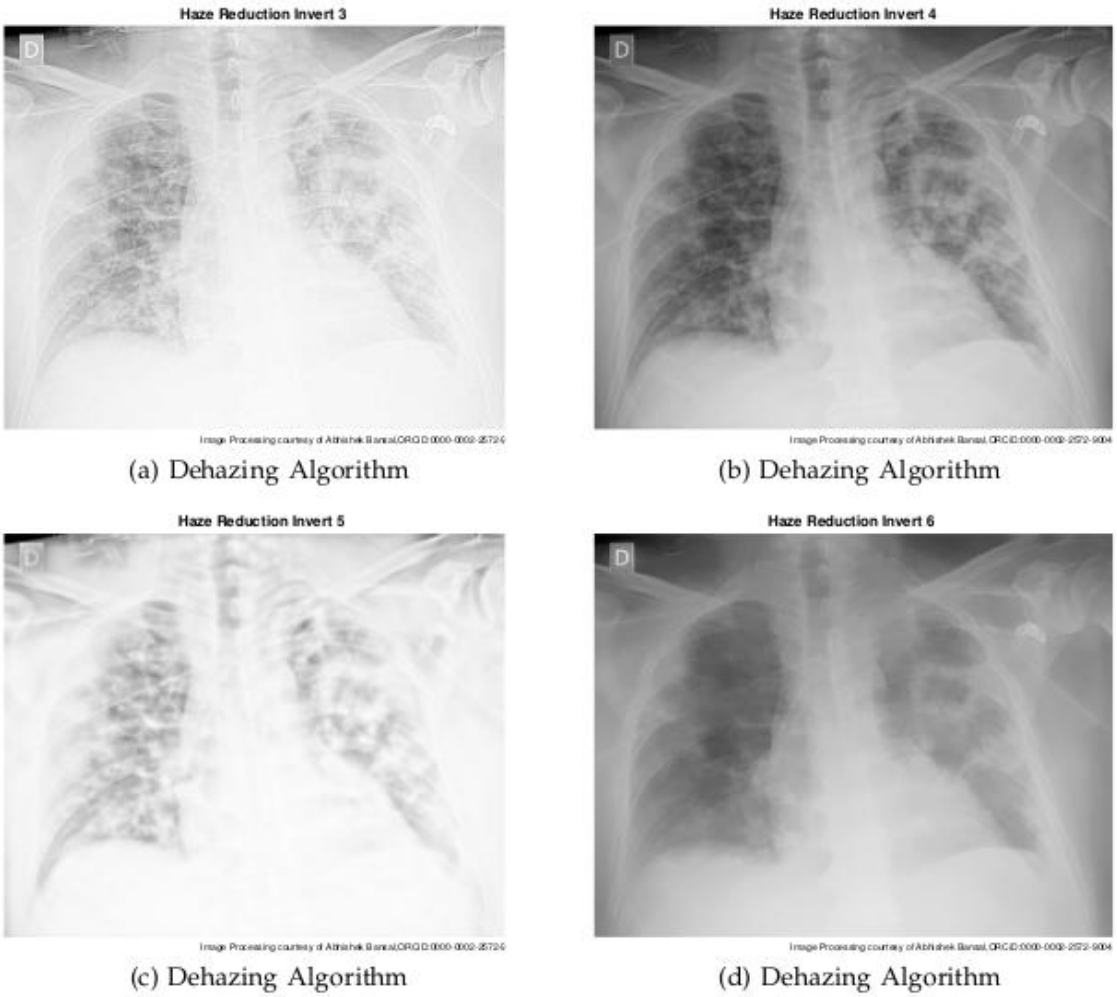


(a) X-Ray Inverted & Illuminated (b) Hazing Reduction Algorithm

(c) Dehazing Algorithm (d) Dehazing Algorithm

Fig. 110: Dehazing Algorithm,Day6

On the new X-Ray of Fig. 110(b), dehazing algorithm is applied and its result is in Fig.110(c,d). Fig. 111[a-d] has four more such combinations on which dehazing algorithm is implemented.



(a) Dehazing Algorithm (b) Dehazing Algorithm

(c) Dehazing Algorithm (d) Dehazing Algorithm

Fig. 111: Dehazing Algorithm,Day6

8. Conclusion & Future Work

The author using various tools and techniques invested his time in order to help doctors or researchers and pharmacologists. The author has successfully presented his image processing results and shown different possible images that can be obtained for analysis and studying ailment.

Though there are already established straightforward rules to read X-rays, e.g. dark gray areas, light area, distances,penetration,adequacy of inspiration,silhouette sign etc., which are adequate; these submitted further processed images can help doctors in

diagnosing and understanding deeper the phenomenon when the infection causes are different. Thus, these can help in the research of new medicine or treatment and can be used in designing of machine or therapy. It also gives researchers a perspective in deciding which image processing technique will not work at all, saving their time.

The submitted image processing results reveal certain patterns which are represented in mathematical form and can be used in the testing of machines. The polynomial fitting equations show the global formulation of complete lungs with various ailments is not possible mathematically whereas the local area (which would of interest) can be more accurately expressed in mathematical equations. The submitted mathematical equations can be more analysed with comparative study on other infections of lungs which the author may submit in future work. The author has used these in his novel model- Novel B-Mathematical Modeling of Respiratory System and Novel B-Bio Models Theory (to be submitted in few months or 20-30 years or never).

*It must be also noted that the clinical usefulness is **not claimed** in these results. As author has already mentioned, many researchers/post-doctorate fellows/clinical doctors, are performing same tasks which even the source[1] reveals, the author has submitted his work in this research paper.*

Funding: This research received no external funding. There are no funders for this submission.The author has himself fully self-financed, (with only objective to help) as it is only wastage of his time.

Acknowledgments: The work reported in this paper has been done independently and exclusively by the single author. The author has himself arranged himself various tools needed to submit this paper, with no support of any kind. The author as such thankful to none and does not have any special name to be acknowledged. He expects all these papers, would be nice Shroud for the passion and the price paid.

Conflicts of Interest: The authors declare no conflict of interest. The author also declares no competing interest. This manuscript has not been accepted or published by any journal.

References

1. Joseph Paul Cohen and Paul Morrison and Lan Dao, Joseph Paul Cohen, Postdoctoral Fellow, University of Montreal, COVID-19 image data collection, covid-chestxray-dataset-master.zip, 525MB, https://github.com/ieee8023/covid-chestxray-dataset
2. COVID-19 Image Data Collection: Prospective Predictions Are the Future Joseph Paul Cohen and Paul Morrison and Lan Dao and Karsten Roth and Tim Q Duong and Marzyeh Ghassemi arXiv:2006.11988, https://github.com/ieee8023/covid-chestxray-dataset, 2020
3. OpenCV team, https://opencv.org/
4. FuzzyLite, https://www.fuzzylite.com/
5. Laplacian Operator, https://en.wikipedia.org/wiki/Laplace_operator
6. Sobel–Feldman operator, https://en.wikipedia.org/wiki/Sobel_operator
7. Mathematical morphology, https://en.wikipedia.org/wiki/Mathematical_morphology
8. Fuzzy Logic, https://en.wikipedia.org/wiki/Fuzzy_logic
9. PyTorch, https://PyTorch.org
10. TensorFlow,www.tensorflow.org
11. Bansal, Abhishek (2023). Image Processing Results of One Week Covid-19 Evolution Pneumonia X-Rays. TechRxiv. Preprint. https://doi.org/10.36227/techrxiv.21778691.v1
12. Bansal, Abhishek (2023). Image Processing Results of One Week Covid-19 Evolution Pneumonia X-Rays., https://www.researchgate.net/publication/369843579_Image_Processing_Results_of_One_Week_Covid-19_Evolution_Pneumonia_X-Rays
13. Bansal, Abhishek (2023), My Research Papers Memoirs Volume 3 Part-I, Paperback, Notion Press
14. Bansal, Abhishek (2023), My Research Papers Memoirs Volume 3 Part-II, Paperback, Notion Press
15. Bansal, Abhishek (2023),My Research Papers Memoirs Volume 3 Part-I: Image Processing Results of One Week Covid-19 Evolution Pneumonia X-Rays Paperback – Large Print, Amazon
16. Bansal, Abhishek (2023), My Research Papers Memoirs Volume 3 Part-I Premium Quality: Image Processing Results of One Week Covid-19 Evolution Pneumonia X-Rays Hardcover, Amazon
17. Bansal, Abhishek (2023),My Research Papers Memoirs Volume 3 Part-II: Image Processing Results of One Week Covid-19 Evolution Pneumonia X-Rays Paperback – Large Print, Amazon
18. Bansal, Abhishek (2023), My Research Papers Memoirs Volume 3 Part-II Premium Quality: Image Processing Results of One Week Covid-19 Evolution Pneumonia X-Rays Hardcover, Amazon

© 2020 by the authors. Submitted for possible open access publication under the terms and conditions of the Creative Commons Attribution (CC BY) license (http://creativecommons.org/licenses/by/4.0/).